DISSERTATION

DOWNDRAFT IMPACTS ON TROPICAL CONVECTION

Submitted by

Katherine Thayer-Calder

Department of Atmospheric Science

In partial fulfillment of the requirements

For the Degree of Doctor of Philosophy

Colorado State University

Fort Collins, Colorado

Spring 2013

Doctoral Committee:

Advisor: David Randall

Richard Johnson
Eric Maloney
Michelle Strout

ABSTRACT

DOWNDRAFT IMPACTS ON TROPICAL CONVECTION

Downdrafts are an integral part of the convective cycle, and have been observed and documented for more than a hundred years. But many questions still surround convective downdrafts and their most difficult to observe properties. These questions have made the parameterization of convective downdrafts in global climate models (GCMs) very difficult. Designers of parameterizations have resorted to a wide range of assumptions and unverified hypotheses in their models of convective downdrafts.

In the last ten years, computing resources have advanced to a point where large domain, high resolution cloud resolving models (CRMs) can easily be run for long simulations. This study uses several simulations with 1 km horizontal resolution from the System for Atmospheric Modeling (SAM) v6.8.2 to examine convective downdrafts. We look at Radiative-Convective Equilibrium (RCE), a 21 day case from TOGA-COARE, Weak Temperature Gradient (WTG) simulations with varied shear profiles, and Lagrangian Parcel data to consider many difficult to observe properties of downdrafts.

We consider a variety of assumptions and questions that arise in the development of convective parameterizations. Our results show that downdrafts are an important mass flux in all simulations, and that cold pools organize convective systems and enhance updraft Convective Available Potential Energy (CAPE). We examine the ability for downdrafts to help couple deep convection to high relative-humidity regions in the tropics, and find that entrainment is likely a more important process in this relationship. We discuss the impact of downdrafts in maintaining boundary layer quasi-equilibrium, and find that, in our simulations, environmental entrainment has a larger impact on low-level most static energy. Finally, we show results from Lagrangian parcel data that illuminate our downdrafts as existing in an unsaturated state, with increasing buoyancy as they

descend. We show that many of our downdrafts have positive buoyancy perturbations, suggesting the presence of warm downdrafts and under-shooting bottoms in heavily precipitating tropical systems.

ACKNOWLEDGEMENTS

I would like to thank my family, including my husband, Mark and my son, Gabriel, for their unwavering support in this process. My extended family were of tremendous and unfathomable support, and without everybody's help, this dissertation would not have been written.

I would like to thank my advisor, Dave Randall, for the amazing educational experience he provided. I am very lucky and thankful that he took a chance and hired me as a student when I had a non-traditional background. Learning atmospheric science and modeling from Dave and CSU has been one of the most rewarding experiences of my life.

I would like to thank my committee, including Eric Maloney, Dick Johnson and Michelle Strout, for their input, advisement, help and comments. This thesis was greatly improved with their suggestions and guidance.

I would like to thank my friends and coworkers in the Randall research group. Their work and support were instrumental in completing these projects.

I would like to thank the funding agency that provided financial support for this project. This work was supported by the National Science and Technology Center for Multi-Scale Modeling of Atmospheric Processes, managed by Colorado State University under Cooperative agreement No. ATM-0425247.

Thank you.

TABLE OF CONTENTS

Chapter 1: Let's Talk About Downdrafts

What is a downdraft?

Convection in a fluid is a simple cycle where more buoyant parcels of fluid rise and less buoyant parcels sink. In the atmosphere, we see this every day in many parts of our world. As the sun warms the surface of the earth, warm near-surface air rises and cooler air aloft sinks to replace it. As buoyant air parcels rise, their temperature decreases, and the relative humidity of the parcel increases. Once the parcel hits saturation, water vapor condenses into liquid droplets and the real fun begins... we get clouds!

Convective clouds are those formed by the motions of buoyant air parcels. They can range from puffy little boundary layer cumulus clouds that are a few hundred meters wide, to huge convective systems that can cover hundreds of kilometers. Even the smallest clouds are very complex systems, influenced by processes on a wide range of scales. Water exists in all three phases in deep convective clouds, and phase changes happening at the scale of a water molecule are a major source of energy for all convective clouds. As these microscopic water droplets or ice crystals move from the interior of the cloud to the edges, cloudy air looses energy through heat radiation and evaporation, and that air begins to move downward (Bohren and Albrecht, 1998).

Every convective cloud contains these basic parts of the convection cycle. Warmer air (positively buoyant) inside of the cloud rises through updrafts, and cooler air (negatively buoyant) sinks in downdrafts. In small clouds, these processes are often turbulent and disorganized, but as the cloud grows the drafts deepen through the troposphere and become more powerful. If they can organize into a long-lived propagating system, a storm is born.

Here, we focus on the downward part of convective clouds - downdrafts. Every convective cloud has some amount of air that sinks due to negative buoyancy, and the rate and depth of the sinking motion is tied to the causes of that negative buoyancy (Knupp and Cotton, 1985). Small

cloud droplets that evaporate or radiatively cool at the edges of clouds create weak downdrafts that may not sink very far. Once cloud droplets are large enough that they cannot be held in suspension by the atmosphere any longer, they fall through the cloud as precipitation, dragging cloud air downward with them. Shafts of precipitation can create deep and powerful downdrafts, through both loading of precipitation and large-scale evaporation as precipitation exits the base of the cloud (Houze, 1993).

As the cooler air of a downdraft enters the sub-cloud layer, also known as the boundary layer, it often cools further due to the evaporation of rain in a sub-saturated environment. This cold air sinks faster, and can be moving at a relatively high velocity as it hits the surface of the earth. A high velocity downdraft is called a microburst. As the cool downdraft air hits the surface and spreads out in all directions, it creates a cold pool region below the cloud. A local frontal zone where the cool air pushes out against warmer surface air is known as a gust front, and for a powerful downdraft a gust front can be damaging and even deadly (Fujita and Wakimoto, 1981).

This study looks at convective downdrafts in-depth in an effort to quantify some of the driving processes and impacts of this complex part of the cloud system. The goal of this work is to examine many of the assumptions and relationships that have been used in climate models for nearly 40 years to represent cloud processes and specifically downdrafts. The grid-scale resolution of most climate models is far larger than convective clouds, so these processes are represented statistically as parameterizations. We will examine the assumptions in downdraft parameterizations by analyzing output from a model that has a high enough resolution to actually simulate the physics of clouds, and use the results to suggest improvements or changes. These changes could improve the ability for many models to simulate current climate and future climate change.

Observational studies of downdrafts

Downdrafts are not easy to observe. They are transient features of clouds that grow and fade in time and space. Traditional methods of atmospheric observations such as radiosondes and remote sensing have difficulties with downdrafts. It is nearly impossible to float a balloon upwards through a downdraft, and remote sensing of temperature or water vapor is difficult inside of a cloud. However, the cool outflow of downdrafts at the surface is a clear manifestation of severe storms, and meteorologists have been trying to learn more about the phenomenon for many years. Humphreys (1914) discusses the observation of cool, gusty winds flowing out of precipitating storms (measured at the surface by weathermen). He notes that these winds are not observed from clouds without rainfall, and concludes that the surface cooling of a thunderstorm is most likely the result of deep columns of evaporating precipitation. Interestingly, he adds observations of intense in-cloud drafts "from the graphic descriptions of the few balloonists who have experienced the trying ordeal of passing through the heart of a thunderstorm", though they were likely too distracted to record careful measurements (Humpreys, 1914).

After World War II, more airplanes and radars were available for meteorological research and observations. The Thunderstorm Project was one of the earliest to focus on using fly-throughs and radar measurements to map the structure and lifecycle of deep convection (Byers and Braham, 1948; Byers and Braham, 1949). This project was the first to define three stages of development during the lifecycle of an ordinary thunderstorm. The first stage they define is the Cumulus stage, where clouds are small and their circulations are dominated by a relatively shallow updraft circulation. The second stage is the Mature stage, where a deep convective cell has a penetrating updraft and long, continuous downdraft. Byers and Braham (1948) propose that these downdrafts are initiated by precipitation loading, maintained through the entrainment of environmental air, which allows some evaporative cooling, and eventually through evaporation of precipitation below cloud base. Their aircraft identify downdrafts beginning at 15,000ft (about 4.5 km) altitude and having vertical

velocities between "a few" and 40 feet per second (1-12 m/s). Figure 1.1 shows the vertical drafts in a "typical" storm cell in the mature stage, with a distinct updraft and downdraft associated with precipitation. The third and final stage is the Dissipating or anvil stage, which occurs after the downdraft has filled the area below the updraft with enough cool air to cut it off from the surface energy source. At this point, Byers and Braham (1948) suggest that the cell is mostly comprised of a "gentle downdraft with negligible vertical motions in the higher levels."

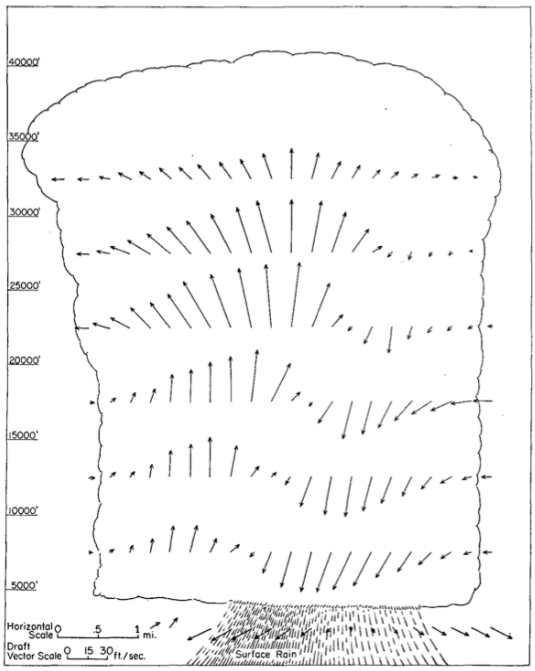

Figure 1.1. Diagram of updrafts and downdrafts in a "typical" mature-stage thunderstorm cell. Figure 11 from Byers and Braham (1948).

Observations of convection and convective circulations were driven to the forefront of the field by Joanne Malkus in the late 1950s. She and her team flew a PBY-6A Navy plane on multiple horizontal transects of tropical clouds in the Caribbean. Their main goals were to document the magnitudes of updrafts, downdrafts and entrainment rates in trade-cumulus clouds (Malkus, 1954). Figure 1.2 is a plot of flight transects through a cloud with a weaker updraft but a noticeably strong downdraft in the upper levels. This draft was measured to have about an 800m width and 4 m/s vertical wind-speeds. Malkus (1954) calculates an entrainment rate based on vertical divergence and then determines (based on thermodynamic properties) that the downdraft was entraining air primarily from the updraft. Malkus (1954) also notes that the air surrounding the cloud with a downdraft was considerably more moist than air near a cloud with no measurable downdraft.

Malkus goes on to use data from these and other flights through small tropical clouds to build a simple steady-state model of downdrafts (Malkus, 1955). Based on this model, they determine that downdrafts originate near the cloud top, and are mostly comprised of updraft air that

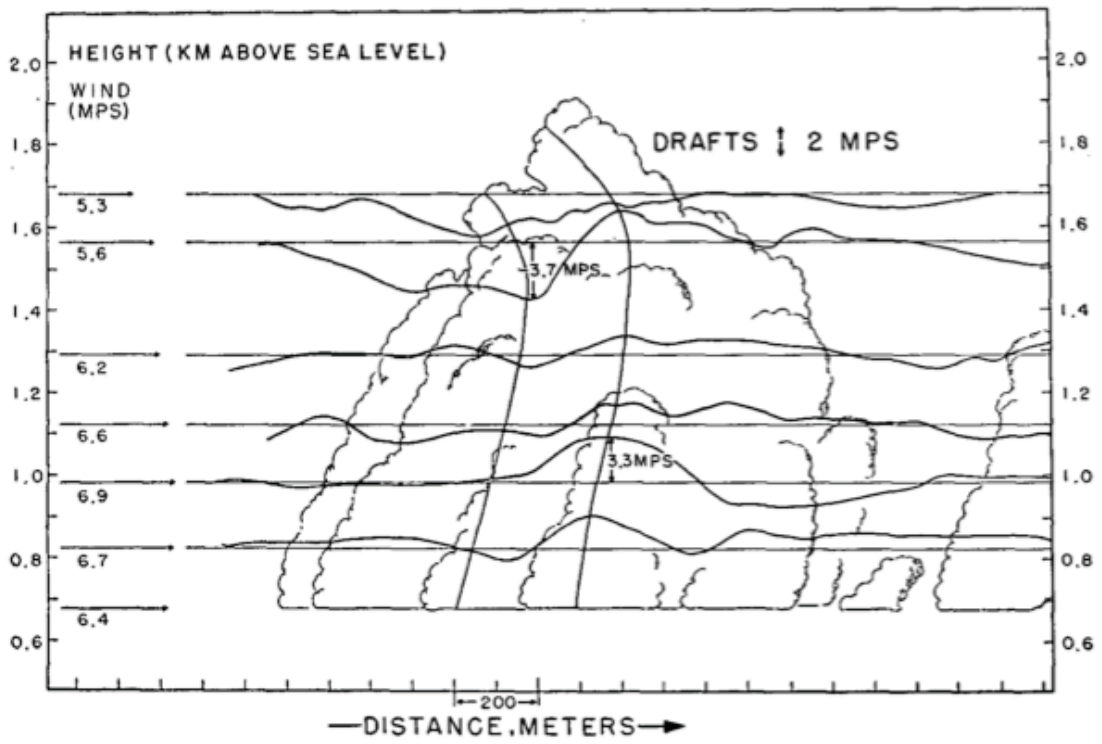

Figure 1.2. Flight traversals and vertical wind speeds through cloud II, Figure 13 from Malkus (1954).

has lost positive buoyancy due to condensate evaporation. In this model, no more than 16 percent of the entrained air could be from the environment in order to agree with the observed thermodynamic properties. The primary source of negative acceleration is due to precipitation evaporation, and the downward speed of the downdraft is damped by constant entrainment of updraft air with positive buoyancy (Malkus, 1955).

In the decades following Malkus' work, there is an explosion in field projects working to observe and quantify cloud properties and dynamics. Knupp and Cotton (1985) give a detailed overview of observations and conclusions about downdrafts to that date. Their analysis separates downdrafts into four categories. Penetrative downdrafts are driven by precipitation and condensate evaporation in the upper levels of both precipitating and non-precipitating clouds. Cloud edge downdrafts are observed in shallow cumuli and are formed as the cloud entrains drier environmental air and the edge condensate evaporates. Overshooting downdrafts are the result of an updraft rising

Table 1.1. Aircraft observations of updrafts and downdrafts, reproduced from Table 2 in Knupp and Cotton (1985)

Location	Reference	Updraft Speed (max/ mean) m/s	Updraft Width (max/ mean) km	Downdraft Speed (max/ mean) m/s	Downdraft Width (max/ mean) km	Cloud Type
Caribbean	Malkus [1954, 1955]	6/-	0.6/-	6/-	0.5/-	Non-precipitating Cu con 2km deep
Australian coastal area	Warner [1977]	8.5/4.5	1.3/0.7	7/3.8	0.8/0.3-0.4	Non-precipitating Cu con
Florida	Hallett et al. [1978]	30/12.6*	>3.5/1.7	8/4.8*	1.8/0.9	precipitating towering Cu
Florida	Keller and Sax [1981]	15.5/7.5*	3/2.5	7/2.5*	4.8/2.1	precipitating towering Cu con to Cb
Florida	Willis et al. [1982]	13/8.8*	1.6/0.9	6/4.1*	1.1/0.8	precipitating towering Cu con
Florida	Wiggert et al. [1982]	31.5/16.8*		23.5/6.8*		precipitating towering Cu and Cb
Illinois	Wiggert et al. [1982]	20.5/7.2*		7.8/3.9*		precipitating towering Cu and Cb
Hurricanes	Jorgensen et al. [1985]	6 (avg)/ 1.5 (med)		5 (avg)/1.5 (med)		four hurricanes, inner core and outer bands
Tropical Atlantic	LeMone and Zipser [1980]	14/2.9 (med)	7/~1.8 (med)	7/~1.8 (med)	7/1 (med)	precipitating and non-precipitating Cu con to Cb
Florida/Ohio	Byers and Braham [1949]	26/7	11.5/1.5	24/5	7/1.2	precipitating Cb
Colorado and Oklahoma	Sinclair [1973]	26/	15/	10/	12/	precipitating Cb

***Mean of maximum gusts**

past its level of neutral buoyancy, cooling and then rapidly sinking downwards. Precipitation associated downdrafts form when a column of precipitation exits the base of a cloud and evaporates into the boundary layer. Their Table 2, reproduced here (in part) as Table 1.1, covers a wide range of aircraft flight data on downdrafts over a 20+ year period. In general, downdrafts are equal or slightly less in magnitude and width as updrafts, and tropical convection has lower magnitude wind fields than continental convection.

One of the most influential studies sited in Table 1.1 is the core updraft and downdraft database compiled by LeMone and Zipser (1980). They used over 10^4 km of flight transects from six days of the GARP (Global Atmospheric Research Program) Atlantic Tropical Experiment (GATE) field study to create a statistical view of up- and downdraft sizes, vertical velocities, and mass fluxes. They found updraft cores to be generally smaller and stronger than downdraft cores, though near cloud base their diameters and velocity distributions were very similar (some values listed in Table 1.1). Updrafts typically had higher mass fluxes than downdrafts, but downdraft mass flux was non-

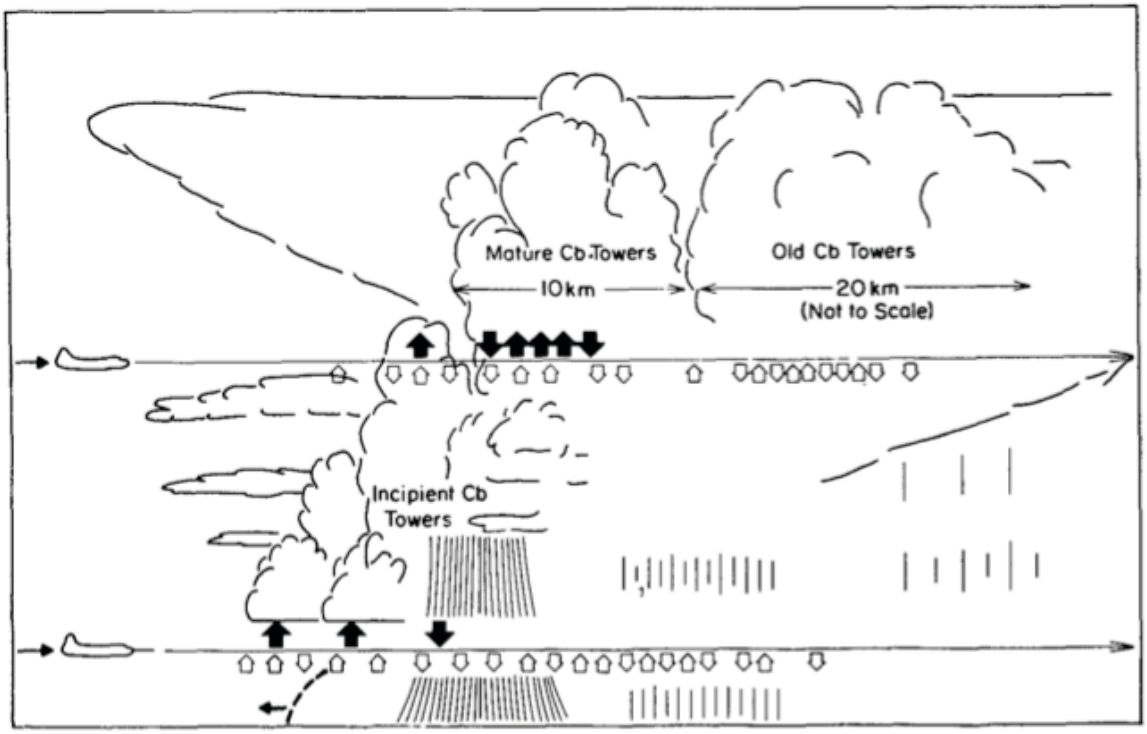

Figure 1.3. A schematic of composite cores and drafts within the tropical mesoscale systems of GATE. From Zipser and LeMone (1980) Figure 4.

negligible, and very nearly the same as updrafts in lower levels. Zipser and LeMone (1980) use this database to build a basic model of tropical convection. A schematic of their results is shown in Figure 1.3. They describe the in-cloud vertical velocities as having a "triangle" profile rather than a "top-hat" shape, suggesting that updrafts and downdrafts mix both thermodynamic and momentum properties as they travel vertically through the cloud.

Jorgensen and LeMone (1989) sampled hundreds of up- and downdraft cores via aircraft during the Taiwan Area Mesoscale Experiment (TAMEX). They were able to get better measurements of in-cloud temperatures using a CO_2 radiometer, and collected drop-size distributions for data on water loading. They found median up- and downdraft diameters to be roughly the same at 1.1km width, and that updrafts had only about 30% more mass flux than downdrafts. The 50th percentile of updrafts and downdrafts were both around +/-2 m/s, but maximum updraft velocities were over 9 m/s, and maximum downdraft values around -6 m/s. Their careful temperature measurements found just as many downdrafts with positive virtual temperature anomalies as updrafts. They conclude that precipitation loading must be a major source of downward acceleration in these clouds.

Wei et al. (1998) examine the impacts of entrainment and precipitation loading on the buoyancy of tropical oceanic clouds in the Tropical Ocean and Global Atmosphere Coupled Ocean-Atmosphere Response Experiment (TOGA-COARE) using flight data in the lower levels of clouds (about 850-700hPa). They define a cloud buoyancy measure as

$$B \equiv \Delta T_v - B_l \quad (1)$$

where $\Delta T_v = T_v - T_{ve}$ is the difference between in-cloud and environmental virtual temperature and $B_l = T_{ve} r_l$ is the reduction in buoyancy due to condensate loading. Using this calculation, and careful measurements of temperature and cloud droplet concentrations, Wei et al. (1998) find that the average downdraft buoyancy is positive. In fact, the stronger downdrafts have *higher* buoyancies than weak ones. They found entrainment to be the main source of the reduction in buoyancy of updrafts

from adiabatic values, and that precipitation loading was secondary in reducing buoyancy of both up- and downdrafts. They suggest that precipitation only temporarily reduces the buoyancy of parcels, and once it falls out the parcel is free to resume buoyant rising motions.

This number of positively buoyant downdrafts in field studies peaked the curiosity of many cloud scientists. Igau et al. (1999) review the results from Wei et al. (1998) and suggest that the assumption of 100% relative humidity in the calculation of in-cloud virtual temperatures positively skews downdrafts towards a higher buoyancy than they actually experience. They find that using the environmental relative humidity values of between 60-80% reduces the buoyancy of downdrafts to negative values for about 1/3 of the strongest cores. Igau et al. (1999) calculate the relative humidity of a downdraft parcel originating at the height of minimum equivalent potential temperature in the environmental sounding and reaching the observed temperature excess at 700hPa. This calculation requires a 30% relative humidity to maintain negative buoyancy, far lower than any observed at these levels in TOGA COARE. And, even assuming 30% relative humidity, the five most intense downdraft cores sampled would maintain their positive buoyancy.

Igau et al. (1999) conclude that many tropical downdrafts are positively buoyant. They suggest that these are the results of "over-shooting downdrafts or the downward-moving parts of gravity waves, or caused by more complex interplay of the forces generated by the surrounding three-dimensional convection and its immediate environment" (Igau et al., 1999). The final result of these field projects and measurements seems to be that tropical downdrafts are more positively buoyant than we can explain, and tropical updrafts are less positively buoyant than we would expect.

Why study downdrafts?

The observations outlined here show that, downdrafts are less intense and move less mass than updrafts (LeMone and Zipser, 1980; Jorgensen and LeMone, 1989), so why bother studying them at all? We have three main motivations for working towards better understanding of downdrafts. The first is that downdrafts can impact human lives and property as a severe weather phenomenon. Fujita and Caracena (1977) document three aircraft accidents resulting from intense downdraft activity in the region. They named these intense, destructive, local downdrafts microbursts and attempt to better explain and document the phenomena in an effort to educate pilots and prevent further death. Fujita and Wakimoto (1981) document severe structural damage to homes and buildings in northern Illinois as a result of microburst and downdraft outflows. They use ballistic calculations from observed damage to calculate surface winds near 100 miles per hour due to microbursts (a 180 kg chimney is thrown over 100m away, shown in their Figure 27, and our Figure 1.4).

Around the world, downdrafts cause damage to infrastructure and occasional loss of lives, they can impact wildfire magnitude and direction (Sun et al., 2009), and they can cause wide-spread dust storms (Middleton and Chaudhary, 1988), among many other destructive and dangerous impacts. But downdrafts also have an impact on the scale of the global climate, and this is our

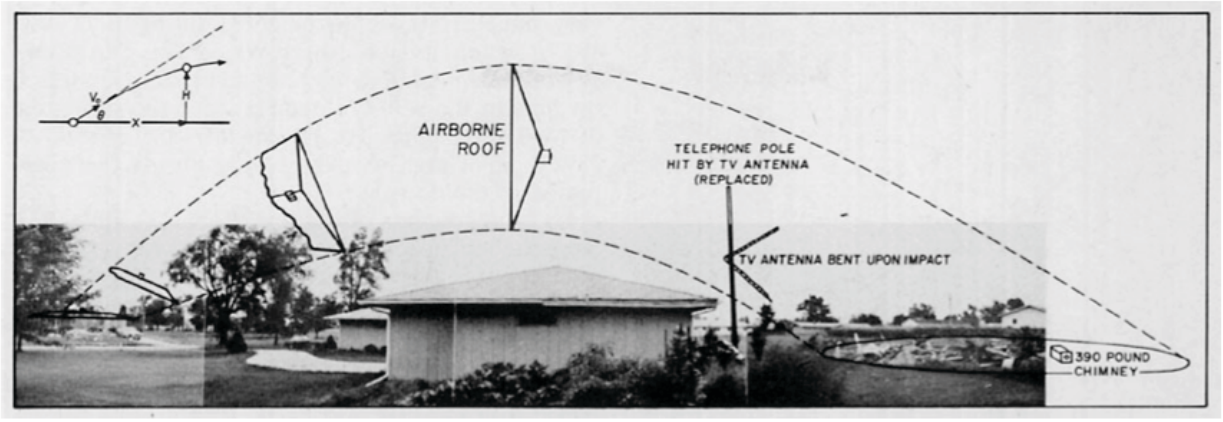

Figure 1.4. A diagram of the ballistic trajectory of a roof and chimney that flew more than 100m in a damaging downdraft gustfront. From Fujita and Wakimoto (1981) Figure 27.

second motivation for studying them. Downdrafts occur almost anywhere precipitation forms in a cloud and modulate the vertical mass transported through convection (Johnson, 1976). In reducing the upward mass transport by deep tropical convection, downdrafts reduce atmospheric subsidence, and reduce the resulting large-scale warming and drying (Cheng and Arakawa, 1997). Downdrafts are very important in coupled atmosphere-ocean systems, through their impacts on surface fluxes via cold pools and gust fronts (Johnson and Nicholls, 1984; Jorgensen et al., 1997). And finally, downdrafts transport upper tropospheric air into the mid- and lower-levels, impacting the mixing of aerosols and other atmospheric constituents on local and global scales (eg. Betts et al., 2002).

It is for all of these reasons that our third, and most specific, motivation arises. Today's global climate models (GCMs) are used by many different groups for climate forecasting, policy planning and scientific research, but their representations of downdrafts have shown a need for improvement. Straub et al. (2010) perform a wide-ranging survey of the ability of GCMs to simulate convectively coupled equatorial Kelvin waves, and found most had severe problems. The authors discuss a missing low-level cooling and drying signal that should be simulated by the model's downdraft parameterization. Several studies, including Maloney and Hartmann (2001) and Sahany and Nanjundiah (2008) have shown the importance of the evaporation of convective precipitation in maintaining an accurate simulation of tropical climate and tropical convection in GCMs. Pritchard et al. (2011) discuss the inability of most global climate models to accurately simulate the eastward propagation of mesoscale convective systems in continental regions. Once they are able to resolve downdraft-boundary layer interactions in the embedded cloud resolving model of the Super-Parameterized Community Atmosphere Model (SP-CAM), the propagation of convection across the Eastern United States is greatly improved.

The goal of our study is to examine convective downdrafts in high-resolution cloud-resolving model output in order to recommend better constraints and more realistic processes in downdraft parameterizations for GCMs. If we can critically examine the assumptions and

simplifications around downdrafts made by GCM convective parameterizations, then we can determine which are most realistic and which are problematic. In doing so, we hope to influence the formulation of future convective parameterizations. Perhaps, these recommendations will help alleviate some of the biases and issues in GCMs, improve our ability to forecast climate, and deepen our understanding of the atmospheric system.

Chapter 2: Downdrafts in Convection Parameterizations

What is a convection parameterization?

Our main motivation in this study is to improve the representation of convective downdrafts in Global Climate Models (GCMs). Climate models divide the world into thousands of pieces, or gridcells, and solve the equations of motion for each piece. These gridcells are much larger than many important atmospheric processes, like convection and boundary layer turbulence. Models producing results for the upcoming IPCC report (AR5), have gridcells that are about 100-200 km wide in the tropics, but the average width of an updraft or downdraft inside of a cloud is about 1km (as we show in the previous chapter). Convection is very important for driving atmospheric circulations, so global climate models use parameterizations to represent the effects of processes too small to resolve on the grid.

Convective parameterizations attempt to calculate the large-scale effects of a gridcell full of clouds, if we were able to simulate them. Figure 2.1 shows this schematically. There are many

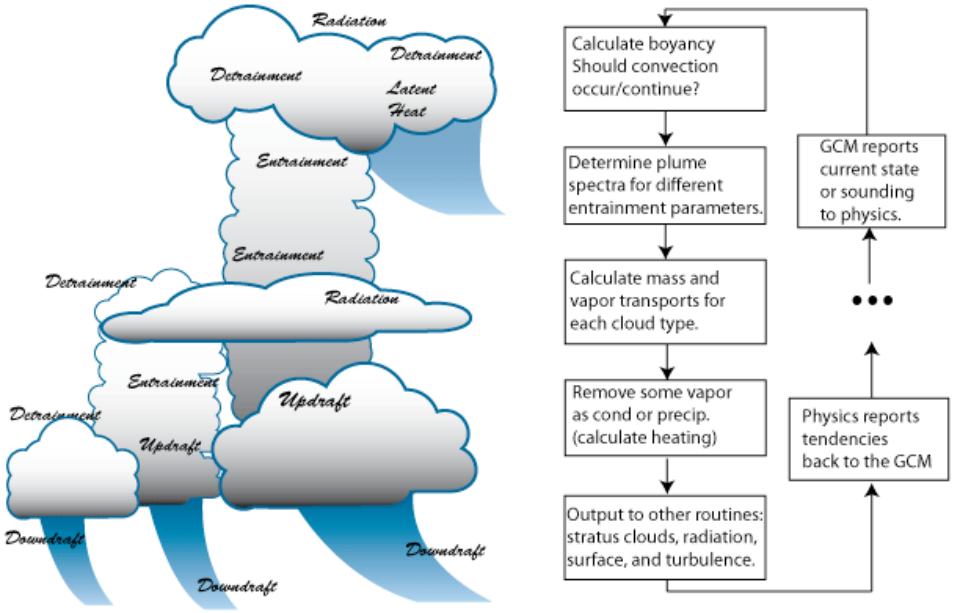

Figure 2.1. Convective parameterizations take the complex and multi-scale processes in cloud systems (left), and distill them into a series of computer procedures, evaluated at each timestep and each gridcell in a climate model (right).

different interacting and complex processes going on within clouds. In a convective parameterization, we choose the ones we think are most important, write equations that describe how these cloud processes are related to grid-scale properties, and then code them up as computer procedures. Most convective parameterizations use grid-scale fields such as profiles of temperature and moisture, convergence, lift, and instability, to calculate the resulting mass flux, heating, and vapor condensation produced by theoretical clouds in that environment. We describe these clouds as theoretical, because they are often modeled as one-dimensional entraining plumes of air, and are simplified from the actual dynamics of convection (Arakawa and Schubert, 1974; Moorthi and Suarez, 1992; Zhang and McFarlane, 1995; etc).

A wide variety of convective parameterizations are implemented in climate models, and each has its own unique properties, assumptions, strengths and weaknesses. Tables 2.1 and 2.2 gives an overview of some of the most prominent climate models used today, and their convective parameterizations. In the next section, we will take a closer look at the methods and assumptions behind these parameterizations.

Current representations of convective clouds and downdrafts

A key strength in our forecasts for climate lies in the unique properties of each global climate model. If every model is formulated differently, it reduces the likelihood of a global bias in forecasts. However, many models have similar pedigrees, and certain assumptions and simplifications have been passed down through many iterations. Every climate model has a similar goal: to calculate the solution to the physical equations that describe the motions of fluids on our planet. And when they fall short of this goal, we should examine our assumptions and consider what processes may be missing or mistaken within our models.

Tables 2.1 and 2.2 list nine different GCMs, each available as a coupled climate model that includes ocean and land surface models, and gives an overview of the representation of deep

Table 2.1. List of popular climate system models, their deep convection parameterizations, and basic properties of their parameterized downdrafts.

Model	Convective Parameterization	Downdraft Mass Flux?	Precip Evaporation?	Unsaturated Downdraft?
GFDL CM2.1	Moorthi and Suarez (1992)/Tokioka et al. (1988)	No	No	No
GFDL CM3/ AM3	Donner (1993)/Donner et al. (2011)	Yes	Yes	No
NCEP CFS/ GFS	Grell (1993)/Hong and Pan (1998)	Yes	Yes	No
CCSM3	Zhang and McFarlane (1995)	Yes	Yes	No
CESM1 (CAM5)	Zhang and McFarlane (1995)/Neal et al. (2008)	Yes	Yes	No
MIROC3.2	Pan and Randall (1998)/ Emori et al. (2001)	No	No	No
MIROC5	Chikira and Sugiyama (2010)	Yes	Yes	No
ECHAM5	Tiedke (1989)/Nordeng (1994)	Yes	Yes	No
IPSL-CM4	Emanuel (1991)	Yes	Yes	Yes

Table 2.2. Models from Table 2.1 and their primary research and development groups.

Models	Primary Research Group (s)
GFDL CM2.1	NOAA/Geophysical Fluid Dynamics Laboratory
NCEP CFS/ GFS	NOAA/National Centers for Environmental Prediction
CCSM3/ CESM1	National Center for Atmospheric Research
MIROC3.2/5	Center for Climate System Research, National Inst for Environmental Studies, and Frontier Research Center for Global Change
ECHAM5	Max Planck Institute for Meteorology
IPSL-CM4	Mateo-France/Centre National de Rechearches Météorologiques

convection and convective downdrafts in each. This list represents a variety of top climate models, with submissions in IPCC assessment reports and CMIP projects. Our list is intended to give a survey overview of the most-used convective parameterizations, so each model listed here uses a slightly different parameterization. Some of these parameterizations are based on the same, older methods, and differ only in details. Others are fairly unique and differ in their basic structure and overall architecture. Since our goal is an examination of downdrafts, we will categorize these parameterizations by their methods for representation of convective downdrafts.

Table 2.1 shows that a few older parameterizations do not include any mention of downdrafts, or calculations for downdraft mass flux. One of the early and most widely used (historically) convective parameterizations is Arakawa and Schubert (1974 - hereafter AS). This parameterization calculates the cumulus cloud-base mass flux based on a diagnosed "cloud work function" that is similar to convective available potential energy (CAPE). To determine the vertical distribution of thermodynamic properties, AS assumes clouds behave as one-dimensional entraining plumes of air. Air enters the cloud in the boundary layer and is lifted and mixed with the environment until it reaches its level of neutral buoyancy and detrains. Air is moved downwards in the dry, subsiding environment only. This parameterization assumes that downdrafts move much less mass than updrafts and the dry environment, and they can be neglected to first order.

1) No Downdrafts

AS has been widely used for several decades, and has been updated and adjusted in that time. In Table 2.1, parameterizations that do not include any downdraft effects, such as Moorthi and Suarez (1992) and Pan and Randall (1998) are direct off-shoots of AS. Moorthi and Suarez (1992) is commonly known as Relaxed Arakawa-Schubert (RAS), because it changes the updraft closure from requiring a balanced state at the end of each timestep, to 'relaxing' it, or performing a few iterations and allowing the system to be near equilibrium rather than enforcing it. Pan and Randall (1998)

change the AS updraft closure to derive the cloud base mass flux from a predicted cumulus kinetic energy (CKE) term. Neither of these parameterizations change the basic AS assumption that downdrafts do not matter. Both parameterizations immediately remove any precipitation formed in their clouds, without allowing any to fall through the column or evaporate.

Each of these "no-downdraft" parameterizations have been adjusted to better agree with observations, but without improving their representation of downdrafts. In the GFDL CM2.1 model, the RAS scheme has been updated with the Tokioka et al. (1988) convective trigger. This adds a second requirement before the deep convective parameterization can run: there must be grid-scale instability, *and* the column entrainment rate must be greater than a threshold. The MIROC3.2 model implements Pan and Randall (1998) with the Emori et al. (2001) criterion. Emori et al. (2001) require the average relative humidity from cloud base to cloud top to be greater than 80% before the Pan and Randall (1998) scheme runs. They show that this simple requirement greatly improves the spatial distribution of summertime tropical precipitation. Using these types of convective triggers creates a tighter coupling between deep convection and high relative humidity regions, as observed (Bretherton et al., 2004). While the theory behind the trigger is based on greater entrainment processes, the actual buoyancy calculations and entrainment in the cloud plumes is not changed.

2) Simple Saturated Downdrafts

The National Centers for Environmental Prediction (NCEP) models are used to forecast climate for both research and operational products. Many user groups look to the NCEP monthly and seasonal forecasts for planning purposes. The NCEP GFS atmospheric model uses a very simple and highly efficient version of the AS scheme described in Grell (1993). It is updated in Hong and Pan (1998) with a convective trigger based on boundary layer turbulence and surface inhomogeneities. Rather than a spectrum of entraining updraft plumes, this scheme uses only a single updraft in each gridcell, but adds a single downdraft plume to the scheme. Because the basic

formulation is the same but the scheme is radically simplified, this parameterization is often called the Simplified Arakawa-Schubert scheme (SAS). Despite the truncation of the updraft spectrum, this scheme has been shown to perform well in simulating climate, and at a fraction of the computational costs.

The simple downdraft plume used in the SAS scheme is typical of "base-model" downdrafts included in convective parameterizations. The downdraft is a single entraining plume, that begins at the column minimum of moist static energy. The mass flux though the downdraft plume is determined as a fraction of the updraft mass flux at cloud base and the precipitation efficiency (dependent on wind shear).

$$m_{d0} = \frac{\beta I_1 m_{ub}}{I_2} = \varepsilon m_{ub} \quad \text{from Eq A.24, Grell (1993)}$$

where m_{d0} is the mass flux at the originating level of the downdraft, $1-\beta$ is the precipitation efficiency, I_1 and I_2 are parameters relating cloud condensate to updraft mass flux and evaporation to downdraft mass flux (respectively), and m_{ub} is the cloud-base updraft mass flux. The thermodynamics of this scheme provide for the maximum possible positive buoyancy for updrafts and negative buoyancy for downdrafts. The updrafts and downdrafts entrain only from the environment, and do not interact with each other. These assumptions are all very similar to the steady-state model of downdrafts proposed by Johnson (1976).

The results of Grell (1993) show that a change from a spectrum of six updraft plumes to a single updraft and downdraft plume does not make much difference in their forecast. However, the loss of the downdraft mass flux greatly increases the drying and heating in the lower troposphere (most intense above the boundary layer), and significantly degrades the simulation of the dynamics of mesoscale convective systems.

The Community Climate System Model (CCSM) and the Community Earth System Model (CESM) are widely used research models based at the National Center for Atmospheric Research

(NCAR). These are "community" models, and development work on the physical parameterizations and numerics of these large, complex models goes on all over the world. The CCSM model contributed to the first four IPCC reports and the first version of the new CESM is included in the upcoming fifth assessment report. The atmospheric component of these climate models is the Community Atmosphere Model (CAM), and this model has undergone many updates and overhauls over the years as well. Traditionally, this model uses the Zhang and McFarlane (1995 - hereafter ZM) scheme, which has been updated with convective momentum transport and a slightly different CAPE-based closure in recent years (Neale et al., 2008).

The formulation of downdrafts in the ZM scheme has not changed in more than 15 years. The downdrafts in ZM are very similar to those of SAS, except ZM allow for a full spectrum of up- and downdraft plumes in the column. Downdrafts in ZM only occur when precipitation forms within a cloud, and all plumes are initiated at the column minimum of saturated moist static energy. These downdrafts also entrain only environmental air, do not interact with the updrafts, and detrain all of their mass and energy below cloud base. Like SAS, the total mass flux through the origination layer of downdrafts is directly related to the mass flux through the updraft at cloud base, as

$$M_d = \frac{-\alpha M_b}{\lambda_m}\left(e^{\lambda_m} - 1\right) \quad \text{from ZM eq 8}$$

where M_d is the mass flux of downdrafts at the origination level, M_b is the mass flux of updrafts at cloud base, α is a proportionality factor, and λ_m is the maximum downdraft entrainment rate. The proportionality factor directly relates the mass flux through the downdraft to the precipitation efficiency, as

$$\alpha = \mu \frac{PCP}{PCP + EVP} \quad \text{from ZM eq 11}$$

where μ is the maximum fraction of evaporation (generally prescribed as 0.2), PCP is the column integral of precipitation and EVP is the column integral of rain water evaporation. So the amount of mass flux through these downdrafts is basically a function of the mass lifted in updrafts, the

entrainment rate and the fraction of precipitation that is allowed to evaporate. The constraints are imposed so that downdrafts disappear in the absence of precipitation, and that the net mass flux at cloud base is always positive.

The Tiedke (1989) convective parameterization in the ECHAM model also uses a simple saturated downdrafts scheme. These downdrafts are modeled in a bulk mass flux scheme as deep penetrating drafts that are associated with convective precipitation. Tiedke (1989) downdrafts form at the highest model level where a 50/50% mixture of cloud air and saturated environmental air results in a parcel with negative buoyancy relative to the cloud-free environment. The mass flux through these downdrafts is *directly* proportional to the updraft mass flux, given by

$$\left(M_d\right)_{LFS} = \gamma \left(M_u\right)_{base} \quad \text{from Eq 16 in Tiedke (1989)}$$

where $\left(M_d\right)_{LFS}$ is the downdraft mass flux at the originating level (the level of free sinking), $\left(M_u\right)_{base}$ is the updraft mass flux at cloud base, and γ is a simple proportionality factor set to 0.2 in the Tiedke (1989) study, but often set to 0.3 when the scheme is implemented in GCMs (eg. Liu et al., 2005). As in the other schemes in this section, Tiedke (1989) evaporates enough precipitation to maintain a saturated parcel decent into the sub-cloud layer, where the downdrafts all detrain.

There are a lot of commonalities in these downdrafts, and they are not the only schemes to use simple saturated plumes to describe downdraft mass fluxes. Cheng and Arakawa (1997) add saturated plume downdrafts to the AS scheme, with a rainwater budget that allows for precipitation loading to effect the buoyancy of downdrafts along with the evaporation of condensate. Cheng and Arakawa (1997) suggest that six variables are required to parameterize downdrafts: the origination height of the draft, the downdraft mass flux at the origination level, the entrainment and detrainment rates of the draft, the thermodynamic properties of entrained air, the thermodynamic properties of the draft itself, and the location of the base of the draft. Each of the simple saturated schemes discussed here outline basic relationships for these six parameters and nothing more. This

may be enough to statistically capture the climatological effects of convective downdrafts, but there are other schemes that go much further in the parameterization of their downdrafts.

3) Complex Convective Downdrafts

Downdrafts can be very sensitive to local thermodynamic and microphysical processes. Where the schemes in the previous section generally drive downdrafts with a determined fraction of the updraft mass flux, and keep their plumes negatively buoyant through the evaporation of precipitation, some convective parameterizations have downdrafts with more degrees of freedom. The Emanuel (1991) scheme, used in the IPSL climate model, employes an episodic mixing model in its updrafts. Updraft parcels are lifted without entrainment to an arbitrary layer between cloud base and cloud top. Cloud water is condensed or precipitated based on a specified fraction, and the cloudy air is mixed with environmental air. The air then either ascends or descends to a new level of neutral buoyancy, where the process is repeated until there is no liquid water left. This allows the parameterization to move air through saturated updrafts and downdrafts using the same rules, driven by their own thermodynamic properties, though the final closure for the system is based on the amount of CAPE available in each column.

Emanuel (1991) also allows for unsaturated downdrafts, which is not included in any of the parameterizations in the previous sections. This scheme specifies a fraction of precipitation falling out of a saturated updraft or downdraft that can be evaporated in the environment. The mass flux of the unsaturated downdrafts are actually based on the conservation equations for momentum, heat, and water using the cooling provided by evaporation of precipitation. To better simulate a convective rain-shaft falling through clear and cloudy air, only a fraction of the precipitation is exposed to the dry environment, and that fraction can vary with time and height. In Emanuel (1991), the results of a radiative-convective equilibrium run are shown, the downdraft mass fluxes

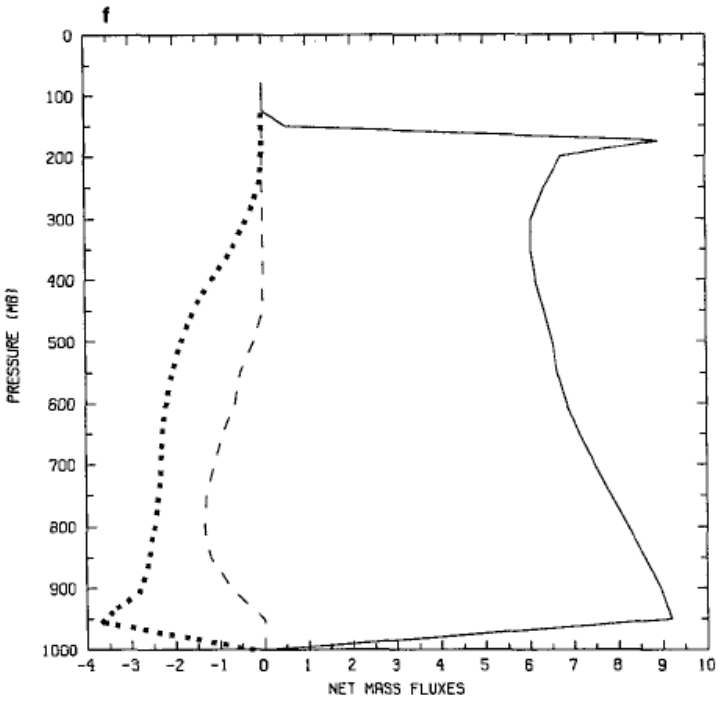

Figure 2.2. Profiles of convective mass fluxes averaged over the last 100 hours of a single column radiative-convective equilibrium run of the Emanuel (1991) scheme. Mass fluxes are in units of [10-3 kg m-2 s-1], the solid line is all updraft mass fluxes, the dashed line is saturated downdraft mass flux, and the dotted line is the unsaturated downdraft mass flux. From Emanuel (1991) Figure 3.

extend through most of the cloudy column, and total about 50% of the updraft mass flux in the mid-troposphere (see Figure 2.2).

4) Mesoscale Downdrafts

Another convective parameterization that permits complex forms of convective downdrafts is the Super-Parameterization, which has generally been used in the Community Atmosphere Model, known as the SP-CAM (Khairoutdinov and Randall, 2001; Khairoutdinov et al., 2005). The SP-CAM replaces the traditional convection parameterizations in the CAM with a 2-dimensional cloud resolving model (CRM) in each GCM gridcell. The CRMs run for the duration of the GCM simulation, and are intensely nudged by the GCM grid-scale environment. At each GCM time step, the CRM outputs are averaged into traditional parameterization outputs (heating and moistening tendencies only, momentum is not shared). Instead of assuming clouds are a spectrum of plumes

with mass fluxes dictated by GCM column instability, the SP-CAM simply runs a small-scale model that solves the equations of motion in two dimensions and determines cloud influences based on this. The CRMs inherently simulate complex updraft and downdrafts, with interactions that we are only beginning to understand (eg. Prichard et al., 2011). Because the CRMs typically run at 4-10km resolution for approximately 64 columns, they can simulate convective organization into small mesoscale structures as well. This means the effects of saturated, unsaturated and mesoscale downdrafts are all included in the resulting tendencies.

The newest version of the GFDL model now implements the Donner (1993) convective parameterization with a few tweaks and updates (Donner et al., 2011). This parameterization simulates a detailed microphysical condensate population, including the effects of phase transformations between all three water phases. In order to do this, the vertical momentum budget must be calculated for each updraft and downdraft plume as well. The Donner (1993) scheme also includes the effects of mesoscale updrafts, downdrafts and anvil clouds. These features distribute water vapor and temperature through the column assuming the clouds are organized into a mesoscale system, and allows for some interactions between updrafts and downdrafts that are not included in typical convective parameterizations. The mesoscale cloud structures also allow for a more complex interaction with the radiation scheme as well, and begins to pull the convective parameterization towards a system where sub-gridscale processes are all tightly coupled, as happens in the super-parameterization.

A few groups have developed cold pool or "convective wake" only parameterizations. These parameterizations take the output of a deep convective scheme and use information about precipitation and mass fluxes to generate a simple model of cold pool activity. Quian et. al (1998) have one example of detailed, complex cold pool parameterization. They model the cold pool as a traveling, rectangular buoyancy wave, with increased surface fluxes near the up-stream side that linearly decrease across the cold pool. Increased surface fluxes in the boundary layer are balanced

through environmental entrainment across the top of the cold pool. This parameterization produces surface fluxes that are more tightly coupled to convection, a boundary layer that destabilizes and re-stabilizes as seen in Quasi-Equilibrium (eg. Raymond, 1995), and a better maintenance and longer propagation period of mesoscale convection.

The idea of mesoscale organization affecting the entrainment and detrainment properties of parameterized plumes has been distilled into a single parameter in the recently published work of Mapes and Neale (2011). They create a time and space-varying parameter called *org* that attempts to replicate the effects of the organization of convection on the properties of entraining plumes. A more organized system of plumes should entrain more moist air, have higher precipitation rates, and more intense convective heating. Their test parameterization for the org parameter is the University of Washington "Shallow" convection scheme (Park and Bretherton, 2009), which includes only two updrafts plumes and no downdrafts. Mapes and Neale (2011) associate higher values of *org* with increased precipitation evaporation, so, they somewhat manage to distill many of the *mesoscale* impacts of downdrafts into a single parameter. While this parameterization is still intended only for research purposes, it is an interesting view into the direction that convective parameterization development is heading. More and more, we are learning that the interactions between updrafts and downdrafts, downdrafts and the boundary layer, boundary layer variability and updrafts, are all important regulating processes that need to be captured for our GCMs to accurately simulate precipitation all over the globe.

Chapter 3: Models and Methods

Using a CRM to improve GCMs

We have discussed a number of problems and assumptions made in downdraft parameterizations that are difficult to address using observational data. Downdrafts are transient structures buried deep within convective clouds, making them difficult to explore by aircraft and hard to observe via remote sensing. Cloud resolving models (CRMs) give us a unique opportunity to examine both case studies and general statistics of convective phenomenon like downdrafts. CRMs are models with a high enough resolution to solve the equations of motion and simulate clouds based on their underlying physics. They usually have domains that are about the same size as a climate model gridcell, which makes them a nice tool for investigating how a parameterization should react given the large-scale behavior of a GCM.

Researchers have been using CRM output to suggest improvements for parameterizations for many years. Weisman and Klemp (1982) use a three dimensional cloud resolving model with various large-scale soundings to produce typical forms of mid-latitude convection. They are then

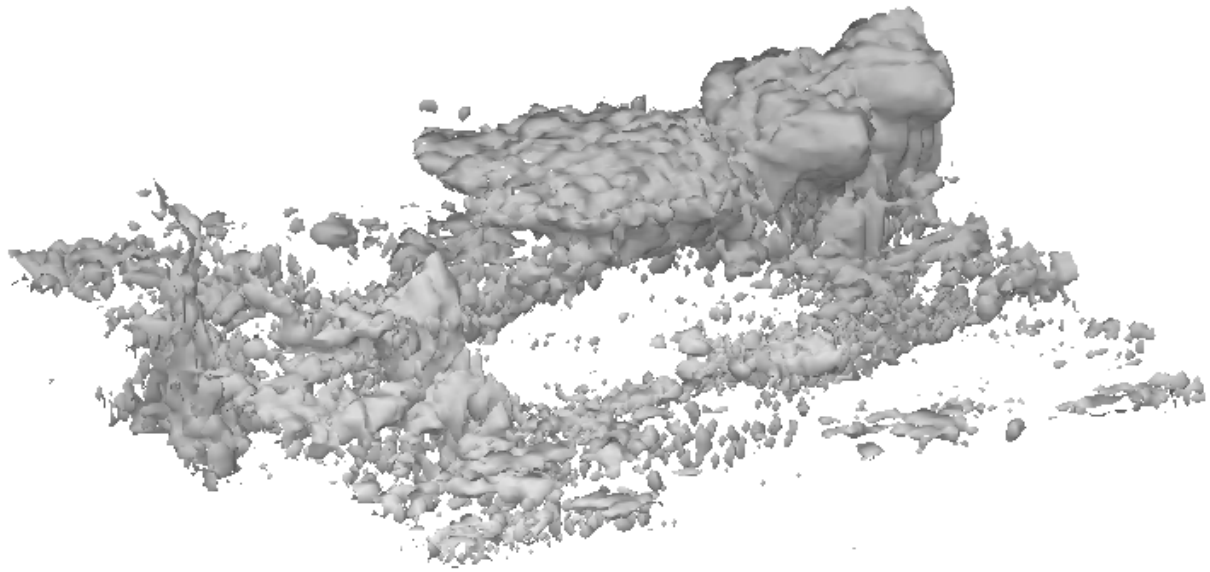

Figure 3.1. Three dimensional rendering of non-precipitating cloud water/ice in our cloud resolving model (from the TOGA simulation).

able to associate patterns of severe weather with the large-scale environment in which they form, and form a good link between the buoyant properties of convective clouds and the large-scale environment.

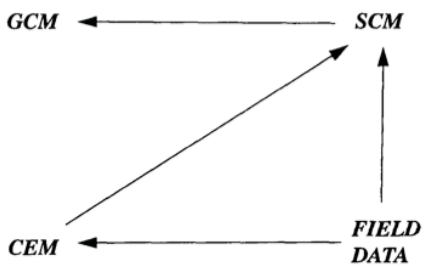

Figure 3.2. Using a single column model (SCM) and Cloud Ensemble Model (CEM - same as a CRM) to improve parameterizations in a Global Climate Model (GCM). From Fig.3 in Randall et al. (1996).

Randall et al. (1996) describe various methods for using CRMs to evaluate and test GCM parameterizations. New parameterizations are built into a single column model (SCM), which is a single column of the parent GCM, and forced with prescribed large-scale tendencies rather than computed dynamics. Field data are used to run simulations in the SCM and the CRM. The results are compared and improvements made to the parameterizations. Further testing and improvements can be done in the SCM until the parameterization is ready for GCM implementation. This allows for a more rapid development cycle of parameterizations than would be allowed by running the full global model.

Xu and Randall (2001) use a different method with their cloud resolving model, this one more similar to the method used in our study. They run the model forced by two different observational datasets, one tropical and one continental, and then compare cloud process statistics from each run and observational data. These statistics are useful as scaling constraints and relationship identifiers when developing new convective parameterizations. This method allows us to view processes in our CRM that are not easily observed in the real world, but very informative for the development of parameterizations. It is a common practice in microphysical development as well, where case-study or radiative-convective equilibrium runs of cloud resolving models are used to investigate different microphysical schemes (e.g. Donner et al., 1999; Noppel et al., 2010; Van Den Heever et al., 2011; and many others).

Another interesting method for utilizing a CRM to improve GCM parameterizations is the implementation of the weak temperature gradient (WTG) approximation as a forcing mechanism

for the CRM. Raymond (2007) describes using this method with a cloud resolving model in order to tune the most sensitive pieces of his parameterization. The WTG approximation was developed by Sobel and Bretherton (2000) as a method of testing parameterizations in single column models. The method stems from the idea that the tropics are held in an equilibrium between the vertical velocities of the clouds and the diabatic heating rates of the average horizontal domain. So the forcing for the SCM or the CRM applies a vertical velocity calculated to just balance the domain-average heating by radiation, latent-heat release, and vertical transport of heat by convection. In a CRM with periodic boundary conditions, the mean vertical velocity must be zero, but the effects of a large-scale lifting or subsidence can be approximated through an implied convergence of temperature and moisture via relaxation of the mean state towards a prescribed sounding. We employ this method to test the impact of vertical wind shear on downdrafts in Chapter 7.

Cloud resolving models have been a useful tool for GCM parameterization development and improvement for many years. They allow us to examine and analyze processes that are difficult to observe in the real world, under strictly controlled conditions that can be very similar to those produced in both the real world and a GCM. For the first 20 years of usage, fully three-dimensional simulations from cloud resolving models were still rather expensive and time consuming. Many studies use two-dimensional simulations or shorter duration simulations to save on computational costs (e.g. Grabowski et al., 1996; Raymond and Zeng, 2005). In the last decade, computers have continued their exponential increase in processing power. We are now able to easily run three dimensional simulations of convection, and we have the processing power to carefully analyze the mass of three dimensional data produced. Our study takes advantage of these computing increases and analyzes downdraft interactions in three dimensional, high-resolution, and long-term simulations.

The System for Atmospheric Modeling (SAM)

Our study uses the System for Atmospheric Modeling (SAM) v6.8.2 cloud resolving model written and maintained by Marat Khairoutdinov. This model uses the anelastic equations of motion on a fully staggered Arakawa C-type grid. Time integration uses a third-order Adams-Bashforth scheme with a variable time step. Advection of scalars (including water species) is done with a fully-three dimensional positive definite monotonic scheme. SAM uses prognostic liquid water/ice moist static energy, total precipitating water (rain, snow, and graupel), and total non-precipitating water (vapor, cloud water, and cloud ice). The model has periodic boundary conditions, a rigid lid top with Newtonian damping, and all simulations here are done over a water-only surface with no topography (Khairoutdinov and Randall, 2003).

SAM has a good record for quality in simulations. Khairoutdinov and Randall (2003) show that the model does a reasonable job simulating long-term weather at the Oklahoma ARM site. Their study does show the model has a low-bias in shaded cloud fraction compared to the GOES-7 satellite observations, but suggest that this could be caused by advection of high-level clouds from outside of the domain in the observations. They show that the three-dimensional model runs tend to have a higher surface precipitation rate for shallow convection and a slightly too-low precipitation rate for intense deep convection, but, in general, matches the observations well.

SAM has participated in a some cloud resolving model intercomparison studies. Xu et al. (2002) compares the above simulation at the Oklahoma ARM site with the same one from seven other models. In this study, SAM does well, but tends to produce a little too much cloud ice, and not as much condensate or cloud fraction as other models. The results, in general, are very comparable with the other models, with SAM showing no egregious biases. Grabowski et al. (2006) include SAM in an intercomparison with 8 other cloud resolving models in a high-resolution simulation of the diurnal transition from shallow to deep convection. SAM performs well in this study, producing reasonable results throughout the simulation. Even the lower resolution (both horizontally and

vertically) simulation from SAM performed about as well as the highest resolution benchmark simulations.

Khairoutdinov et al. (2010) use SAM as a large-domain high-resolution large-eddy simulator (LES), and are able to simulate tropical deep convection on a very fine resolution that is usually reserved for shallow boundary-layer simulations. The model simulates deep convective clouds for a full day at 100m horizontal resolution in a 200km horizontal domain. Their vertical profiles of updraft and downdraft velocities and mass fluxes match very well with those observed by LeMone and Zipser (1980).

One more important reason to use SAM as our model in this study is because this model is the CRM used in building the Super-Parameterization in the SP-CAM (Khairoutdinov and Randall, 2001; Khairoutdinov et al., 2005). We discuss the SP-CAM and its implementation in the previous chapter. It has been shown to do a better job at representing convectively-coupled global-scale waves, but the exact reasons for this are still hypothetical (eg. Thayer-Calder and Randall, 2009; Pritchard et al., 2011). Here, we hope to shed a little more light on these connections by investigating how convective downdrafts respond to large-scale forcing in SAM.

Simulations Used in This Study

This study uses two main simulations for the analysis of downdrafts. The first is a simple radiative-convective equilibrium run (hereafter referred to as the RADCONV simulation). This simulation is run over an ocean surface with a high temperature (303K) and an initial moist, tropical sounding. There is no large-scale forcing in this simulation, and no diurnal cycle (the sun is kept at zenith). Surface fluxes are computed locally in each grid-column. Our domain is 128km by 128km in the horizontal, with 1km horizontal resolution, and a 10 second time step. We use an increasing vertical grid with 64 levels between sea-level and about 28km in height (1010hPa to 5hPa). This results in approximately 100m vertical resolution in the boundary layer and increases above. This

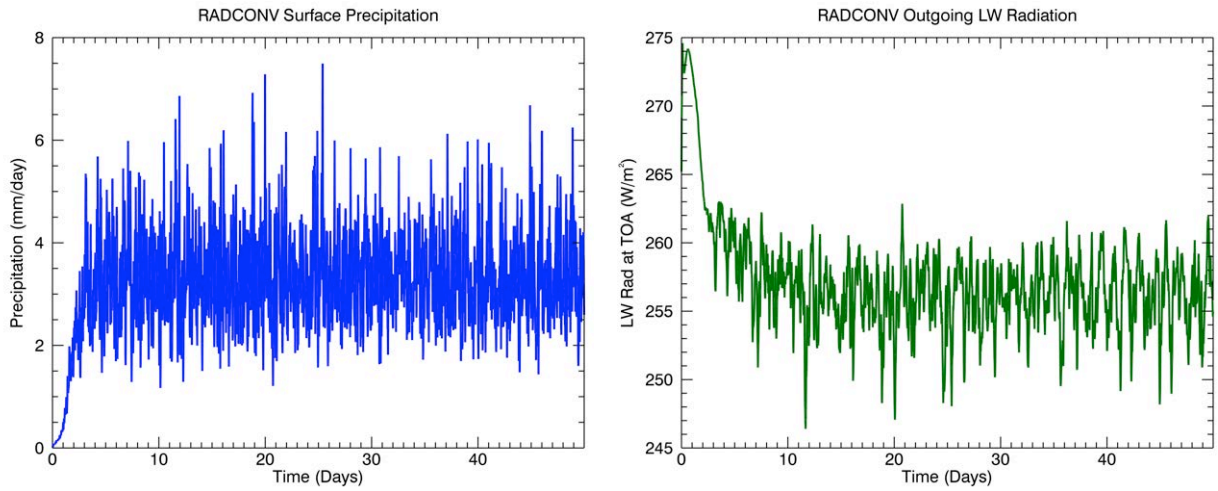

Figure 3.3. Surface precipitation (left) and outgoing longwave radiation (right) from the entire RADCONV simulation. The last 20 days are used in our analysis.

simulation uses the RRTM radiation scheme (Pincus et al., 2003) the Smagorinsky-type sub-grid scale turbulence parameterization, and single moment microphysics.

We run the simulation for 50 days, and use the last 20 days in our analysis. We have statistical output every half hour and three dimensional output every hour. The simulation oscillates about a steady mean, but relatively low, precipitation rate after about four days. The cloud field does not fully reach a steady state until after 10 days, however, as seen in the outgoing longwave radiation field in Figure 3.3 and in the precipitable water time series (not shown). Convection in this steady case is unorganized and appears all over the domain. Our cloud fraction is below 25% once the system reaches equilibrium, so our domain size seems reasonable for this study. It is relatively shallow and seems dependent mostly on warm rain processes.

The second main simulation we analyze in this study is a 21 day simulation forced with TOGA-COARE data (hereafter referred to as the TOGA simulation). This simulation is also run over an ocean surface, but with observed SSTs and large-scale temperature, moisture and momentum tendencies derived from the TOGA-COARE intensive observation period (at the end of December 1997 and beginning of January 1998). Surface fluxes are also computed individually in each grid-column, but then nudged back towards the observed values on the same nudging timescale

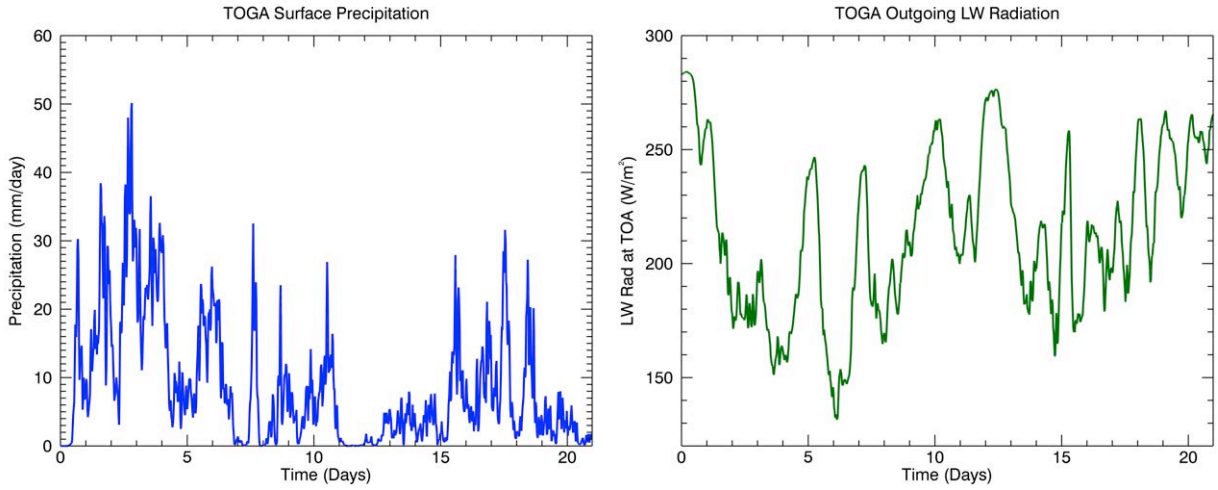

Figure 3.4. Surface precipitation (left) and outgoing longwave radiation (right) from the entire TOGA simulation.

as the moisture and momentum variables. Just as in the RADCONV run, our domain is 128km by 128km in the horizontal, with 1km horizontal resolution, and a 10 second time step. Again, we use an increasing vertical grid with 64 levels between sea-level and about 28km in height (1010hPa to 5hPa). The TOGA simulation also uses the RRTM radiation scheme, the Smagorinsky-type sub-grid scale turbulence parameterization, and single moment microphysics.

This simulation lasts 21 days and captures a wide variety of convective events. The simulation begins with the passage of an MJO event, and the first six days consist of extremely moist, very deep convection. A westerly wind-burst begins to build around day 7, and days 11 through 15 are heavily suppressed. The remainder of the simulation has low observational forcing values and is effectively simple diurnally-forced tropical convection. Our CRM does not have a coupled ocean surface, so convection will not be able to mix and cool the surface below. However, we do nudge towards observed SSTs from the TOGA period, and this allows us to emulate the surface temperature changes that actually occurred. The high amount of large-scale variability in this simulation allows us to analyze downdrafts in very moist and very dry environments, and in shallow and deep convection. We have three dimensional, surface, and column average data every half hour for this entire simulation, giving us ample opportunity to investigate these complex cloud processes.

Structure of This Study

Our goal in this work is to examine many of the assumptions and simplifications used in convective parameterizations when calculating the impact of downdrafts. Downdrafts are difficult to observe, so many parameterizations of downdrafts are built on assumptions and simple calculations that are rarely, if ever, examined in detail. In each of the chapters in this thesis, we present one or more assumptions present in at least one prominent convective parameterization. We will discuss the parameterizations that use the assumption, and then examine its validity in our CRM data. The assumptions are grouped into chapters covering general aspects of convection and downdrafts, and occur as follows: Chapter 4 covers the mass budgets and updraft/downdraft mass transfer, Chapter 5 examines boundary layer variability and surface fluxes in relation to downdrafts, Chapter 6 discusses the sensitivity of downdrafts to environmental relative humidity, Chapter 7 explores the impact of vertical wind shear on downdrafts, Chapter 8 considers the boundary layer quasi-equilibrium hypothesis, Chapter 9 examines some Lagrangian parcel data, and Chapter 10 gives a summary and direction for future work.

Chapter 4: Downdraft Mass Budgets

Assumption: Downdrafts move less mass than the dry, subsiding environment, and are secondary in importance for the mass budget of cumulus convection.

There are several examples of cumulous parameterizations where the designers have assumed that much less mass is moved downward through clouds than in the dry, subsiding environment outside of the clouds (Arakawa and Schubert, 1974; Moorthi and Suarez, 1992; Pan and Randall, 1998; Park and Bretherton, 2009). If this were the case, then very little would change in the boundary layer due to the passage of convection. Simple personal experience can refute this assumption, as anybody who has experienced the passage of a convective event has experienced the gustiness and cooling associated with downdrafts. In this chapter, we simply examine the mass budgets of downdrafts, updrafts and the subsiding environment in two different simulations with the SAM cloud resolving model. In our model, is it true that most mass is lifted inside of clouds and then slowly subsides in the dry regions between them? Or do downdrafts move a significant amount of mass downward as well, and how does it compare in magnitude to the dry environment?

We analyze each three dimensional snap-shot of the model state, and categorize each gridcell as belonging to either an updraft, a downdraft, or the surrounding environment. Our criteria for updrafts is a vertical velocity greater than 1 m/s, continuous for two levels and containing at least 1.0e-5 g/kg of non-precipitating condensate (in a cloud). The criteria for downdrafts is similar, except the vertical velocity must be less than -1 m/s, continuous for two levels and contain some precipitating or non-precipitating condensate. Everything else (including gridcells with condensate and a vertical velocity between -1 and 1 m/s) is considered part of the surrounding environment. In the RADCONV simulation, our convection is light and dissipates quickly. The cloud fraction at each level is less than 25%, and the fraction of environmentally classified but cloudy gridcells is very small compared to the cloudless cells. Because we limit our gridcells to those that contain condensate, we filter out much of the gravity wave activity in the surrounding dry environment.

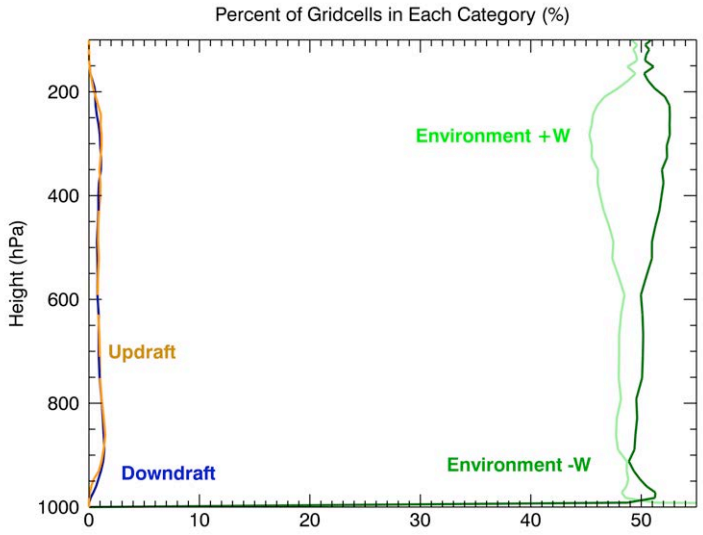

Figure 4.1. Percent of gridcells categorized as updrafts, downdrafts or the environment in one 3D snapshot from RADCONV.

However, large-scale gravity waves, such as those that top a convective cloud and have condensed water, might be counted (though, it is unlikely those waves have large magnitude vertical velocities on our scale).

We begin with the simple radiative-convective equilibrium case, referred to as RADCONV. The model configuration and a general overview of this case are given in Chapter 3. Figure 4.1 shows how many gridcells are part of each category as a function of height for one three dimensional snapshot of RADCONV. In general, updrafts and downdrafts make up less than 3% of the overall number of gridcells in each snapshot. The largest numbers of updraft and downdraft cells occur in the lower troposphere, between 950 and 800hPa. However, there are cells categorized as updrafts and downdrafts through most of the free troposphere, extending from just above the surface at 995hPa and reaching to 150hPa. While this is only a single snapshot, during the last 10 days of RADCONV used in our analysis, these percentages (and convection in general) do not change very much.

Figure 4.1 also shows the percentage of gridcells categorized as the environment is much larger than those considered updrafts and downdrafts. In this figure, any environmental cell with a vertical velocity greater than zero is plotted in the light green line, and any cell with a vertical velocity less than zero is plotted as a dark green line. The number of slightly upward moving gridcells and slightly downward moving cells is close at all levels, with more downward moving cells by only a few hundred. This contradicts the general view of the cloudless environment as stable and largely

subsiding. Rather, it suggests the view of a turbulent mass of air, filled with small waves and eddies, that has the net effect of slowly moving mass downward.

We can calculate a simple vertical mass flux by multiplying the vertical velocity in each gridcell by the density of air in the cell and the horizontal area through which the mass moves. Our mass flux for each type of draft is

$$M = \overline{\rho w_v A_H} \qquad (1)$$

where M is the mass flux, ϱ is the layer density, w_v is the gridcell vertical velocity, A_H is the horizontal area of the gridcell, and the bar indicates an average over the entire domain. Figure 4.2 shows the average vertical mass flux by each category averaged over the last 10 days of RADCONV as a function of height. In this case, downdrafts move more mass downward than the environment through almost all of the height of the column. Only a few levels near the upper reaches of convection see larger mass flux by the environment than convective downdrafts. Updrafts and downdrafts also display two distinct peaks in mass flux, one around 850hPa and another in the upper levels near 300hPa. These are likely related to the two major types of convection occurring during this snapshot: shallow convection that occurs just above the boundary layer and deeper convection (though not as deep as seen in the TOGA simulation).

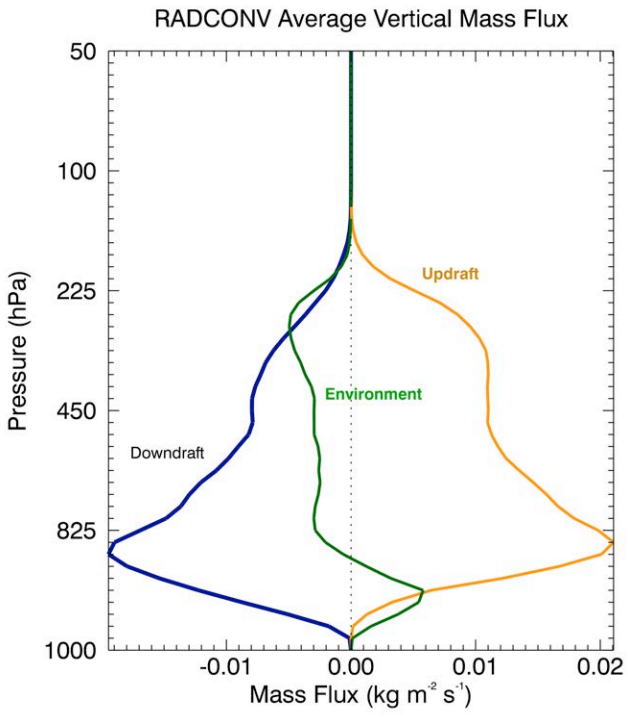

Figure 4.2. Vertical mass fluxes by updrafts, downdrafts and the environment from the last 10 days of RADCONV.

We look at the average vertical mass flux for different levels of the atmosphere

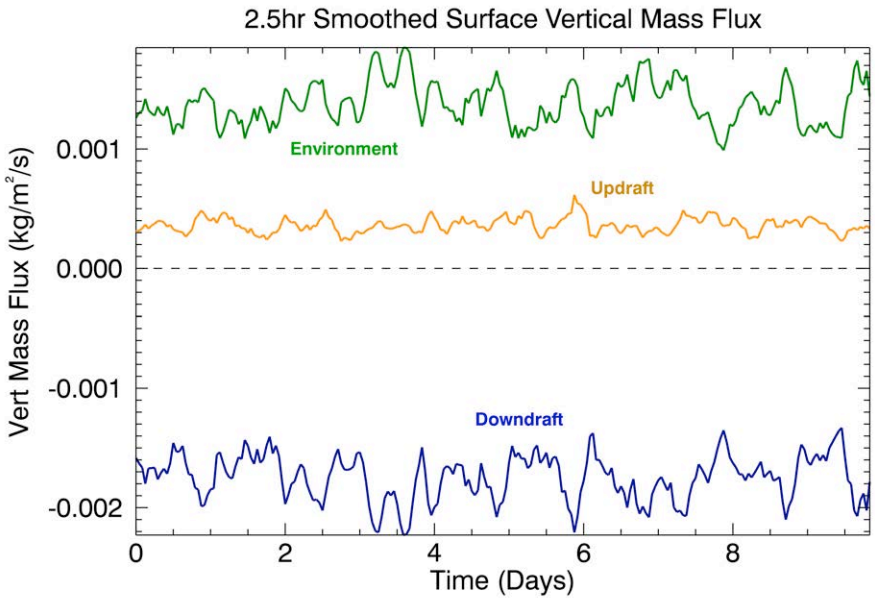

Figure 4.3. Vertical mass fluxed by updrafts, downdrafts and the environment over the last 10 days of RADCONV, averaged across the lowest 50hPa.

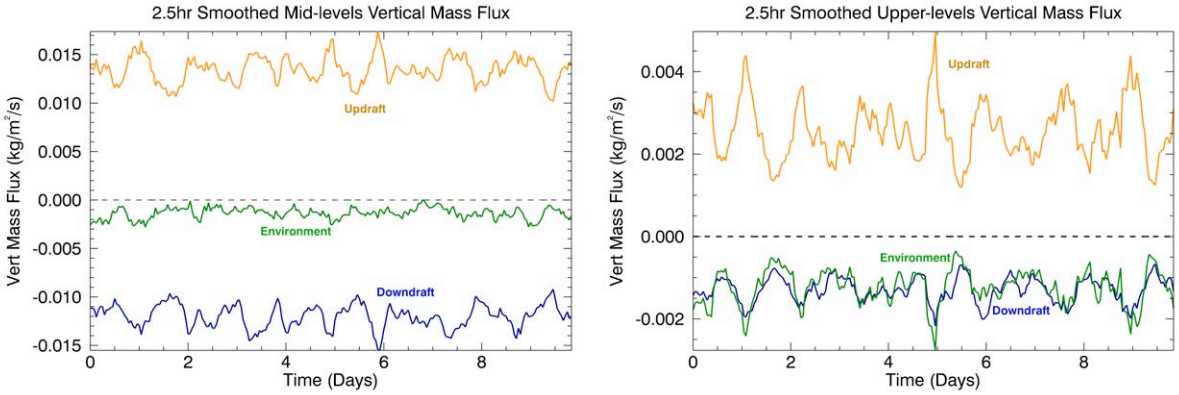

Figure 4.4. Vertical mass fluxed by updrafts, downdrafts and the environment over the last 10 days of RADCONV, averaged between 950 and 350hPa (left) and and 350-50hPa (right).

during the last 10 days of RADCONV in Figures 4.3 and 4.4. Figure 4.3 is the vertical mass flux averaged over the lowest 50hPa, and shows how mass moves vertically near the surface. Counter-intuitively, gridcells categorized as the environment have a net lift in the lowest levels. This is probably caused by two issues. The first is that updrafts are required to have some cloud condensate, so upward-moving air below cloud base will be categorized as "environmental" in this framework. Secondly, downdrafts are injecting cool air into the lowest levels, which pushes the rest of the

atmosphere just a little bit higher. A generally positive environmental mass flux and larger negative flux by downdrafts occurs throughout the lowest layers of RADCONV (Figure 4.3).

Figure 4.4 shows the average vertical mass flux through the middle of the troposphere, and updrafts and downdrafts clearly dominate this region during RADCONV. The environment has a small, net downward movement of air, but is much less than downdrafts. In the upper part of the atmosphere, the amount of downward mass flux by downdrafts and the environment is more comparable. However, the average amount of mass moved vertically reduces substantially in this region of the atmosphere (see change in y-axis scale between left and right panels of Figure 4.4), as convection in this simulation tops out around 200hPa. The upper levels are likely dominated by overshooting cloud tops and air detrained from anvils at the tropopause.

The vertical profile of vertical mass flux by updrafts, downdrafts and the environment is slightly different for the TOGA run compared to the RADCONV run. This simulation includes large-scale forcing that describes moisture and temperature convergence as well as large-scale wind profiles, so the variability of convective events is much higher (see Chapter 3 for a description and overview). When all of these different periods of convective activity (deep convection, suppressed shallow convection, and simple diurnally forced convection) are averaged together over time, we get the vertical profile of mass flux shown in Figure 4.5. In this run,

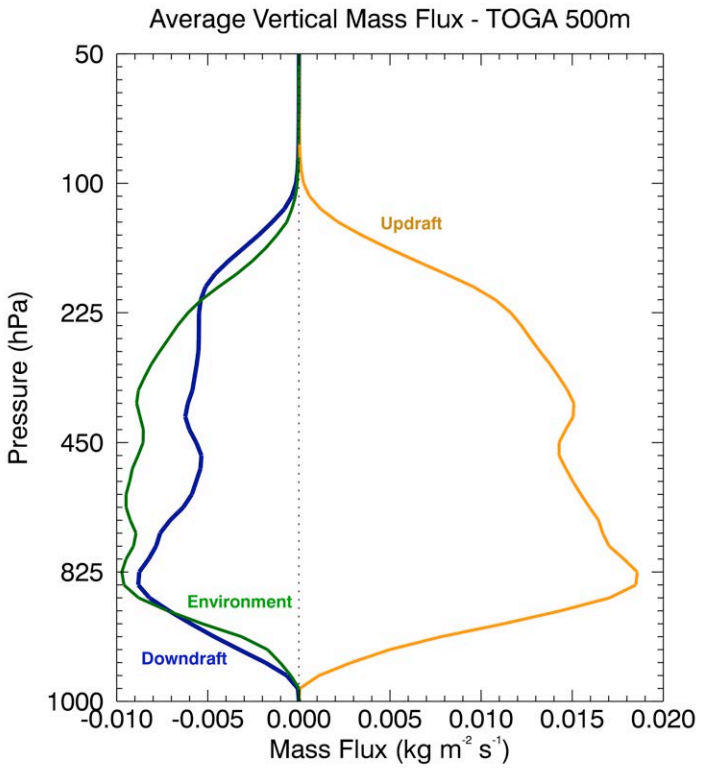

Figure 4.5. Vertical mass fluxed by updrafts, downdrafts and the environment averaged over the entire 21 day period of TOGA.

downdrafts and the environment have similar magnitudes and both are required to balance the updraft mass flux through most of the column. In the lowest levels, downdrafts dominate. Through the mid-levels of the troposphere, however, the environment moves slightly more mass.

Also, this profile has a tri-modal structure (rather than the bimodal shape seen in RADCONV), which is most obvious in the downdrafts and environmental mass fluxes. Peaks in downdraft mass flux occur around 850 hPa, around the freezing level at 600hPa, and near the top of the convective troposphere at about 150hPa. This structure could be due to propagating tropical waves, with convection at low levels building to mid-level cumulus congestus (Johnson et al., 1999), and finally into deep cumulonimbus clouds (described in Kiladis et al., 2009). The tropical wave passage of an MJO event in the first third of the simulation may be the feature that dominates this structure and produces this tri-modal vertical mass flux distribution.

The average mass flux in the surface layers of TOGA is more complex than the RADCONV case, but similarities abound (Figure 4.6). In this case, downdrafts and the environment move a similar amount of mass, with downdrafts dominating some events and the environment dominating in others. Similar to the RADCONV case, there are times when the average environmental mass flux near the surface is upwards, especially in periods of lighter or newly formed convection. The variability in convective events produces variability in the ratio of updraft to downdraft mass flux. This relationship is discussed in more detail in Chapter 5. The mid-level and upper-level averages shown in Figure 4.7 reinforce the relationships seen in the profile figure (Figure 4.5). In both cases, downdrafts and the environment move a nearly equal amount of mass, and both are needed to balance the updraft mass flux. As we saw in RADCONV, the magnitude of the upper level mass fluxes (right panel of Figure 4.7) are much smaller than the mid-levels, as these layers are less convectively active than ones below.

Based on the results shown here, we conclude that downdraft mass flux is not secondary to environmental mass flux in the amount of mass carried through the column. In our model,

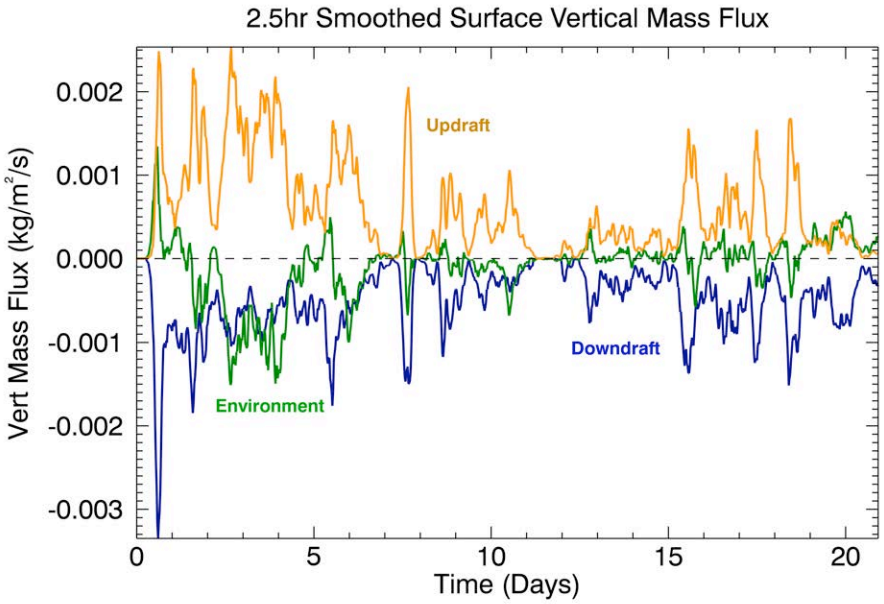

Figure 4.6. Vertical mass fluxed by updrafts, downdrafts and the environment over the last during the 21 days of TOGA, averaged over the lowest 50hPa.

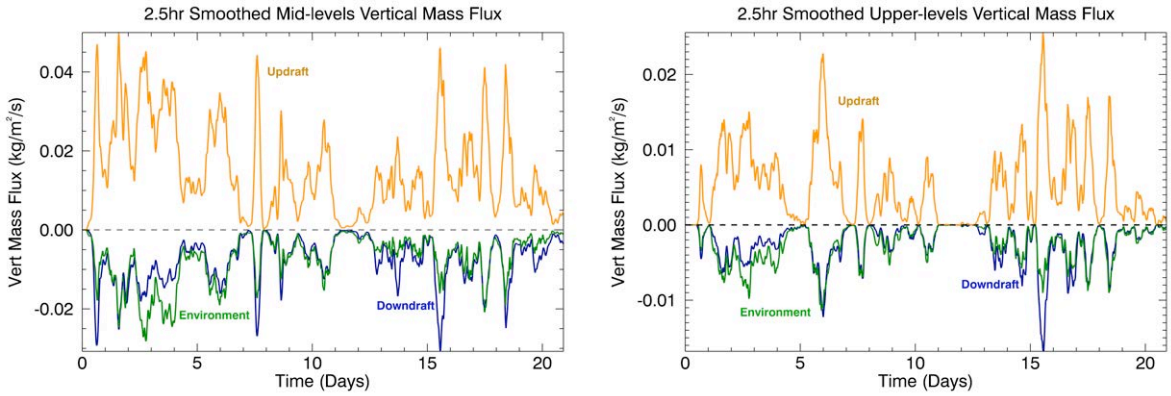

Figure 4.7. Vertical mass fluxed by updrafts, downdrafts and the environment during the 21 days of TOGA, averaged between 950 and 350hPa (left) and and 350-50hPa (right).

downdraft mass flux is nearly the same magnitude or greater than the mass flux by slow downward movement outside of the clouds, and quite significant in the sub-cloud layer.

Assumption: Downdrafts entrain only environmental air and do not interact with updrafts.

Another common assumption in convective parameterizations that do include downdrafts is that up- and downdrafts do not interact (Tiedke, 1989; Emanuel, 1991; Sud and Walker, 1993; Cheng and Arakawa, 1997). These downdrafts entrain only environmental air as they move downward, and

then detrain below cloud base. Figure 4.8 shows a three dimensional rendering of gridcells inside of a cloud with positive vertical velocities (left) and negative vertical velocities (right) for one small cloud during RADCONV. This shows a complex turbulent structure, with updrafts filling the center of the cloud and downdrafts cascading down the periphery, flowing between billowing turbulent eddies towards the surface. It seems unlikely that complex and turbulent cloud structures such as updrafts and downdrafts rarely exchange mass, especially as they share cloud-space and precipitation.

To address this assumption, we can return to our categorization of updraft and downdraft gridcells, and find where each type borders another type exactly horizontally along a shared cell wall (corners are not considered). Are updrafts and downdrafts only bordered by environmental gridcells? Or do they share cell walls, and is there any significant mass fluxes across those walls?

Figure 4.9 shows the fraction of updraft gridcells that border downdraft gridcells averaged over the last 10 days of RADCONV. This fraction is greater than 0.4, and well over 0.5 for updrafts, so about 50% of updrafts do border downdrafts in the mid-troposphere. Between 40 and 50% of downdrafts gridcells share a border with an updraft cell between 900hPa and 600hPa. This number decreases above and below this region. The maximum occurs where a maximum number of gridcells meet the updraft/downdraft criteria, and the cloud width often narrows (either in a warm tower of cloud or at the top of a boundary-layer cumulus), forcing more interaction between the types. There is a good bit of variability about this mean, even in the RADCONV run, and almost the entire profile differences between

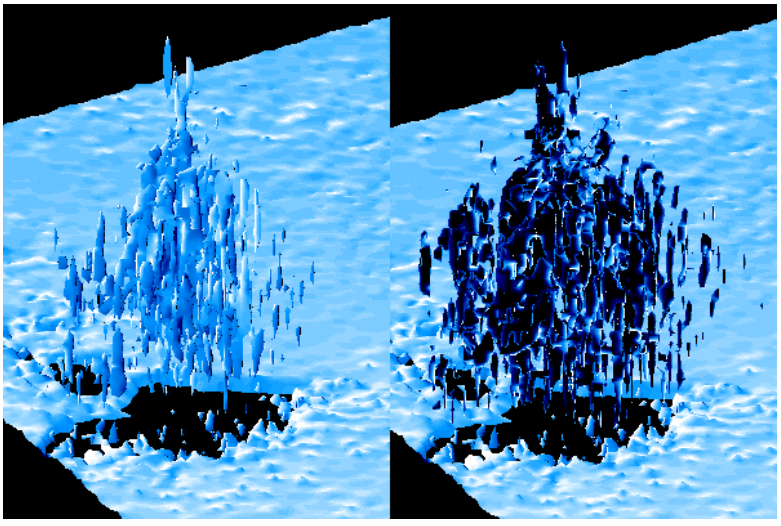

Figure 4.8. A 3D rendering of positive vertical velocities inside of a cloud (left) and negative vertical velocities in the same cloud (right) in a small cloud during RadConv.

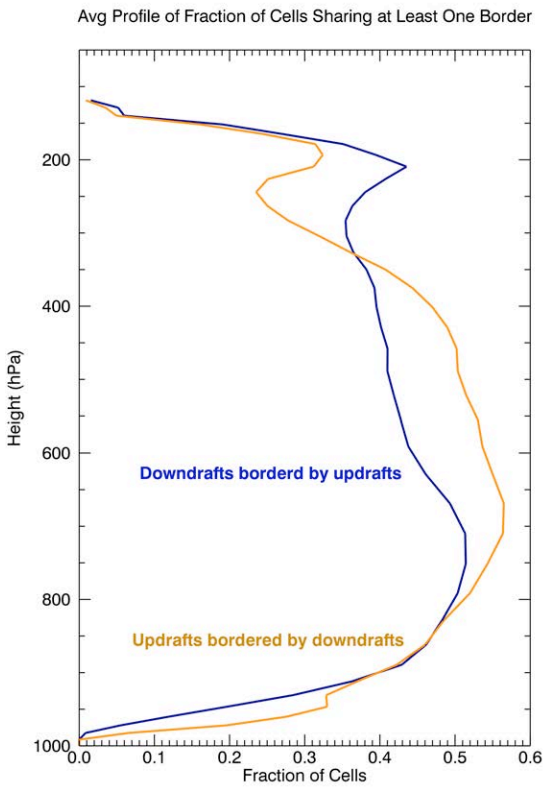

Figure 4.9. The fraction of gridcells categorized as updrafts that share a cell wall with a gridcell categorized as a downdraft, averaged over the last 10 days of RadConv.

border downdrafts, this means that 50% do not, and that the assumption of entraining environmental air may not be completely outrageous. However, if updrafts are entraining even a small fraction of their air from downdrafts, this will decrease their buoyancy, and have significant impacts on the height and structure of convection (see entrainment discussion in Chikira and Sugiyama, 2010). Similarly, a downdraft that entrains air from an updrafts bordering downdrafts, or downdrafts bordering updrafts, is not statistically significant. There are two layers near the surface (960 and 946hPa) where the larger fraction of updrafts bordering downdrafts is outside of two standard deviations, and is due to the fact that there are far more downdraft gridcells in these layers than there are updraft cells.

It is worth noting that if 50% of updrafts

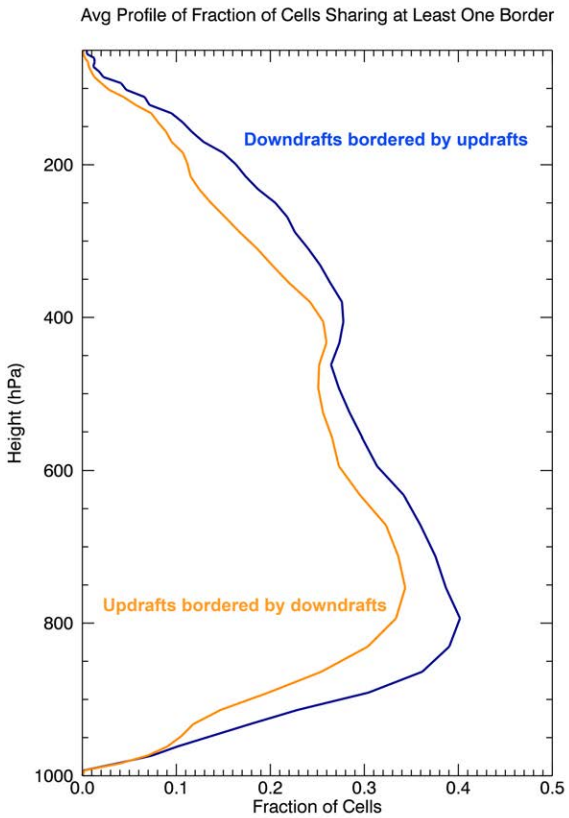

Figure 4.10. The fraction of gridcells categorized as updrafts that share a cell wall with a gridcell categorized as a downdraft, averaged over all 21 days of TOGA.

updraft rather than the environment will have a *higher* buoyancy than one assumed to be entraining only dry environmental air. This will affect the thermodynamic drivers of downdraft vertical momentum. As discussed in the first chapter, observed tropical updrafts seem to have a lower buoyancy than we expect, and observed downdrafts have a higher buoyancy.

We performed the same analysis of shared updraft and downdraft borders for the TOGA run, averaged the results over the entire 21 days, and the final profiles are shown in Figure 4.10. In this case, the average fractions of updrafts and downdrafts that border each other are smaller, but this is likely the result of averaging in days with "zero" fractions (where there is no convection and no updrafts or downdrafts) with days of deep convection. This higher variability results in a lower fraction. Despite this, updrafts and downdrafts share borders about 30% of the time through the column, and 40% of downdrafts border an updraft at the peak of the distribution near 800hPa.

To get a feel for the actual ranges of up- and downdrafts that border each other during the TOGA simulation, a time-height plot is more useful. These are shown in Figure 4.11. Because this simulation encompasses such a large variability in precipitation amount and mean profiles, there is a wide variety of bordering profiles as well. In general, we see that fractionally more downdrafts share borders with updrafts than vice versa. And we see a strong peak in the fraction bordering at around 800hPa for both

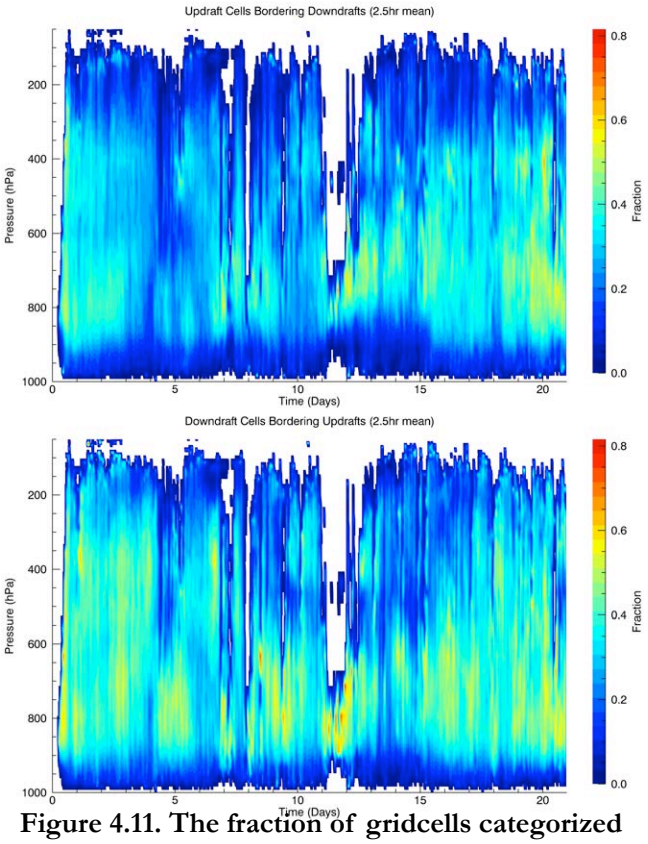

Figure 4.11. The fraction of gridcells categorized as updrafts that share a cell wall with a gridcell categorized as a downdraft (above, and vice versa below), in a profile-time contour for the TOGA simulation.

profiles. For the strongly suppressed days 11 and 12, nearly 80% of downdrafts border updrafts at the top of the clouds. During the heavily raining period of the first 8 days, the fraction of updrafts sharing a border with a downdraft is much lower throughout the profile than seen at other times, and is much lower than the fraction of downdrafts that share a border with an updraft. During the diurnally forced period of the last 5 days of the run, we see a profile very similar to the average from RADCONV.

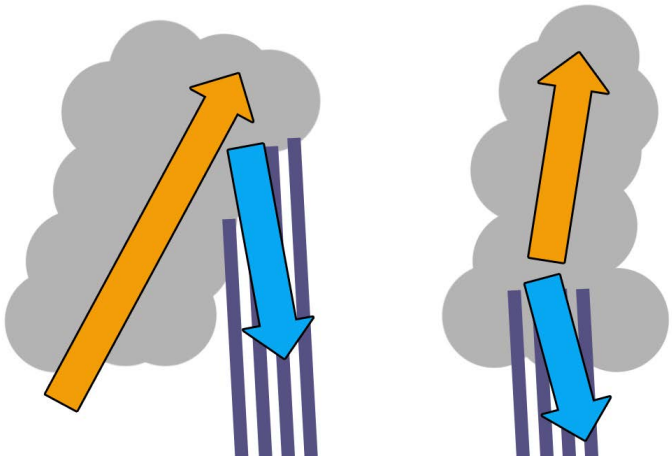

Figure 4.12. Possible updraft and downdraft geometries. Updrafts can loose mass into downdrafts as they shed precipitation (Left), or they could form above downdrafts and not interact with them at all (Right).

When we talk about three-dimensional model data such as these, we have the opportunity to study the geometry of updrafts and downdrafts within a cloud. These interactions impact the heat and moisture content of up- and downdrafts inside the cloud, and should be considered in detail. Parameterization developers are forced to consider difficult questions about how updrafts and downdrafts share mass. Figure 4.12 shows two possible, and very different, cloud updraft and downdraft geometries. On the left, rising updraft air condenses water and lifts it until the condensate is too heavy to be supported by the temperature perturbation. Updraft air then moves into a downdraft shaft. This allows for downdrafts to gain mass from both the cloudy updraft and the surrounding environment (depending on how much tilt and mixing is allowed to occur). This downdraft will be less negatively buoyant than the one on the right. In the righthand figure, updrafts form above downdrafts. These updrafts entrain from the environment and downdrafts form below. These downdrafts will be strongly negatively buoyant as they entrain only from the environment. We

will look more closely at the thermodynamic properties of up- and downdrafts and their geometry within clouds in Chapter 6. For now, we focus on the issue of simple mass flux across these shared borders, and whether or not updrafts and downdrafts exchange mass.

We calculate a horizontal mass divergence for each gridcell, and for those categorized as updrafts or downdrafts, we sum all of the mass diverging (a positive flux out of the gridcell) across a shared border and plot the result in Figure 4.13. This is a total divergence of mass flux rather than a domain average, as given by the equation

$$M = \rho(u_{out} - u_{in})A_V \qquad (2)$$

where M is the total mass flux divergence, ϱ is the layer mean density, A_V is the area of the shared gridcell wall, and u_{out} and u_{in} are horizontal winds (in both the U and V directions). So a positive M

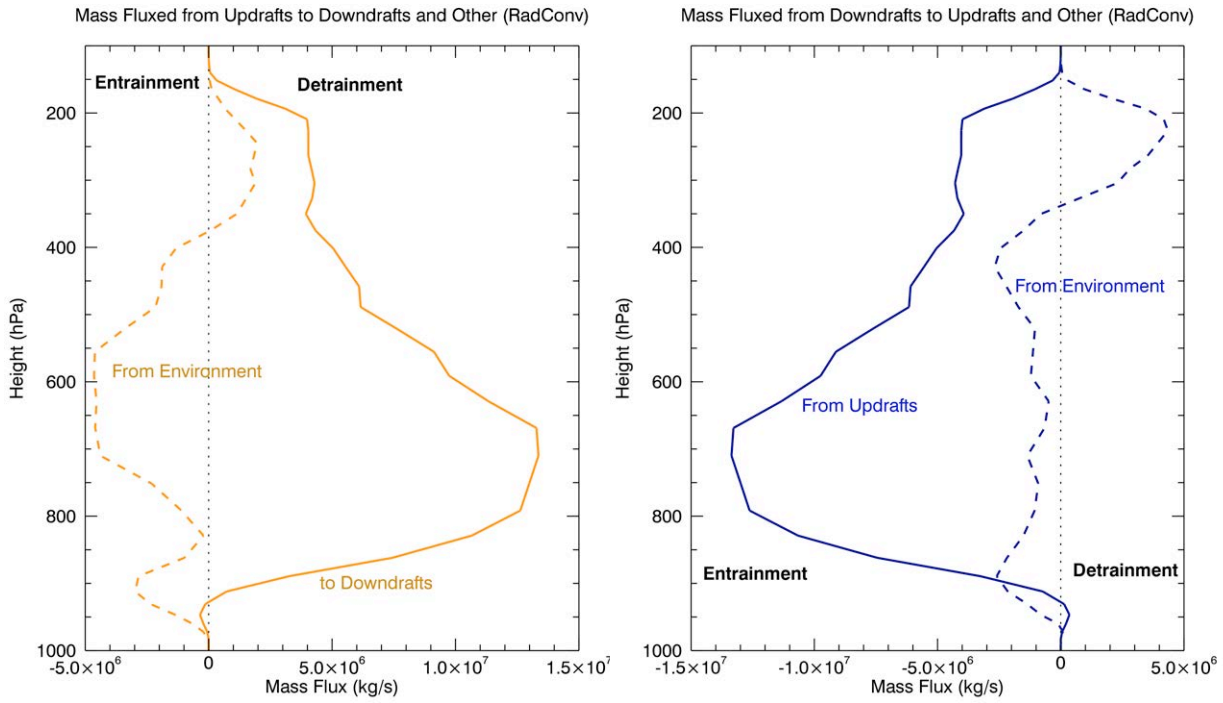

Figure 4.13. Profiles of the total mass fluxed across shared borders between updrafts and downdrafts (solid line) and other borders (dotted line) averaged over the last 10 days of RadConv. Mass fluxed from or to updrafts in orange (left) and from or to downdrafts in blue (right). For this calculation, *a positive mass flux is leaving the up- or downdraft and a negative one is entering the draft.*

is air leaving the cell and a negative is entering it. We plot these results for updrafts in orange lines and downdrafts in blue. Each plot shows horizontal mass flux from or to a different cell type. So, the orange plots show mass flux starting in an updraft and moving elsewhere (positive flux) or starting elsewhere and ending in an updraft (negative flux). And the blue plots show mass flux starting in a downdraft and moving elsewhere (positive flux) or starting elsewhere and ending in a downdraft (negative flux). When we look at the 10-day average of RADCONV, we see a significant amount of mass flux from updraft gridcells into downdraft gridcells. This mass flux has a maximum between 800hPa and 650hPa, in the same layers with the maximum percentage of shared borders occur for updrafts (see Figure 4.9). The profile of air moved from updrafts to downdrafts in the left panel is the same, but opposite signed, as the right panel where we consider air moving into downdrafts from updrafts. This means that mass is conserved across these borders.

The movement of mass across other borders (generally into the environment) is different for updrafts and downdrafts in RADCONV. Updrafts tend to have a net flux of air from the environment into the gridcell. Through most of the column, updrafts are entraining from the environment, and near the top of the column, they diverge or detrain to the environment. Downdrafts also entrain air from the environment through most of the column, and detrain air in the upper layers. This is a bit upside-down from what we might expect, but is likely an artifact of our categorization methodology. The detrainment at upper levels could be from negative buoyancy gridcells associated with the evaporation of precipitation and condensate in anvil clouds. It could also be related to overshooting tops, where updraft air rises, sinks quickly and then detrains. The lack of an expected detrainment near the surface is probably due to fewer gridcells categorized as downdrafts in the lowest levels. In these regions, the vertical velocities decrease as the convective air mixes in the turbulent boundary layer, and even though a gridcell may be the continuation of a downdraft as it slows and spreads out in the boundary layer, if its vertical velocity is not less than -1 m/s or it is not vertically continuous across two layers, we do not count it in this mass budget.

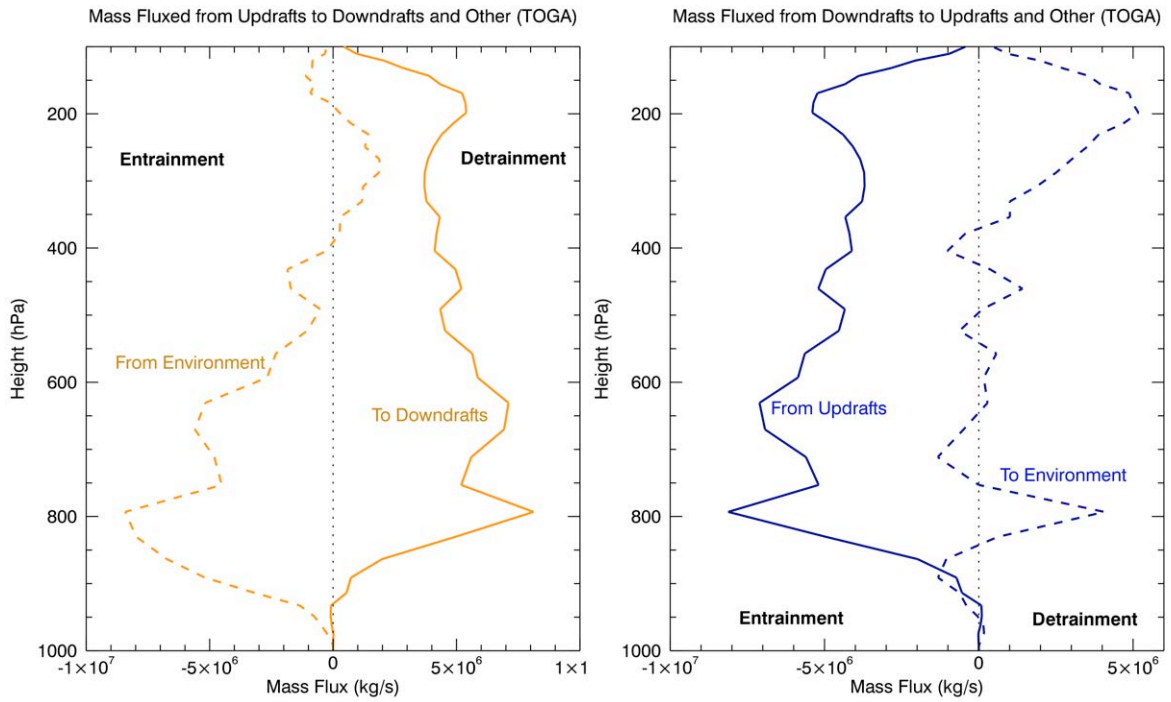

Figure 4.14. Profiles of the total mass fluxed across shared borders between updrafts and downdrafts (solid line) and other borders (dotted line) averaged from one 3D snapshot every two hours during the 21 days of TOGA. Mass fluxed from or to updrafts in orange (left) and from or to downdrafts in blue (right). For this calculation, a positive mass flux is leaving the up- or downdraft and a negative one is entering the draft.

The important characteristics of Figure 4.13 are that the majority of net horizontal mass flow is from updrafts into downdrafts. Updrafts and downdrafts both entrain some environmental air, though more environmental air flows into updrafts than downdrafts. We present a very similar plot from the TOGA simulation in Figure 4.14, but this is the average is from the entire 21 days of simulation, across many different convective events. Even in this case, we see a general net mass flux from updrafts to downdrafts throughout the entire column. We also see more air entrained from the environment into updrafts than into downdrafts in the net. And we see that gridcells categorized as both updrafts and downdrafts are part of the detrainment of cloud and precipitation at upper levels.

Because the TOGA simulation encompasses so much variability in convective events, an average over all 21 days is not very meaningful. We can break apart the 3D data from the simulation into different categories of convection to find a better understanding of how different magnitudes of updrafts and downdrafts interact. In this case, we will use precipitation as a proxy for convective

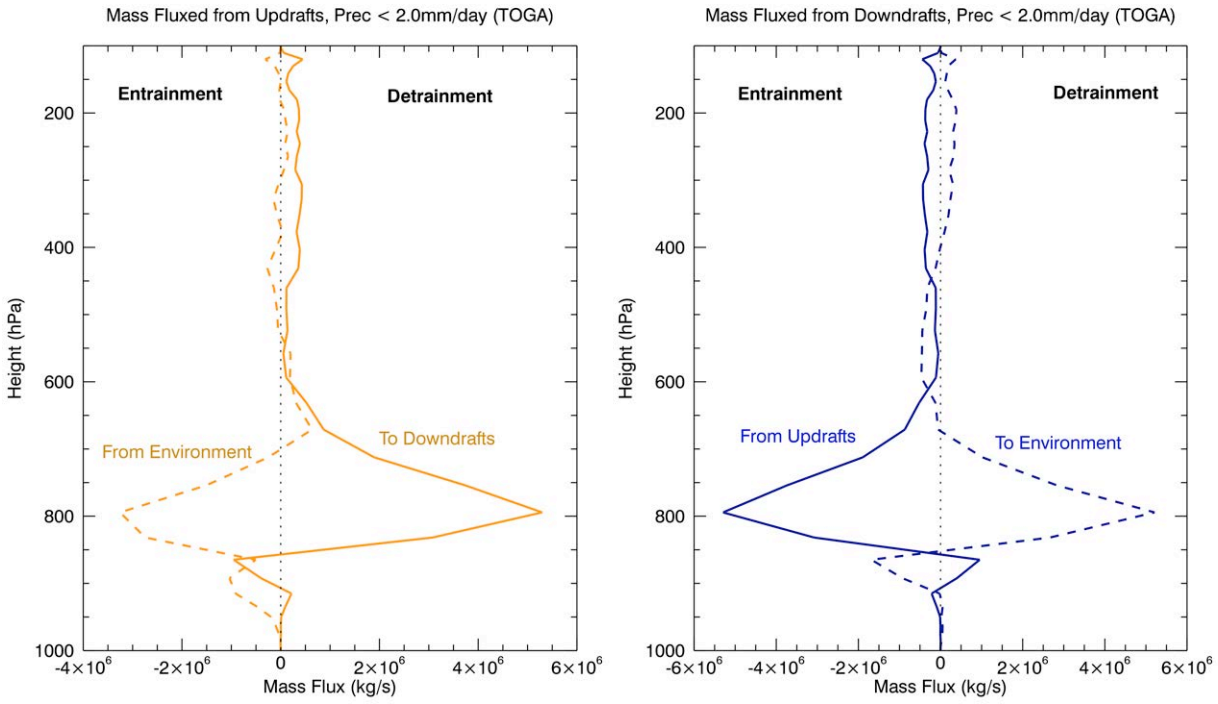

Figure 4.15. Profiles of the total mass fluxed across shared borders between updrafts and downdrafts (solid line) and other borders (dotted line) averaged from 3D snapshots where the average surface precipitation is less than 2 mm/day. Updrafts in orange (left) and downdrafts in blue (right). A positive mass flux is leaving the up- or downdraft and a negative one is entering the draft.

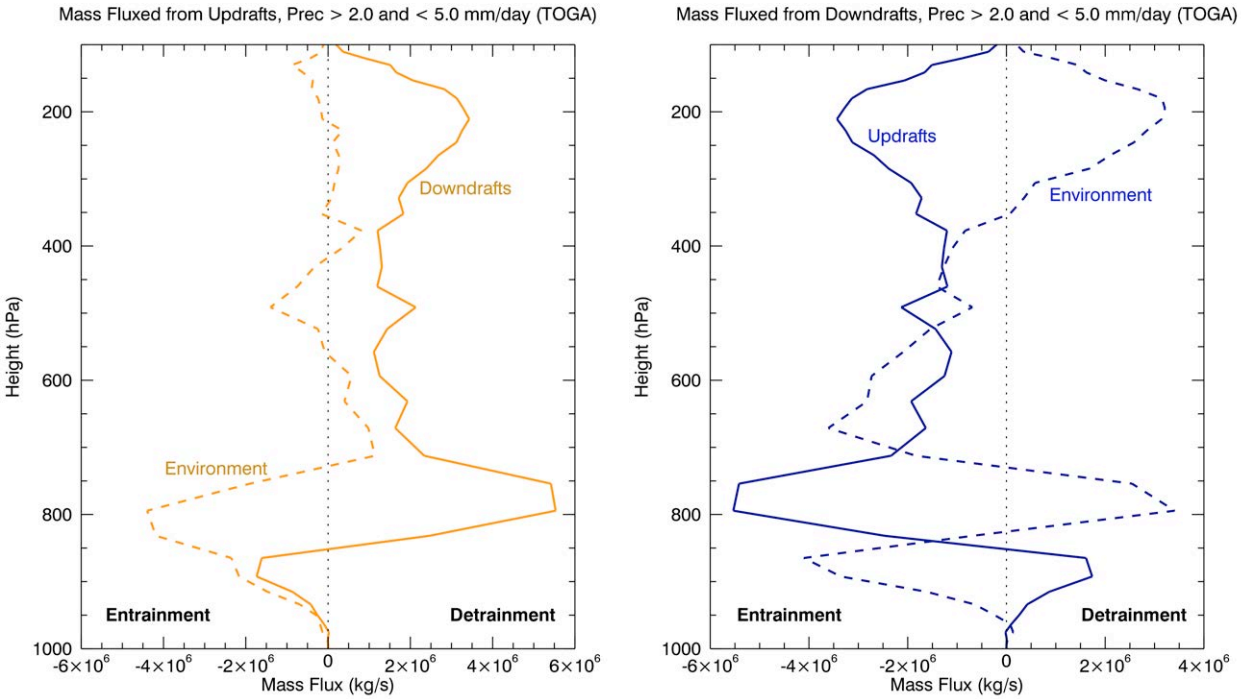

Figure 4.16. As in Figure 5.14, but averaged from 3D snapshots where the average surface precipitation is between 2 and 5 mm/day.

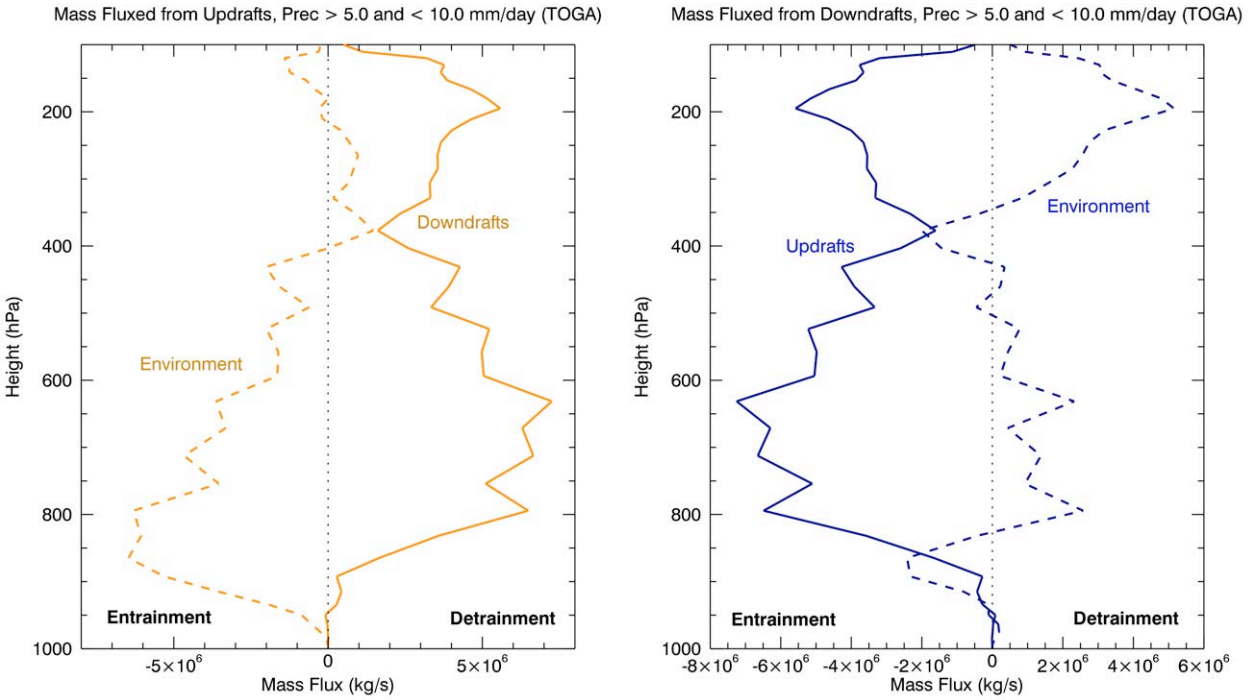

Figure 4.17. As in Figure 5.14, but averaged from 3D snapshots where the average surface precipitation is between 5 and 10 mm/day.

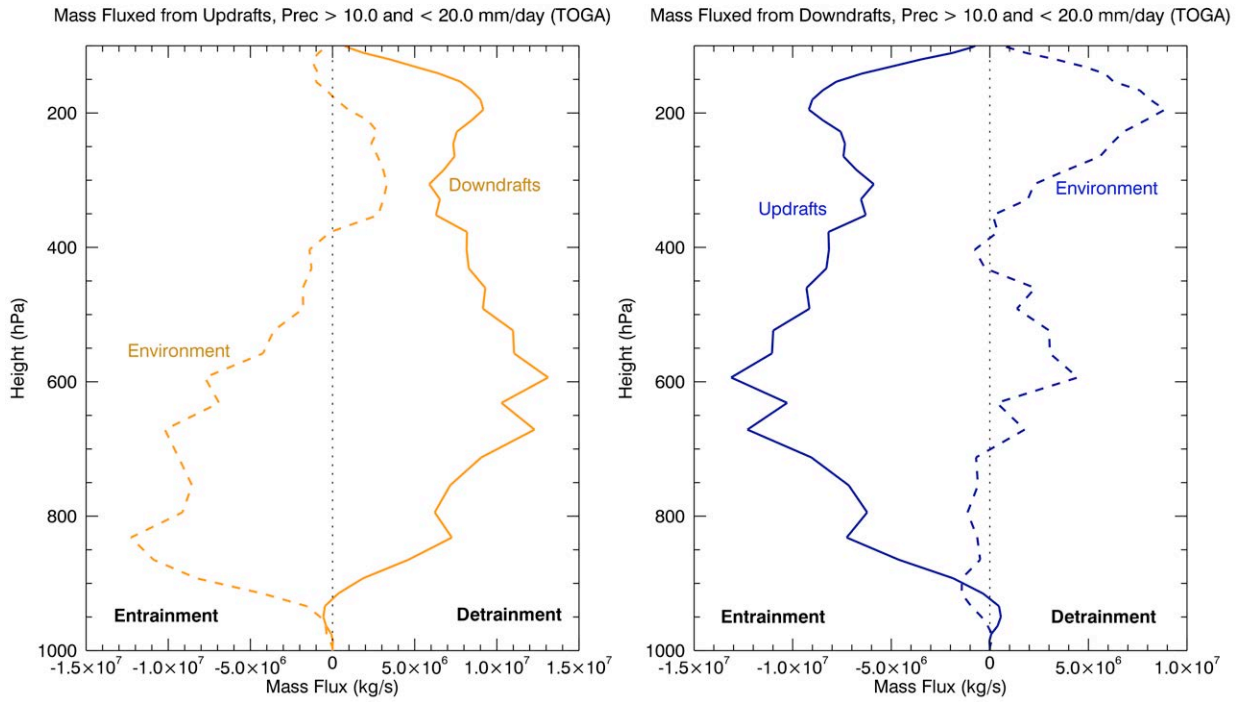

Figure 4.18. As in Figure 5.14, but averaged from 3D snapshots where the average surface precipitation is between 10 and 20 mm/day.

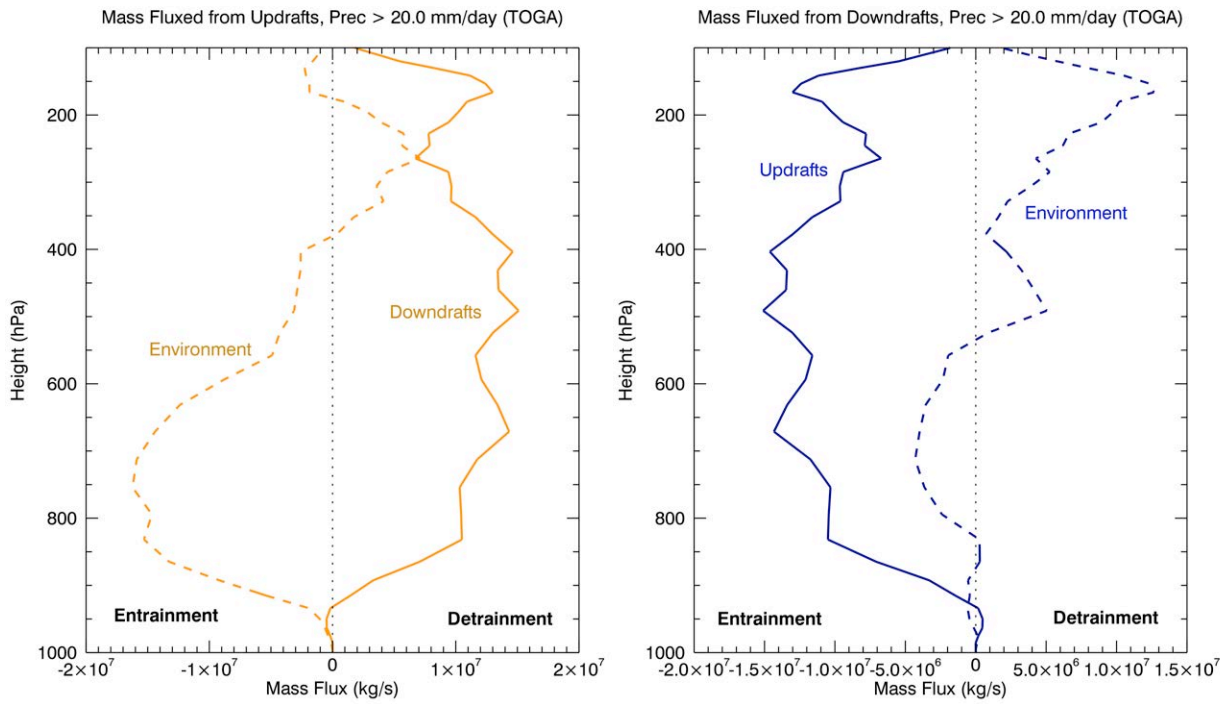

Figure 4.19. As in Figure 5.14, but averaged from 3D snapshots where the average surface precipitation is above 20 mm/day.

strength. Based on the mean precipitation at the surface, we bin the 3D data and produce composite profiles of horizontal mass exchange for different magnitudes of convective activity. These profiles are shown in Figures 4.15 through 4.19.

There are plenty of interesting features in these figures, but the most important structures are persistent in all categories. In all precipitation regimes, there is a horizontal flux of mass from updrafts to downdrafts through most of the column. In the lowest precipitation cases, there is a relatively large amount of mass flux from downdrafts to updrafts below 850hPa. This feature is strongest in the 2-5 mm/day regime, but shows up slightly in others (Figures 4.18 and 4.19), though much closer to the surface and small compared to the horizontal fluxes at mid-levels. It is possible that this opposite direction of mass flux is related to the formation of updrafts on the edges of cold pools and air lifted by downdrafts in the boundary layer. This could also simply be the signature of scattered shallow convection.

For all cases above 2 mm/day, downdrafts consistently lose mass to the environment between about 350hPa and 100hPa. Updrafts, however, do not show a large detrainment to the environment in the upper levels until the precipitation becomes larger. This suggests that in the 2-10 mm/day mid-magnitude precipitation regimes, there are deep clouds where the updrafts run to high levels, and the air rapidly becomes less buoyant (over-shooting tops), and sinks quickly before leaving the cloud from the downdraft-type sinking air.

Finally, the changes in the profiles of entrained environmental air for both updrafts and downdrafts are very interesting. Updrafts generally entrain environmental air beginning at about 850hPa. This layer of environmental air flux into the updraft gridcell is shallow for lightly precipitating regimes, and then deepens and increases in magnitude as precipitation increases. Downdrafts, on the other hand, have a wildly varying interaction with the environment. With low precipitation (less than 2 mm/day, or Figure 15), there is a slight amount of environmental air flux into downdraft gridcells in the mid-levels (700 to 400hPa). This convergence of environmental air becomes quite large in the next figure (Figure 4.16), but disappears almost entirely for heavier rain rates (Figure 4.17). In fact, when precipitation is between 10 and 20 mm/day, there is a slight divergence to the environment between 700 and 400hPa, and the converging region moves downward, to between 950 and 700hPa. In the highest precipitation regimes (greater than 20 mm/day, or Figure 4.19), there is a clear convergence of environmental air into downdraft gridcells, and it extends through a large part of the column, but has a maximum between 850 and 550hPa. We are not clear on why this happens, but the most basic take-away from these plots is that updrafts seem to have much more continuous intake of air from the environment than downdrafts do, so convection may be more sensitive to environmental properties via updraft entrainment than through downdrafts. We explore this idea further in Chapter 6, when we take a close look at the sensitivity of downdraft cooling to environmental relative humidity, and in Chapter 7 where we consider the effects of shear on downdrafts and cloud geometry.

Returning to the basic assumptions being addressed in this section, our results indicate that there is a significant amount of updraft to downdraft interaction and mass flux. In general, updrafts entrain air from the environment and detrain it into downdrafts. This is not altogether different from the assumptions made by some convective parameterization as far as updrafts go, but it is significantly different for downdrafts. Downdrafts gain more mass from updraft air than environmental air in the net in all cases, and so their negative buoyancy could be due less to the evaporation of precipitation, and more to the loading of condensate into air that is just slightly cooler than the surrounding updrafts.

Recommendation: A more complete downdraft/updraft mass budget for a convection parameterization.

Rather than the classic view of cloud plumes as updrafts surrounded by clear, slowly subsiding air (Arakawa and Schubert, 1974), or the basic view of downdrafts as entirely separate structures from updrafts (Johnson, 1976), the results of this chapter suggest a slightly different mass flow for cumulus parameterizations. First of all, downdrafts should have at least as much mass flow as the subsiding environment. The RADCONV average profiles show downdrafts dominating the environment from the middle troposphere downwards, but the TOGA simulation has the two fluxes in nearly equal amounts at almost all levels. The large variability in the relative magnitudes of downdrafts and environmental mass fluxes in the TOGA simulation (Figures 4.6 and 4.7) suggests that downdrafts need to be controlled by time-varying properties (such as the amount of precipitation or precipitation evaporation) rather than a simple fraction of updraft mass flux. We investigate this idea further in the next chapter.

Finally, it seems that the majority of mass entrained into downdrafts comes from updrafts. So, in outlining a possible mass budget for future use in convective parameterizations, this transfer of air and moisture should not be neglected. Figure 4.20 shows the major mass flux directions from

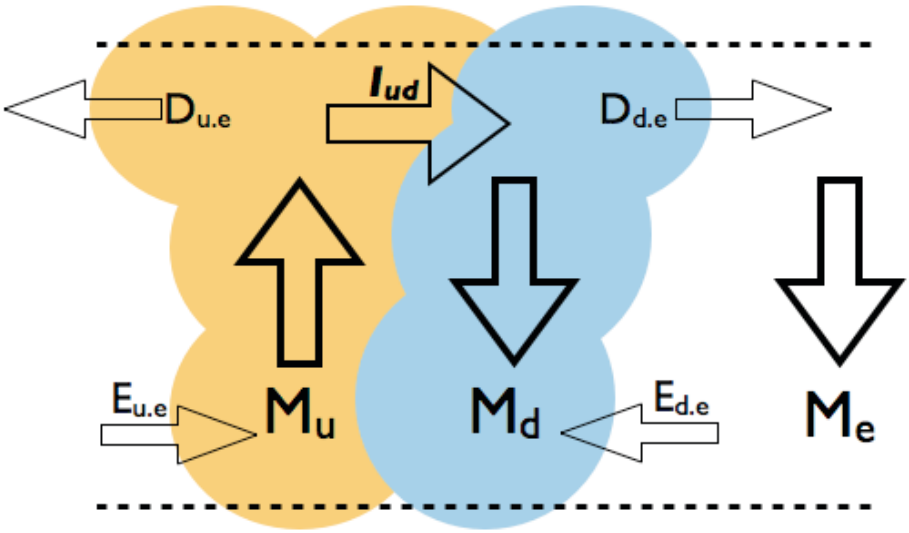

Figure 4.20. A diagram of the convective mass fluxes outlined in the suggestions for a parameterization.

our results. Updraft, downdraft and environmental vertical fluxes should all be included in convective parameterizations. Updrafts and downdrafts seem to both entrain in the lower troposphere and detrain in the upper levels. There does not seem to be a significant or persistent flux from downdrafts to updrafts. The impacts of cold pools and downdraft-related turbulence on shallow clouds is investigated in later chapters. For now, we suggest neglecting the flow of mass in that direction for simplicity. However, the significant mass flux from updrafts to downdrafts should not be neglected.

Chapter 5: Cold Pools and Boundary Layer Variability

Assumption: Downdraft mass flux is a set fraction of updraft mass flux at cloud base.

We have shown that a common downdraft closure relates the mass fluxed through downdrafts to the cloud base updraft mass flux via a fixed parameter. For example, in the Tiedke (1989) scheme, the downdraft mass flux at the level of free sinking is determined by the simple equation

$$(M_d)_{LFS} = \gamma (M_u)_{base} \quad \text{where } \gamma = -0.2 \qquad (1) \text{ (Equation 16 from Tiedke, 1989).}$$

They point out that changes in this parameter have a strong influence on the vertical profile of convective heating, and are a large source of uncertainty in their parameterization (Tiedke, 1989). This assumption follows a similar assumption in Johnson (1976), and puts two important constraints on convection. The first is that the net cloud base mass flux is upward, and the second is that downdrafts cannot occur without some upward cloud mass flux. These are both good rules for convection in most cases, though there are times at the end of a cloud's lifecycle where it is possible that neither is true.

The basic relationship of downdraft mass flux as a fixed fraction of updraft mass flux is another simplification that may not hold up well to scrutiny. We have already looked at a general mass budget of the troposphere, including the boundary layer, in the previous chapter. To examine the current assumption, we need to dive more deeply into how clouds modify the boundary layer. Can the mass fluxed back into the boundary layer by downdrafts be directly related to the amount of mass lifted from the layer by updrafts?

Because we want to look at how clouds are modifying the boundary layer at its interface with the convective troposphere, we introduce a new category of mass flux: a simple cloud mass flux. In the previous chapter, we use a strict definition of updrafts and downdrafts to describe the way mass moves vertically through the atmosphere. Our updrafts are constrained to two continuous levels of

greater than 1 m/s vertical velocity inside of a cloud, and our downdrafts are two continuous levels of less than -1 m/s vertical velocity inside of cloud. All other air, including cloudy air that moves slowly, is considered part of the environment. This could be considered a 'core' mass flux definition. For our cloud mass flux, we will include any air inside of a cloud or rain-shaft. If it is moving upward, it is part of the upward cloud mass flux and if it moves downward it is part of the downward cloud mass flux, regardless of the speed or vertical continuity.

A benefit of this reclassification in the lower part of the troposphere is that we can include upward and downward mass fluxes in very shallow cloud layers, or in cloud regions where the air is moving more slowly in the vertical (for instance, as a downdraft diverges horizontally in the boundary layer, its vertical velocity decreases). Also, the "environment" is now defined to be cloudless, so mixing of clear and cloudy air is more clear. Figure 5.1 shows that the upward and downward cloud mass fluxes include far more air movement than the core mass fluxes. A drawback of this classification is that it could draw gravity wave and stratiform turbulence into the mix. This

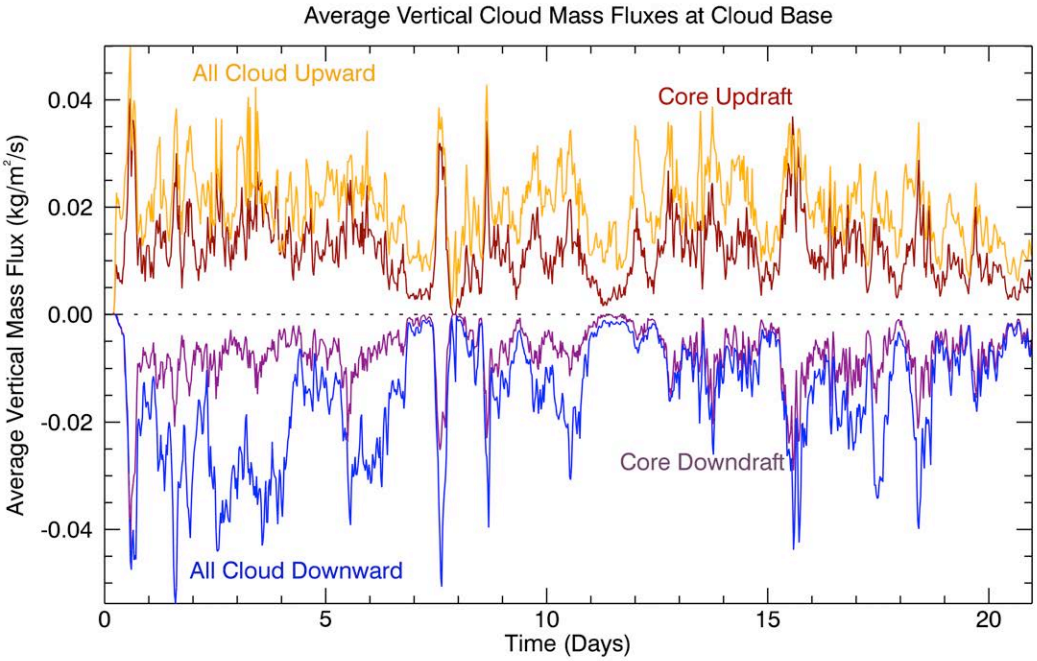

Figure 5.1. Vertical mass fluxes at cloud base during the TOGA run for core up- and downdrafts (red and purple), and for upward and downward cloud mass fluxes (orange and blue).

classification scheme is possibly too inclusive for the upper troposphere, where shallow wave motions could pollute the statistics. Figure 5.2 shows a profile of core and cloud mass fluxes from one 3D snapshot on Day 4 of the TOGA run. This is a day when the core definition of up- and downdraft is far more restrictive than the cloud definition. We can see more boundary layer mass flux is included in the downward cloud mass flux than in the core downdraft definition, as well as more mass flux near the melting level and at the tropopause.

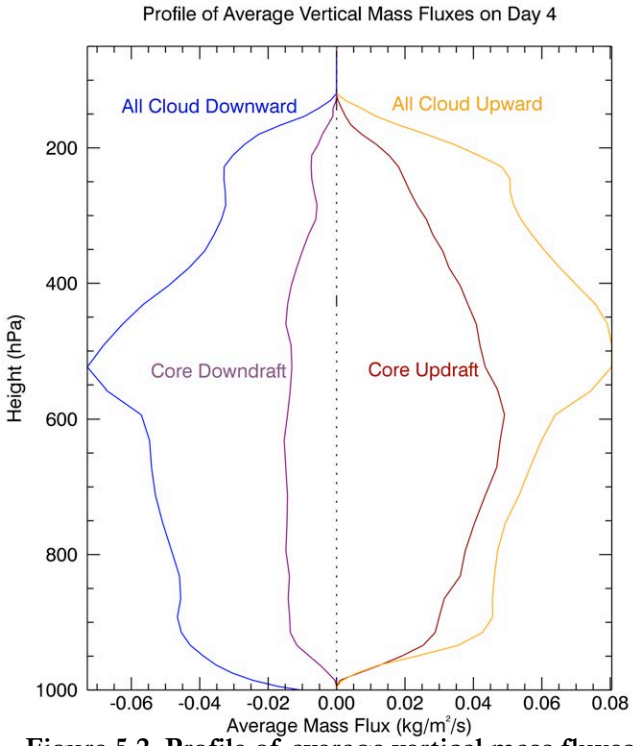

Figure 5.2. Profile of average vertical mass fluxes during one 3D snapshot from the TOGA run for core up- and downdrafts (red and purple), and for upward and downward cloud mass fluxes (orange and blue).

To look at our current assumption, that downdraft mass flux can be parameterized as a set fraction of updrafts, we simply plot the ratio of upward and downward mass fluxes at the cloud base and between the cloud base and the level of free sinking (LFS, defined here as the column minimum of mean saturation moist static energy). Figure 5.3 shows the ratio of cloud-base upward mass flux to the downward mass flux at both the LFS and

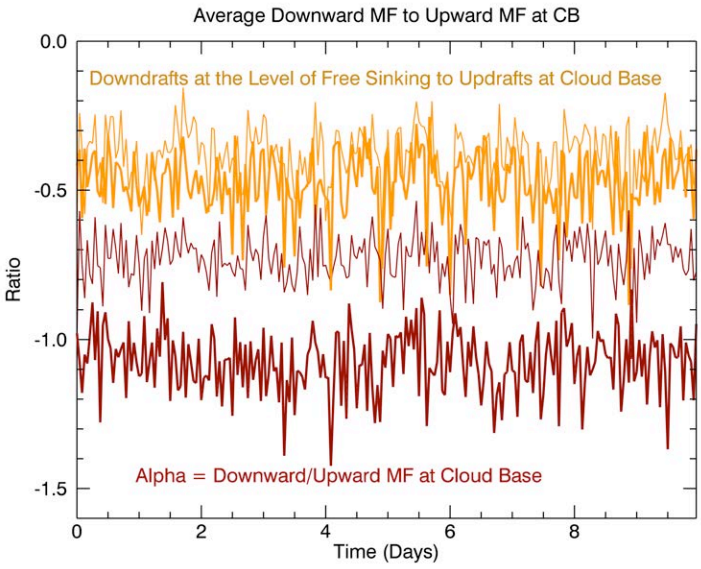

Figure 5.3. RADCONV Ratio of cloud base upward mass flux to downward cloud mass flux at the LFS (orange) and downward cloud mass flux at the cloud base (red). Heavy line is the core mass fluxes and lighter lines show cloud mass fluxes.

at cloud base for the last 10 days of the RADCONV simulation. Both of these ratios have plenty of variability. The cloud mass flux ratio of upward mass flux at cloud-base to downward flux at the LFS ranges from less than 0.2 to around 0.6 in extreme cases. Because this ration oscillates about a single mean value here, one could argue that the approximation made by Johnson (1976) and Tiedke (1989) and described in Equation 1 is reasonable. The magnitude of 0.2 that they use is slightly off the average of our results. A better assumption, however, would allow for more variability than a fixed coefficient can provide.

The ratio of downdraft to updraft mass flux at cloud base (shown in red in Figure 5.3) is called the alpha parameter in Raymond (1995), where he describes a balance in the boundary layer between downdraft cooling and surface flux warming. We will look at this balance in more detail later in this chapter, but right now we introduce alpha as a method of gauging the downdraft activity in the boundary layer. Alpha is defined as

$$alpha = \alpha = M_d / M_u \text{ at cloud base} \quad (2).$$

Figure 5.3 shows the interesting result that, as expected in equilibrium, the downdraft core mass flux balances the core updraft mass flux, and the thick red line oscillates around -1.1. However, if we include all cloud mass fluxes, we see that upward cloud mass flux dominates in the RADCONV run. This means if we re-made Figure 4.3 using the cloud mass flux, we would see a downward flux by the environment outside of the clouds, and that the upward environmental mass flux that we did see is produced in large part by shallow cumulus updrafts that were not included in our updraft core definition. Regardless, in the last 10 days of the RADCONV run, we see a balance between upward and downward cloud mass flux activity at the top of the boundary layer, with a net positive cloud mass flux (and an alpha parameter less than 1.0).

Beyond the case of simple radiative-convective equilibrium, our TOGA simulation gives more insight into the variability of these updraft and downdraft mass flux ratios. Figure 5.4 shows

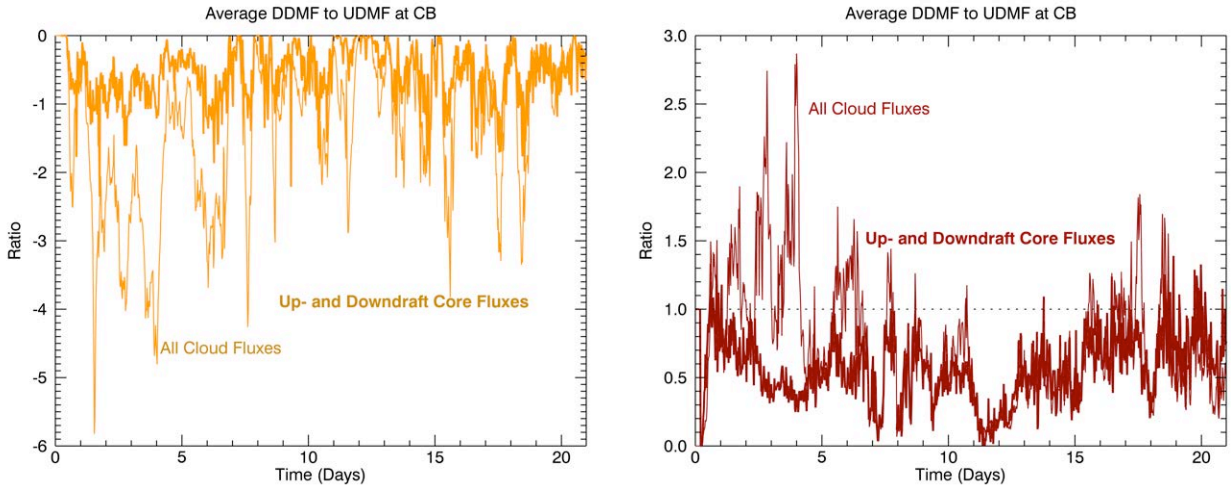

Figure 5.4. TOGA Ratio of cloud base upward mass flux to downward cloud mass flux at the LFS (orange, left) and absolute value of downward cloud mass flux at the cloud base (red, right). Heavy line is the core mass fluxes and lighter lines show cloud mass fluxes.

these same ratios for the entire 21 days of the TOGA run, and there is much more variability than what we see in Figure 5.3. The ratio of upward mass flux at cloud base to downward mass flux at the LFS is shown in orange on the left. The core mass fluxes have a pretty wide range of variability, moving from near zero to less than -2.0 in some cases. The cloud mass flux ratio is even more variable, ranging from near zero to occasionally less than -4.0, with a maximum near -6.0. This is 3000% larger than the 0.2 estimate from Tiedke (1989), and occurs during an intensely raining period with very active downdrafts. The differences between the cloud mass flux and core mass fluxes are very clear in this figure. During strong convection, the ratio of downward cloud mass flux to upward cloud mass flux is much more variable than that of the core mass fluxes. This variability better mirrors the variability of precipitation during the simulation, and we will be using the cloud mass fluxes extensively for the rest of this study.

The absolute value of the alpha parameter is shown in the right hand panel of Figure 5.4. By definition, it will be negative (a negative flux divided by a positive flux), but looking at the absolute value gives a clear positive correlation to precipitation, and other atmospheric properties that strongly relate to downdrafts. In Figure 5.4, even the core mass flux ratio at the top of the boundary layer has a wide range of variability, ranging from near zero to above 1.0 in some periods of intense

convection. The ratio of cloud mass fluxes exhibits even more variability, starting near zero during the suppressed convection on day 11 to nearly 3.0 on some of the heaviest raining periods of the first five days.

The results of this section indicate that a single constant parameter relating the mass fluxed by updrafts to downdrafts is probably a poor assumption, especially if the goal is to capture the variability of precipitation and convection in the tropics.

Assumption: Parcels are lifted by parameterizations considering only mean layer properties.

Convective parameterizations that include plume or draft-based cloud models are an attempt to gather information about important sub-gridscale cloud processes in a GCM column. But many of these models base the appearance or intensity of convection on layer mean properties in each column. When Arakawa and Schubert (1974) close their system of equations, they relate the amount of mass moving through cloud base to the 'Cloud Work Function', which is very similar to a calculated CAPE using mean layer properties. This function lifts a parcel with the horizontal mean moist static energy and vapor mixing ratio out of the boundary layer and determines its positive buoyancy based on the horizontal mean column temperature and moisture profile. However, as we just discussed, cloud mass fluxes in the boundary layer can be extremely variable. And one of the biggest impacts of downdrafts in the boundary layer is the increased sub-gridscale spatial variability associated with the injection of mass below cloud base.

Using the alpha parameter described in the previous section as a measure of downdraft activity in the boundary layer, we can take a look at just how much impact downdrafts have on various properties in the boundary layer. If we think of the temperature or the amount of moisture at each point as a distribution about the layer mean value, than convection could change this layer mean property slightly, but change the variance significantly. Figure 5.5 compares the value of alpha to the variances of different variables in the sub-cloud layer during TOGA. Variance of total water

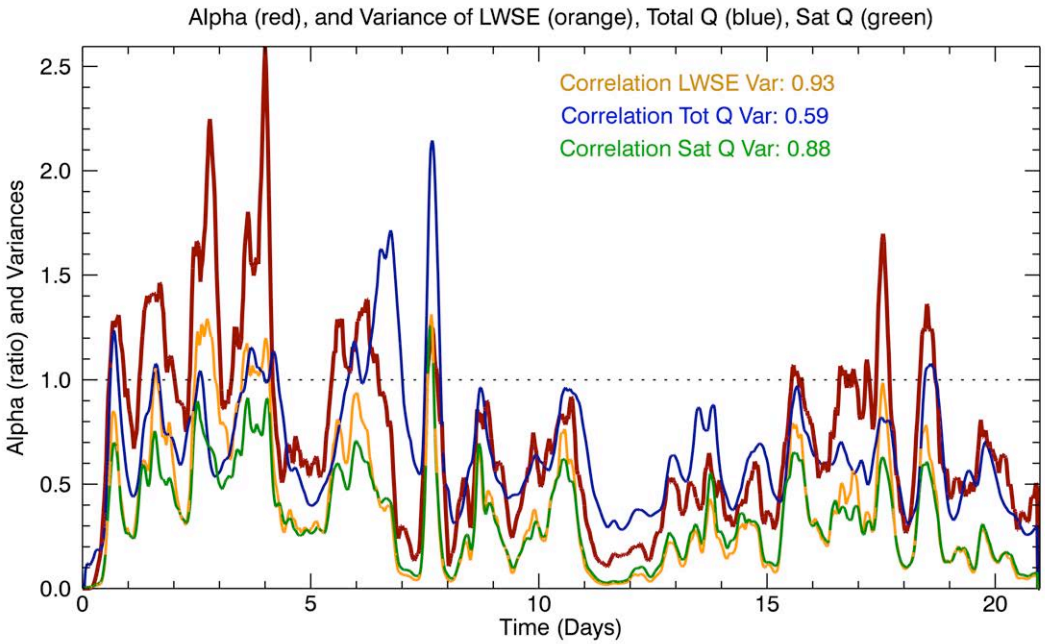

Figure 5.5. TOGA cloud mass flux alpha ratio and variance of Liquid Water Static Energy (K^2), Total water mixing ratio (g^2/kg^2) and saturation mixing ratio (g^2/kg^2).

mixing ratio (blue) is the least correlated at only 0.59, but follows the general trends in alpha. As expected, when downward mass flux dominates at the cloud base, alpha increases above 1.0 and all variances plotted here increase as well. Variables that have more dependency on temperature, such as saturation mixing ratio (green) and liquid water static energy (orange) have a higher correlation to alpha. This indicates that while downdrafts are associated with moisture changes in the boundary layer, properties with the highest correlations involve temperature changes.

Temperature and moisture are not the only boundary layer properties that feel the impacts of downdrafts. Downdrafts can also "stir-up" the boundary layer, injecting mass that falls rapidly toward the surface and then spreads out - creating a cold pool below the cloud. This process increases the gustiness below the cloud, and increases the variances of surface winds. Figure 5.6 shows the correlation of alpha to the variances of the U and V components of the local winds in the boundary layer. As downdrafts hit the surface and spread out, they dramatically increase the variances of horizontal winds. Air flows in all directions from the base of a downdraft, and creates strong convergence as these wind gusts converge against the prevailing boundary-layer flow.

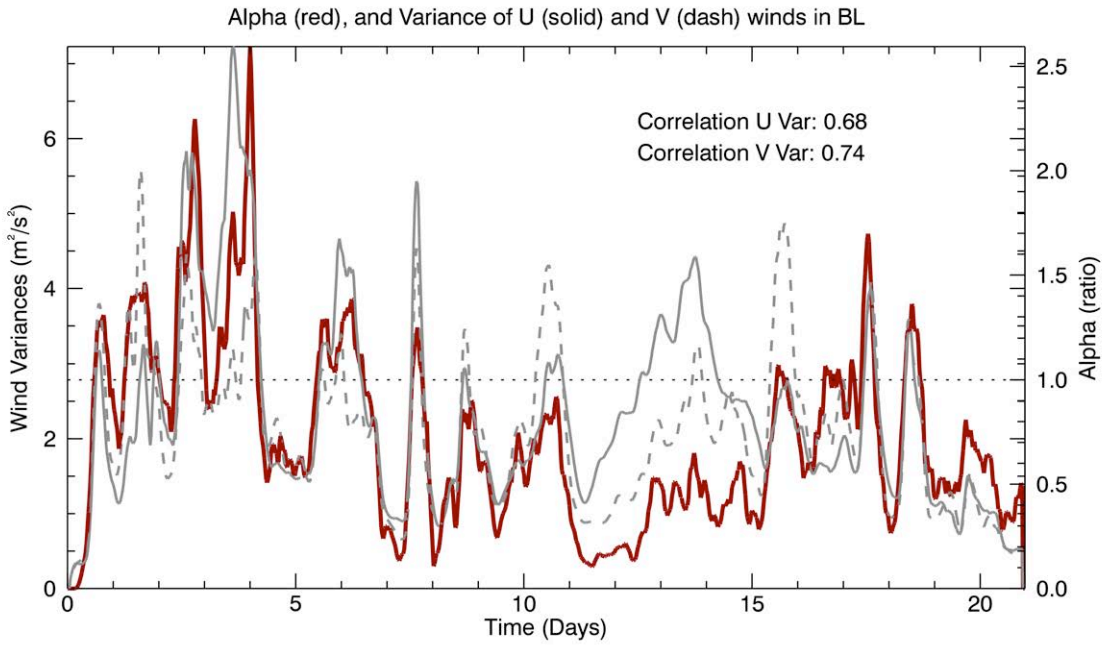

Figure 5.6. TOGA cloud mass flux alpha ratio and variance of the U and V component of winds (m^2/s^2).

As discussed in Chapter 1, cold pools have differing influences on convection. The region of cold diverging air below a downdraft can reduce the amount of heat and moisture locally available to the updraft. However, the convergence of mass along the edges of a cold pool can create a prime location for new convection. The variances of temperature and moisture increase not simply because cool air is added to the distribution, but because the cool pool winds can sweep warm moist air into convergence zones, and produce small regions that are slightly warmer and slightly more moist than the mean.

To give an example of how downdrafts and cold pools can impact the properties of updrafts, we will start by examining data from one 3-dimensional snapshot from the TOGA simulation where a strong cold pool has formed below intense convection. Figure 5.7 shows the mass convergence in the lowest atmospheric level from the snapshot, which occurs around noon on Day 7 of the TOGA simulation. Looking at Figures 5.5 and 5.6, this is a period of intense downdraft activity, and high variances of boundary layer LWSE, total water mixing ratio, and winds. The map of horizontal convergence in Figure 5.7 shows the outline of a large cold pool that

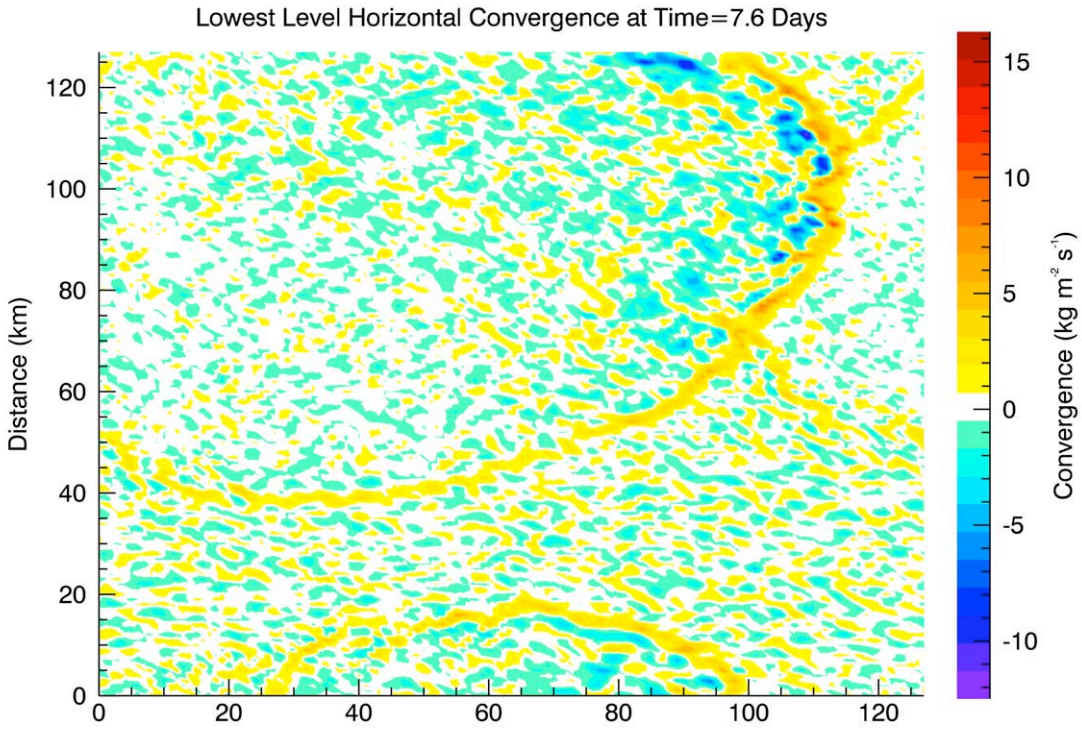

Figure 5.7. Horizontal mass convergence in the lowest layer of one 3D snapshot from TOGA.

dominates the domain during this time period. Dark blue signifies places with divergence, and where downdraft air has hit the surface and is spreading out in every direction. A large orange and red ring surrounds the cold pool, showing a wave of converging air that spreads out as downdrafts dump more and more cold air into this expanding cold pool.

Figures 5.8 and 5.9 continue our study of this cold pool, with maps of temperature and water vapor anomalies in the lowest atmospheric level of this three-dimensional snapshot. The boundaries of the cold pool on the north, east, and south sides are regions of high temperature gradient. The cool mass of air that comprises this cold pool stands out starkly against the red backdrop of the undisturbed boundary layer. At the same time, the center of the cold pool is filled with relatively dry air, and the entire structure is surrounded by a ring of air with a higher vapor content than in the undisturbed (dry environmental) boundary layer. These maps show that the region of high convergence is associated with a strong temperature gradient and an increase in water vapor, making it a prime location for new convective updrafts to form.

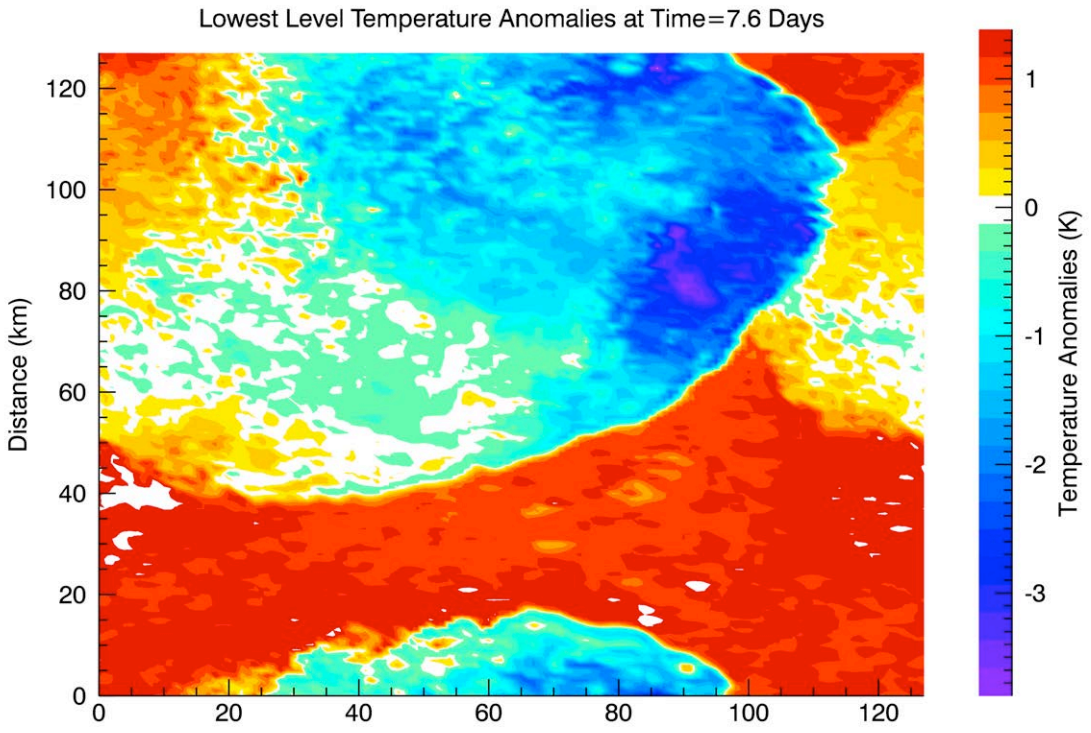

Figure 5.8. Temperature anomalies in the lowest layer of one 3D snapshot from TOGA (same snapshot as Figure 5.7).

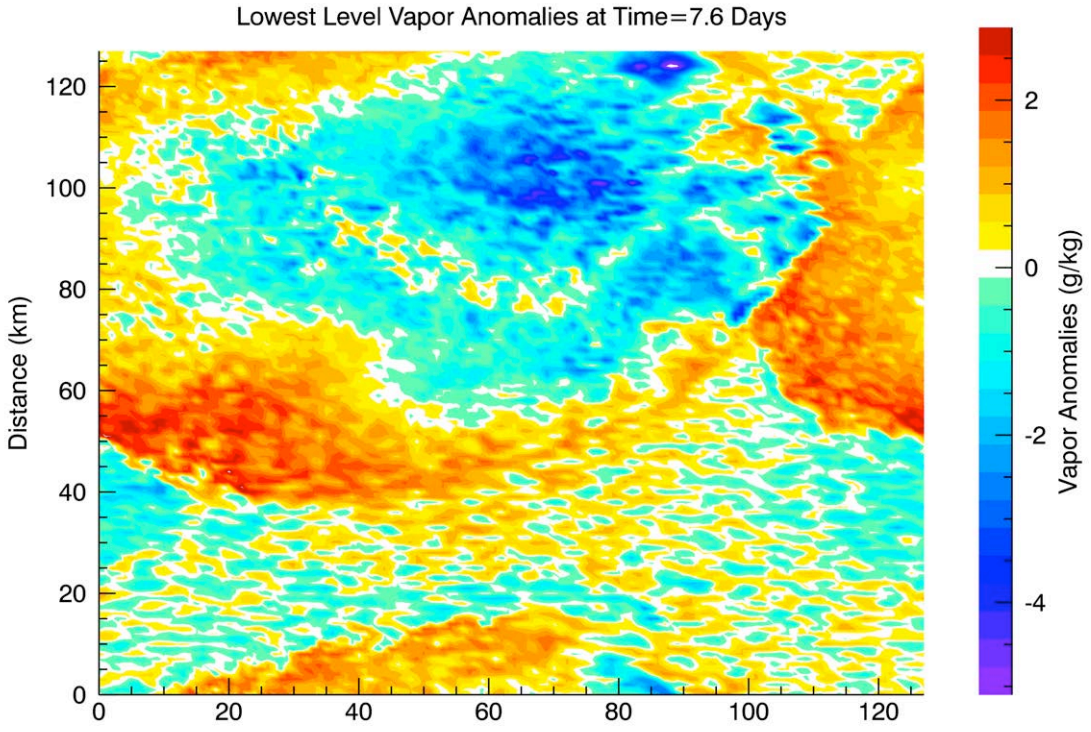

Figure 5.9. Water vapor anomalies in the lowest layer of one 3D snapshot from TOGA (same snapshot as Figure 5.7).

Throughout this work we will use a thermodynamic variable called moist static energy (MSE). The MSE of a parcel is defined as

$$h = C_p T + gz + Lq_v \quad (3)$$

where C_p is the specific heat of dry air, T is the temperature, g is the acceleration due to gravity, h is the height, L is the latent heat of vaporization, and q is the water vapor mixing ratio. The MSE of a parcel is conserved for adiabatic motions in the absence of ice. Going back to the top of the boundary layer, we see in Figure 5.10 that many updrafts form at the edge of the cold pool, where convergence, temperature, and moisture and therefore MSE are all higher than the mean. This shows that the parcels entering the base of newly formed clouds at this time period have MSE profiles *higher* than the mean values of the domain, and the assumption that lifting a parcel with mean properties may be a poor one. Figure 5.10 is only a single time-step, and to really cement this conclusion, we need to look at the statistics for updrafts and downdrafts during the entire TOGA

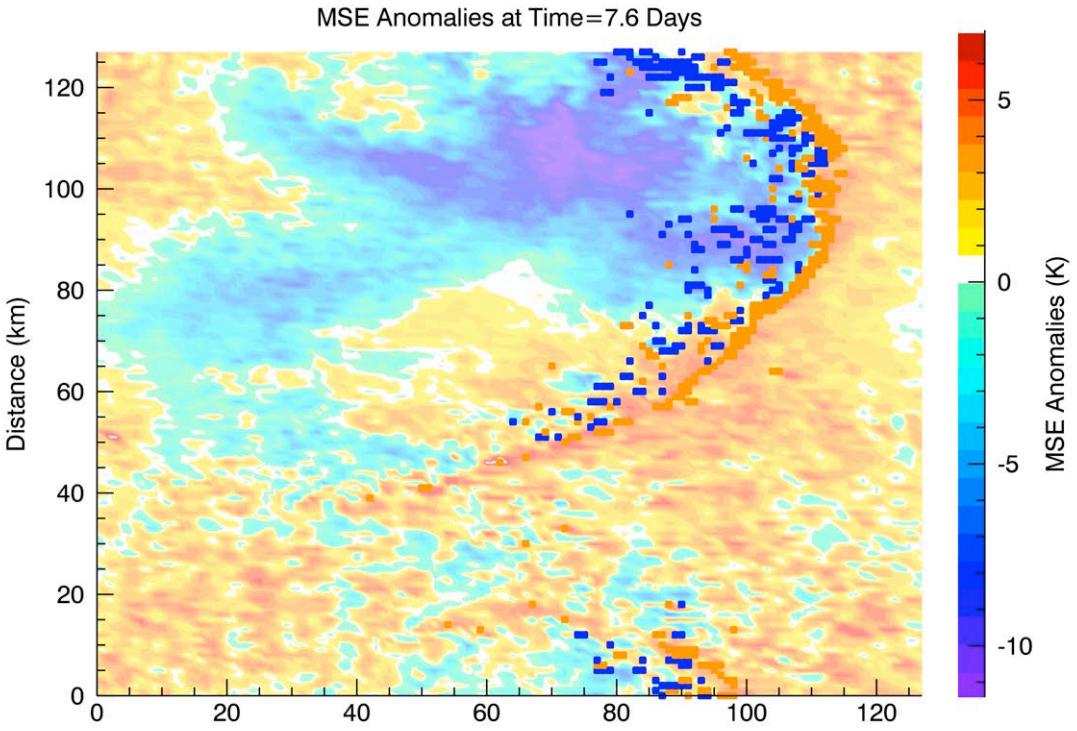

Figure 5.10. Moist static energy anomalies at cloud base of one 3D snapshot from TOGA (same snapshot as Figure 5.7), with core updrafts and downdrafts identified by orange and blue squares.

simulation. In Figure 5.11, we look at the moist static energy (MSE) anomalies relative to the mean of the cloud base layer, associated with 3D gridcells categorized as core updrafts and downdrafts at cloud base. Every 3D snapshot from the run can be categorized by the precipitation rate, and then the values of MSE for updrafts and downdrafts are binned, and added to the histograms of all of the other time steps in that precipitation range. In each of the panels of Figure 5.11, the distribution of MSE for up- and downdrafts at cloud base is plotted, and the mean is denoted with a thin vertical

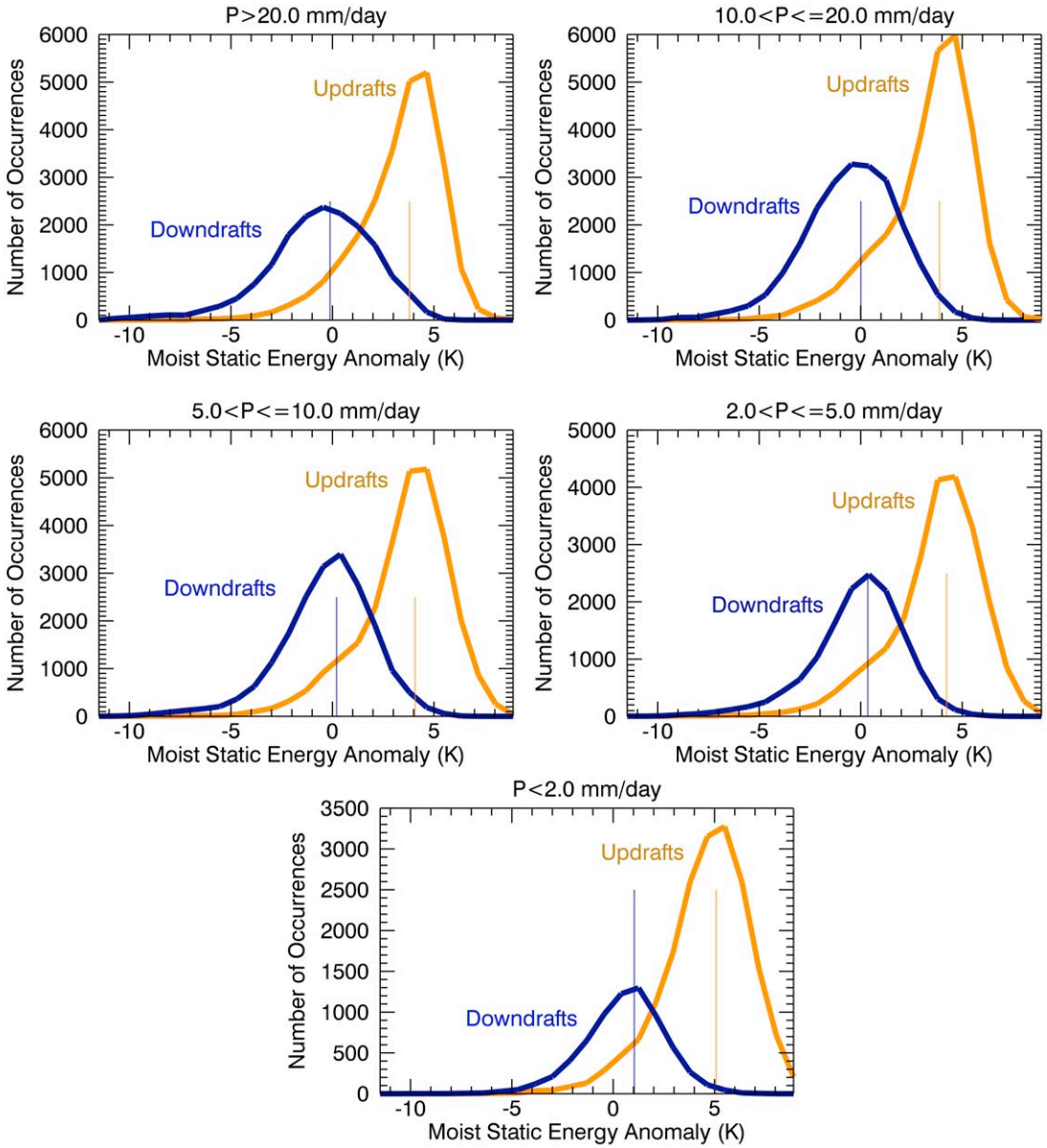

Figure 5.11. Histograms of moist static energy anomalies of core Updraft and Downdraft gridcells at cloud base for various precipitation amounts during TOGA. The mean for each distribution is marked as thin vertical line.

line. In each of the panels of Figure 5.11, the majority of updraft gridcells have a higher MSE than the mean, and the average of the updraft distribution in each panel is several degrees warmer than the domain mean. As precipitation gets lighter, the average updraft MSE gets higher. But the change between different precipitation regimes is not very large. Downdrafts have a much more even distribution, and a mean much closer to the average domain mean. As the precipitation rate decreases, the mean downdraft MSE increases *above* the domain mean.

The assumption that the intensity of convection can be directly related to the mean column CAPE, or a lifted parcel with mean layer properties, is probably not the best one. It seems that updrafts regularly have values of MSE much higher than the mean. The decrease of updraft MSE as precipitation increases in Figure 5.11 indicates a possible relationship between updraft properties and cold pools. Intense downdrafts and cold pools are associated with heavier precipitation, and these may lead to more mechanical lifting of parcels, requiring *less* buoyancy from updrafts. As downdrafts become less intense, updrafts may have to rely solely on temperature and vapor for thermodynamic lift, and the MSE required to lift parcels out of the boundary layer becomes larger.

We have discussed the usage of CAPE in convection parameterization a bit in this chapter, but we have not examined the effect of downdrafts on CAPE. Figure 5.12 shows a map of CAPE anomalies from the same snapshot shown in Figures 5.7, 5.8, 5.9 and 5.10. These CAPE anomalies are calculated in each grid column by lifting a parcel from every level and then taking the highest possible value. As expected, the cold, dry regions in the center of the cold pool have a very low CAPE, and converging regions around the edges of the cold pool have a much higher CAPE. The eastern edge of this cold pool is the epicenter of updraft activity (see Figure 5.10), and has some of the highest CAPE values. The range is impressive, and these updraft regions have as much as 4000 J/kg more CAPE than the center of the cold pool.

Figure 5.13 shows the relationship between CAPE variance and the alpha ratio during the TOGA simulation, which is less correlated than other boundary layer variables at only 0.49.

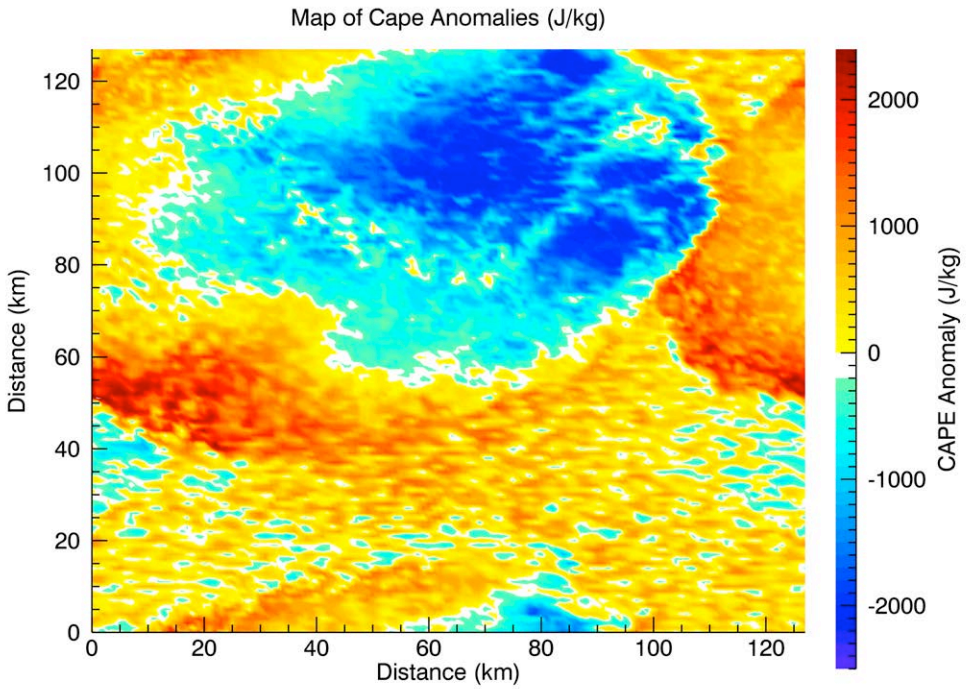

Figure 5.12. Convective available potential temperature anomalies in the lowest layer of one 3D snapshot from TOGA (same snapshot as Figure 5.7).

However, there is a stronger (and negative) correlation between the alpha ratio and mean CAPE (-0.58). This means, as downdrafts get stronger, alpha increases and the mean CAPE decreases. As CAPE increases, updrafts begin dominating and alpha decreases. While the general convective activity is related to the mean values of CAPE in the column, the actual CAPE values of updrafts

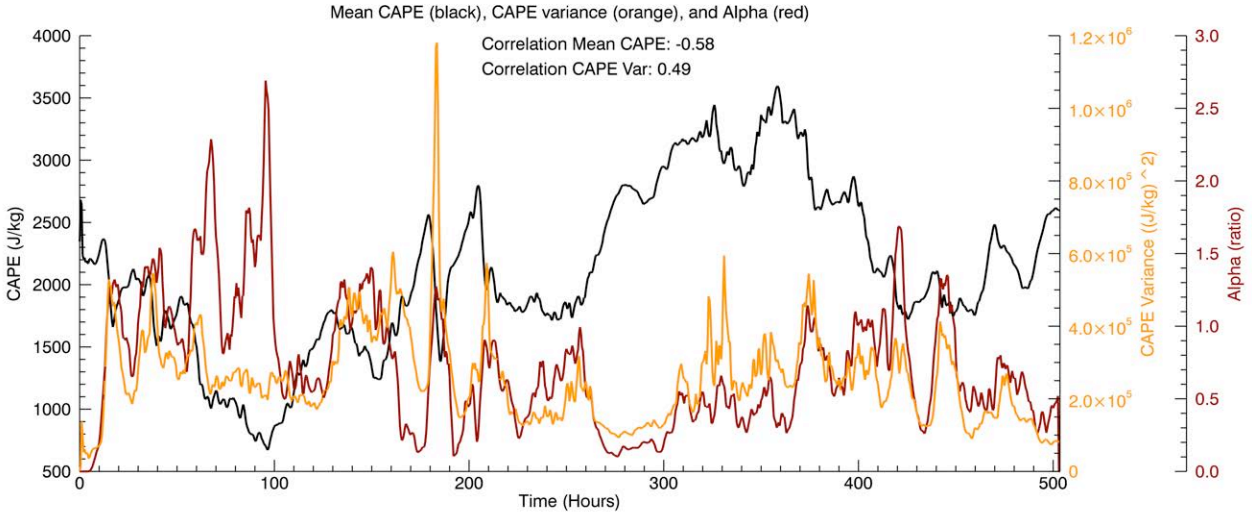

Figure 5.13. Mean CAPE (black), CAPE Variance (orange) and cloud mass flux Alpha ratio (red) for the entire TOGA simulation.

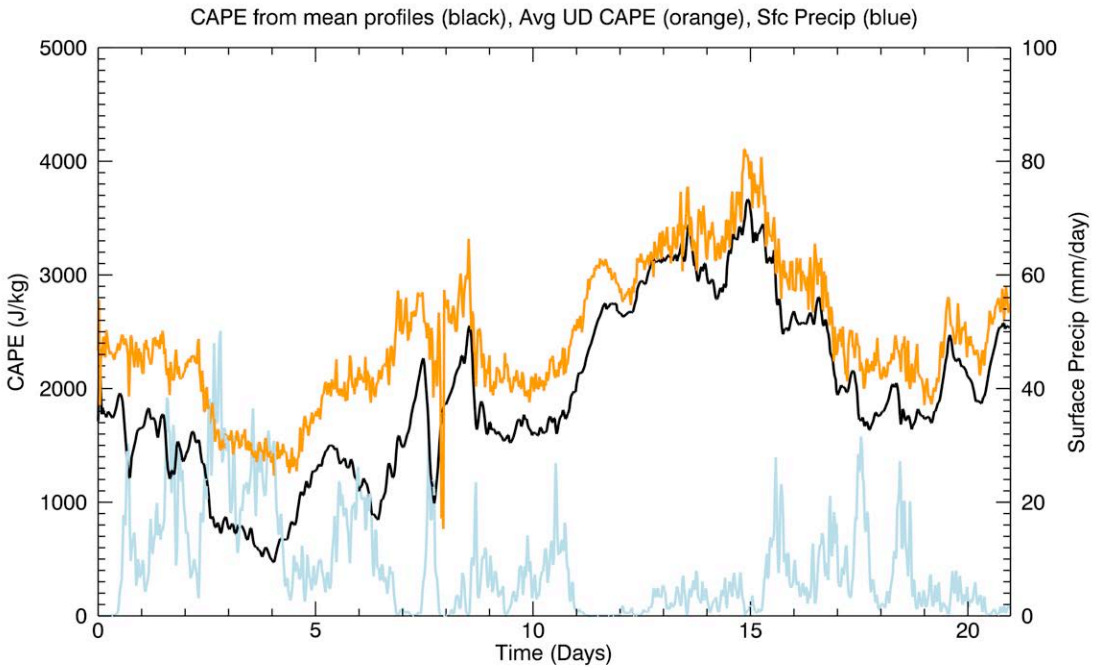

Figure 5.14. Mean CAPE (black), average CAPE in parcels identified as updrafts at cloud base (orange) and surface precipitation (light blue) for the entire TOGA simulation.

can be different from the mean. Figure 5.14 shows the average CAPE of gridcells categorized as updrafts at cloud base compared to the mean CAPE during the TOGA simulation. The black line is the calculation for CAPE used in most convective parameterizations, and the orange line is the amount of CAPE in core updrafts in our CRM. Throughout the simulation, the actual amount of CAPE in updrafts is much higher than the mean values. Using only wide-area mean values of CAPE to calculate updraft mass flux may be misleading, and adding in some method of parameterizing boundary layer variance seems to be a good idea.

Assumption: Surface fluxes are unrelated to convective activity.

Traditionally, surface fluxes in climate models have been parameterized outside of the convective scheme. Parameterizations such as bulk aerodynamic formulas are used in many GCMs, and they relate the amount of moisture and heat transferred from the surface to the atmosphere to only grid-scale mean variables. For example, the formulations used in CAM 3.0 are

$$E = \rho_A |\Delta v| C_E \Delta q \quad \text{and} \quad H = \rho_A |\Delta v| C_p C_H \Delta \theta \quad \text{from Collins et al. (2004)}$$

Where E is the latent heat flux and H is the sensible heat flux from the surface, ϱ is the density of surface air, $|\Delta v|$ is the area mean difference between surface and lowest-level wind velocities, C_E and C_H are drag coefficients, C_p is the specific heat of air at constant pressure, and Δq and $\Delta\theta$ are the differences between surface and lowest level moisture and temperature (Collins et al. 2004). Both equations relate the flux of energy from the surface to the difference in mean winds between the surface and lowest atmospheric layer, and the difference in temperature or moisture between the mean surface and mean properties of the lowest layer. This means that the transfer of sensible and latent heat from the surface depends on the mean large-scale properties, and is not directly coupled to large-scale convective activity.

However, past observational evidence has pointed to a strong relationship between convection and surface fluxes, which may be too small to resolve on the GCM grid. Johnson and Nicholls (1984) observed an order of magnitude increase in sensible heat flux and an order of 3 increase in latent heat flux associated with the passage of a squall line during GATE. Jorgensen et al. (1997) calculated surface fluxes from low-level flight measurements through a squall line late in the TOGA COARE project, and found a distinct increase in both latent and sensible heat flux associated with the convective edge of a cold pool. Many observational studies have found an increase in surface fluxes along the initial out-flow boundary (or gust front) of convective downdrafts, so it makes sense to suggest that GCMs should include this increase in surface fluxes in their parameterizations.

The maps of surface convergence, temperature and moisture anomalies in the previous section show that cold pools are associated with low-level variability that could impact surface fluxes (Figures 5.7, 5.8 and 5.9). However, we should consider the question carefully: How does convection, and downdrafts in particular, influence surface heat fluxes?

Starting with domain mean surface heat fluxes, we see a surprising result. Figure 5.14 shows the domain average latent heat flux, the domain average sensible heat flux, and the alpha ratio from

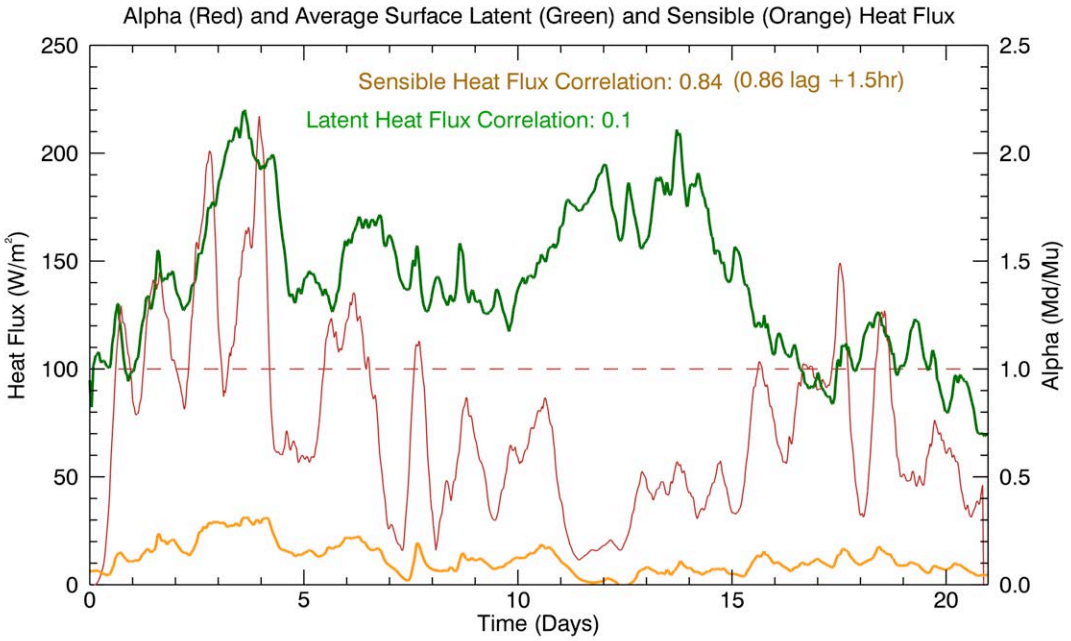

Figure 5.14. Mean Latent heat flux (green), mean sensible heat flux (orange) and cloud mass flux Alpha ratio (red) for the entire TOGA simulation (3.5 hour running mean applied).

the TOGA simulation. The domain mean latent heat flux is almost uncorrelated with the alpha ratio, at a mere 0.1. The sensible heat flux, while much lower in magnitude than the latent heat flux, is very well correlated to the alpha ratio (0.84). So, while the temperature flux from the surface is very sensitive to downdraft activity (as observed in previous studies), the latent heat flux seems to be completely unaffected by downdrafts. How can this be?

Figure 5.15 shows the standard deviations of sensible and latent heat fluxes over the entire TOGA simulation. These have a much higher correlation to the alpha parameter, for both moisture and temperature flux. So, like other boundary layer variables discussed in this chapter, these fluxes see an increase in variability when downdrafts are dominant. This is understandable, as downdrafts impact only a fraction of the surface. In the areas that feel the cool, gusty air, surface fluxes are increased. Regions that are outside of convective activity retain surface fluxes similar to those of a dry, lightly convecting boundary layer. Figure 5.16 looks at the actual distributions of sensible and latent heat flux anomalies on another day with relatively intense downdrafts (Day 18 of the TOGA simulation). The map of precipitation in the top left shows that most of the convection is confined

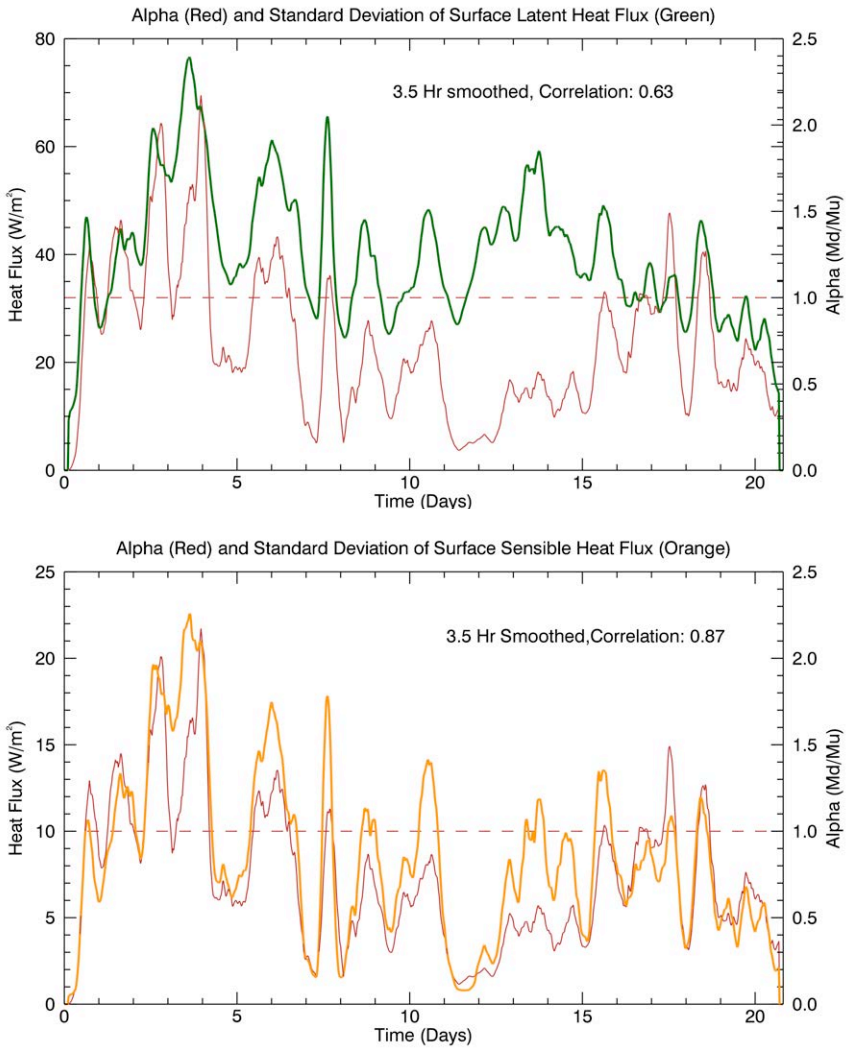

Figure 5.15. Standard deviations of latent heat flux (green, top) and sensible heat flux (orange, bottom) with cloud mass flux Alpha ratio (red) for the entire TOGA simulation.

to the lower right quadrant of the map, though periodic boundaries allow for precipitation to wrap around to the top of the domain. Sensible heat flux anomalies on this day are very closely related to the locations of intense precipitation. Areas that are not near the convective activity have very little (or slightly negative) anomalous sensible heat flux. So, the cold air from downdraft outflow creates perfect conditions for an increase in surface sensible heat flux, and that is the main driver for this source of energy. This results in a tight correlation between sensible heat flux and downdraft activity throughout the TOGA run. Latent heat flux anomalies are much less organized. While the convective region does have a large amount of anomalously high latent heat flux, other areas of the

domain, that are not directly affected by convection, also have positive latent heat flux anomalies. Looking at a map of surface winds, we see that the convective downdrafts have very high wind speeds and are co-located with the highest latent heat flux anomalies. But the other positive anomalies are located in regions with light surface winds, unrelated to downdraft activity.

While the sensible heat flux in this run is directly correlated to the intense surface temperature changes resulting from downdrafts and cold pools, the latent heat flux is sensitive to many different processes. Increased radiation and large-scale surface winds can result in an increased surface evaporation. As the cool air in the cold pool mixes with boundary layer air, it increases the

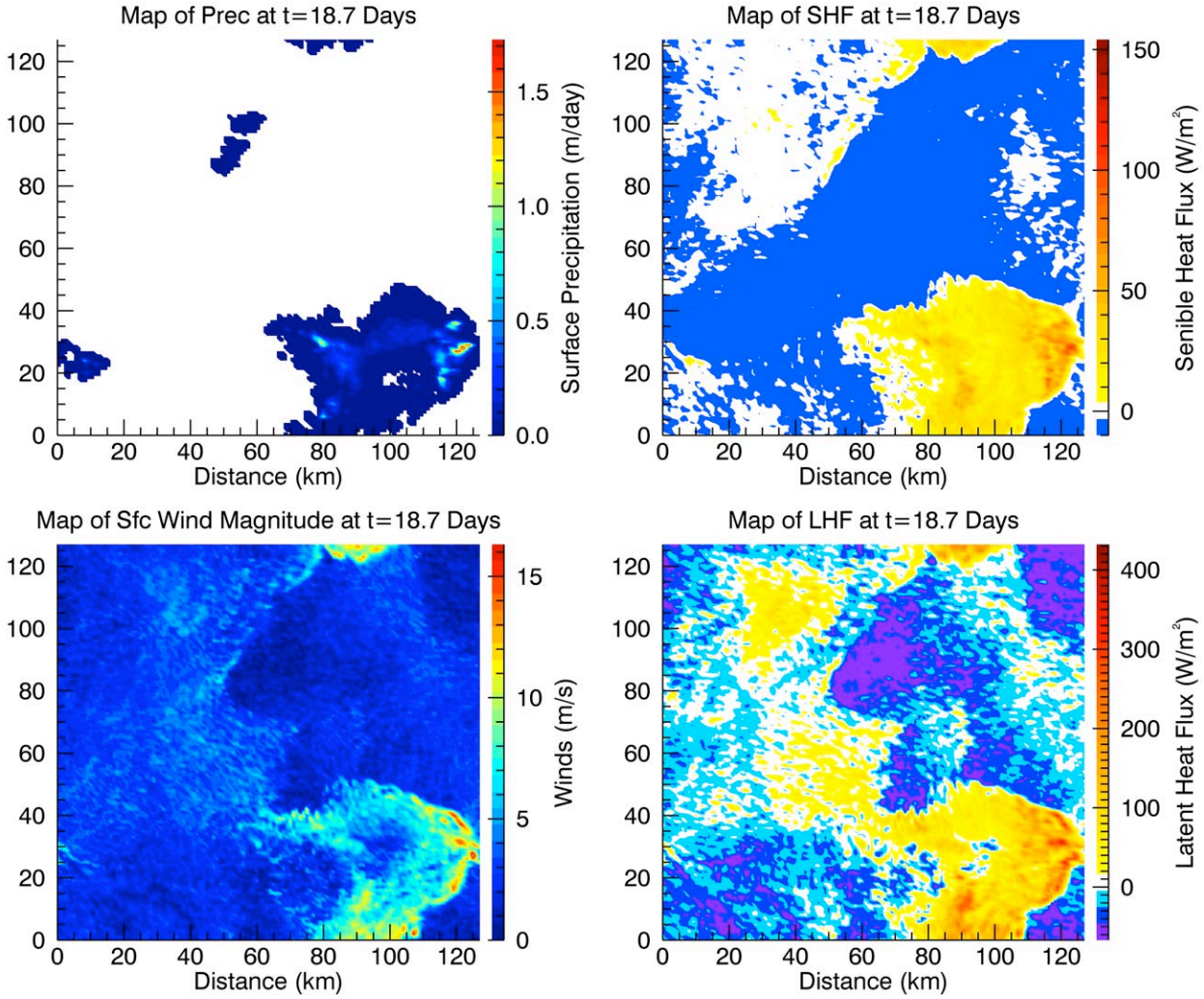

Figure 5.16. Maps of surface variables for a single 3D snapshot at 18.7 Days in TOGA. Clockwise from top left: Surface precipitation, Sensible heat flux anomalies, Latent Heat flux anomalies, and total magnitude of horizontal surface winds.

local surface relative humidity and can decrease the surface latent heat flux. As described in Chapter 3, midway through this simulation there is a strong increase in mean winds associated with a westerly wind-burst following an MJO disturbance. This is a time period associated with light convection, so the surface is receiving quite a bit of insolation as well. These other processes are enough to greatly increase latent heat flux, completely apart from convective activity.

To answer the question posed in this section, cool air from downdrafts is a main driver of surface sensible heat flux in this simulation. Temperature fluxes should be tied more closely to convective activity in GCMs. The latent heat flux is more complex, and the result of many competing processes is a decoupling of the mean surface moisture flux from convective activity. For a large GCM gridbox, the bulk moisture flux parameterization is probably good enough, however as GCM gridcells become smaller, there will be more of a chance for convective downdrafts to dominate an entire cell, and the surface moisture flux will need to be sensitive to these local effects.

Recommendation: A better representation of boundary layer variability and downdraft influences.

Based on the results of this chadpter, there are three main features of downdrafts in the boundary layer that should be captured by a convective parameterization.

1. If downdraft mass flux is regulated through a direct relationship with updraft mass flux, a fixed parameter will not capture the true variability. In Figure 5.4, the shape of the relationship between updraft mass flux at cloud base to both the downdraft mass flux at the LFS and at cloud base (alpha) were remarkably similar. Both ratios varied widely, so if this relationship is used to close the downdraft parameterization, the ratio should be allowed to vary based on the thermodynamic properties of both updrafts and downdrafts.
2. Downdrafts and the presence of cold pools increase the variability of all temperature and moisture-related properties in the boundary layer. Core updrafts in regions of strong cold

pool activity are actually less buoyant than scattered updrafts. Cold pools could help produce longer lasting, persistent convection. The long-lasting effects of cold pools and gust fronts on new updraft parcels would be difficult to parameterize without an available prognostic variable related to convection.

3. Surface sensible heat flux is tightly correlated to downdrafts in our model, so we recommend adding in some downdraft-based temperature adjustment to the sensible heat flux parameterization. Latent heat flux is more complex. If the author of a parameterization includes downdraft drying and gustiness in their surface flux parameterization, it should be as a fraction related to the area of the gridcell covered by intense downdrafts.

Each of these recommendations points to small areas where changes in the way convection interacts with the boundary layer could affect the overall climate in a model. The issue of persistence is likely the most important. The formation, expansion and impacts of a large cold pool last much longer than the typical 20-30 minute time step in a GCM. To really include these features in a climate model, at least the adjustments to updraft parcel buoyancy should continue from one time step to the next. Parameterizations such as Pan and Randall (1998) have implemented prognostic cumulous kinetic energy, which allows convection to "remember" its state from the previous time step. A prognostic cold pool kinetic energy might be useful as well, and help produce longer-lasting, more organized convection in a GCM (e.g. Elsaesser and Kummerow, 2013; Mapes and Neale, 2011).

Chapter 6: Downdrafts and Mid-Tropospheric Relative Humidity

Assumption: Downdrafts are very sensitive to environmental relative humidity through the evaporation of precipitation.

Updrafts are formed by air rising through the atmosphere due to increased buoyancy, usually the result of surface warming or convergence. Downdrafts are air sinking through the atmosphere due to decreased buoyancy, which is generally thought to be driven by precipitation loading and evaporation. Observations as to the microphysical drivers of downdraft negative buoyancy are difficult to find. Knupp and Cotton (1985) performed a wide-ranging survey of observations and model results related to downdrafts and concluded that the relative roles of condensate evaporation, melting and loading in driving downdrafts was particularly unclear.

Intense observational campaigns of tropical convection have attempted to answer this question. Jorgensen and LeMone (1989) found the majority of downdraft cores sampled by air craft in the TAMEX (Taiwan Area Mesoscale Experiment) campaign have positive virtual temperature perturbations. Thus condensate loading was expected to be a major source of negative buoyancy above cloud base. Igau et al. (1999) found similar positive virtual temperature anomalies in downdraft cores in aircraft data from the TOGA COARE campaign. They used parcel theory to show that relative humidities near 20% would be required to evaporate enough precipitation to create negatively buoyant downdrafts. This is not a commonly seen relative humidity in the tropics (though it might be found in continental air) so they conclude that downdraft cores analyzed in their study were likely produced through precipitation loading.

Climate modelers are forced to simplify all of these complex cloud processes and traditionally, they choose precipitation evaporation to be the main (or only) source of negative buoyancy in downdrafts. Zhang and McFarlane (1995) use a simple saturated downdraft parameterization where downdrafts are required to maintain a saturated column through the evaporation of precipitation. The beginning level of these downdrafts is just below the layer of

updraft detrainment, and their mass flux at this level is a fraction of the updraft mass flux determined by the precipitation efficiency, calculated as

$$\alpha = \mu\left[\frac{P}{P+E}\right] \quad \text{where} \quad \mu = 0.2 \quad (1)$$

where P is the total vertical integral of in-cloud precipitation and E is the evaporation required to maintain the saturation of the column, and negative buoyancy of the downdraft. The weight and loading effects of the precipitation or cloud condensate is not considered in the magnitude of these downdrafts at all.

The assumption that convective downdrafts are mainly driven by precipitation evaporation could cause them to be very sensitive to environmental relative humidity in the area. Downdrafts in a dry column would evaporate more water, and be colder. They could create larger cold pools, and cool the boundary layer more quickly than a downdraft in a very moist column. Many studies propose this to be an important process for the regulation and organization of tropical convection. Emanuel (1989) proposes that the transition of downdrafts from a dry regime with strong boundary layer cooling to a moist regime and weaker downdraft cooling is fundamental in the formation of tropical cyclones. Thayer-Calder and Randall (2009) theorize that the buildup of mid-tropospheric moisture allows for a similar transition from disorganized convection with stronger downdrafts to deep convective regions with relatively weak downdrafts in the Discharge-Recharge Cycle of the Madden-Julien Oscillation (MJO).

Several studies have pointed to the interaction of convection and downdrafts as a possible weak point in the simulation of MJO variability, as discussed in Chapter 1. Many of the models with poor tropical convective variability lack the build-up of cloud from shallow to deep convection as the wave passes. Their deep convective parameterizations are firing too quickly, and re-stabilizing the tropical atmosphere before there is a chance to trigger a wave. (DeMott et al., 2007; Thayer-Calder and Randall, 2009; Kim et al., 2009; Maloney and Hartmann, 2001; Straub et al., 2010).

There are three main ways to decrease the frequency of convection and allow for a buildup of low-level moisture via shallow convection. The first is to simply put a relative humidity trigger in your parameterization. Emori et al. (2001) improved the simulation of tropical mesoscale waves by simply requiring the column average relative humidity be above a certain level before allowing deep convection. Tokioka et al. (1988) find they are able to greatly improve the simulation of the MJO in their model after preventing the deep convection parameterization from running until the column is nearly saturated by using a minimum entrainment rate. Zhang and Mu (2005) show that a change in the Zhang-McFarlane parameterization that includes the addition of a relative humidity criterion also improves the representation of convection in the Community Climate Model (CCM). While adding this criteria for the triggering of deep convection seems to help, it is not exactly based on a physical process, only the basic observation that deep convection is tightly coupled to high relative humidity environments in the tropics (as in Bretherton et al., 2004).

Another method of reducing the frequency of convection is to increase convective entrainment. Del Genio (2012) explains that modelers have long thought the only way to get deep convection penetrating to the tropopause (as often observed) is through undiluted ascent, or allowing some fraction of updraft plumes to rise without entraining any environmental air. However, recent studies have shown this is extremely unlikely to be occurring in the real tropics (Romps and Kuang, 2010). Allowing some entrainment of environmental air increases the sensitivity of convection to mid-tropospheric moisture levels, and prevents deep convection from occurring until the column is sufficiently moist. Neale et al. (2008) updated the Zhang-McFarlane convection scheme discussed here to include entrainment in the calculation of CAPE for a lifted parcel, and greatly improved the representation of tropical phenomena such as the El Nino Southern Oscillation (ENSO). Other studies have shown that increasing entrainment in a plume parameterization improves tropical convective variability, but often at a cost to the mean climate (Hannah and Maloney, 2011; Del Genio, 2012).

A third option for reducing the frequency of deep convection in climate models focuses on downdrafts. This is similar to the relationship between evaporation-driven downdrafts and column relative humidity discussed here. If deep convection occurs in a model column with low relative humidity, precipitation evaporation should create a very cool downdraft, and reduce low-level CAPE for future convection. At the same time, precipitation evaporation will moisten the column and reduce the moisture deficit. Once the column is sufficiently moist, evaporative-driven downdrafts would not be as powerful, and deep convection will have to reduce CAPE through tropospheric heating. To our knowledge, this process has been described in theoretical studies (Emanuel, 1989; Raymond, 1995; Thayer-Calder and Randall, 2009), but never fully implemented or tested in a GCM or evaluated using a CRM. The possibility of a downdraft-relative humidity convective feedback drives our discussion in this chapter. How sensitive are downdrafts to the vertical average relative humidity through a portion of the column (mid-troposphere versus below cloud base, for instance)? Can a dry environment produce stronger downdraft cooling?

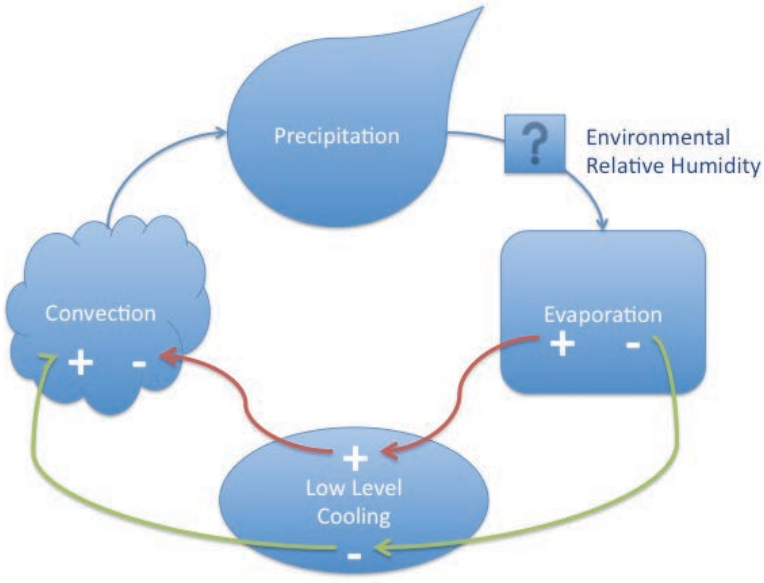

Figure 6.1. A diagram of the proposed downdraft regulating mechanism. Convection forms precipitation that falls through the atmosphere. If the environmental relative humidity is low, evaporation increases, downdraft cooling increases, and convection decreases. If the environmental relative humidity is high, evaporation decreases, decreasing downdraft cooling and convection is allowed to increase intensity.

We could start this investigation at any point on the cycle in Figure 6.1, but the most straightforward place is to examine the simple relationship between downdraft cooling and environmental relative humidity. In order to do this, we need to define low-level downdraft cooling. To do this, we look at the flux of virtual temperature across a model layer very near 500m. We use a definition of virtual temperature that includes liquid and ice condensate, such as

$$T_v = T(1 + 0.608q_v - q_n - q_p) \quad (2)$$

where T is the absolute temperature in a gridcell, q_v is the vapor mixing ratio, q_n is the non-precipitating condensate mixing ratio, and q_p is the precipitating condensate mixing ratio. We use the virtual temperature here because it is a good measure of the power of the downdrafts. If evaporation increases or precipitation increases, the virtual temperature will decrease and downdrafts become less buoyant. Moist static energy, as defined in Chapter 5 eqn 3, is conserved regardless of precipitation evaporation amounts, and is not the best variable for looking at sensitivity to relative humidity. We calculate the downdraft cooling (DDC) or eddy flux of virtual temperature at 500m as

$$DDC = C_p \rho (\overline{w' T_v'})_{DD} \quad (3)$$

where Cp is the specific heat of dry air, ϱ is the density at 500m, w' is the vertical velocity anomaly from the layer mean, T_v' is the virtual temperature anomaly from the layer mean, we use only gridcells categorized as downdrafts in the cloud mass flux definition (see Chapter 5), and then average over the whole domain. Our flux of downdraft virtual temperature at 500m for the TOGA simulation is shown in Figure 6.2.

If downdrafts are sensitive to the environmental relative humidity as described in this chapter, we should see an increased cooling (due to colder temperatures or larger downdraft mass flux) when relative humidity is lower. Figure 6.3 shows a scatter plot and correlation between downdraft cooling and relative humidities at different heights in the column. Surprisingly, these two properties are not highly correlated, with a linear correlation of only 0.42 for mid-levels, and 0.14 at

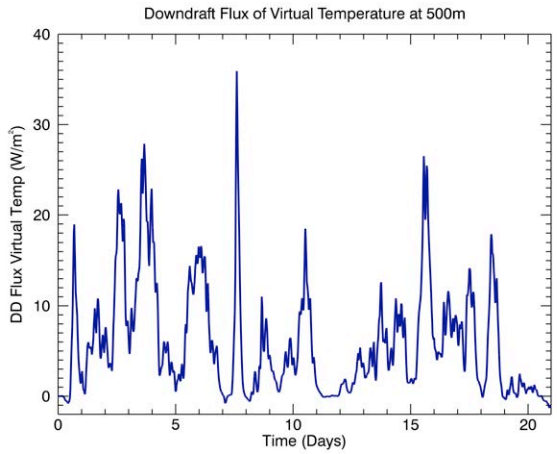

Figure 6.2. Downdraft cooling of the lowest 500m during the TOGA simulation, as calculated in Equations 2 and 3, and smoothed with a 2.5 hr running mean.

low levels. Upper level relative humidity (500-100hPa, not shown) is also poorly correlated to downdraft cooling, at 0.2. In fact, these positive correlations indicate that downdraft cooling increases with *increased* environmental relative humidity! This is the exact opposite of the expected relationship.

Figure 6.3 shows that many days with low convective activity, or very light downdraft cooling, are associated with a wide range of values for low level and mid-level relative humidity. We include a polynomial best-fit line in the figure for completeness, but its shape is not much different from a straight linear fit. Both relationships are positive, and in the mid-level plot, there is a distinct lack of light cooling events in high relative humidity time periods. Again, this is the opposite of what is expected for evaporative-driven downdrafts. When precipitation falls through the moist atmosphere, less evaporation should occur, and light cooling should be the dominate mode. Even though higher downdraft cooling is

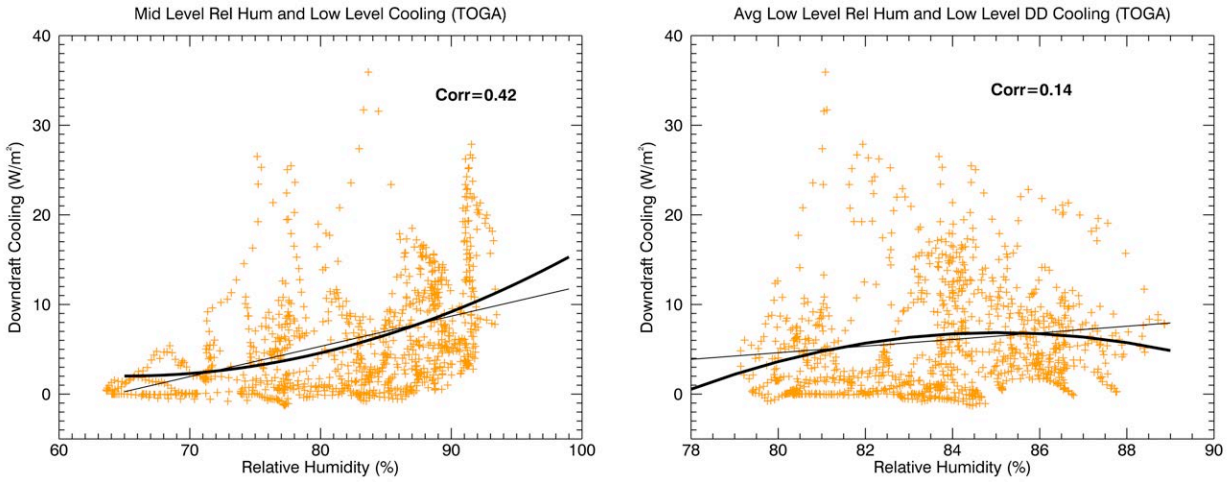

Figure 6.3. Scatter plots of downdraft cooling versus mid-level relative humidity (850-500hPa, left) and low-level relative humidity (1000-850hPa, right), both smoothed with a 2.5 hr running mean.

associated with higher relative humidities in the low levels, the highest values of downdraft cooling are associated with a drier sub-cloud layer (right-hand panel Figure 6.3).

Since we have such an unexpected result here, we need to look at the proposed relationship and see where it does not work. Looking back at the cycle illustrated in Figure 6.1, we can examine each of the proposed relationships and determine where the theory is no longer supported. Figure 6.4 looks at the relationship between precipitation evaporation and environmental relative humidity. Here we use a total column evaporation rate, which is simply the sum of the evaporation through the height of the convective column. This is actually better correlated with mid-level relative humidity, at +0.6, and poorly correlated with low-level relative humidity (+0.21) and upper-level relative humidity (+0.2, not shown). Even though there is a better correlation between mid-level relative humidity and precipitation evaporation, again it is in the direction opposite what we would expect. Our results show higher evaporation occurring in high relative humidity environments.

Another way to look at precipitation evaporation is through a calculation of precipitation efficiency. The basic definition of precipitation efficiency is the fraction of vapor condensed into water or ice particles that reaches the surface as precipitation. After vapor condenses, it can potentially re-evaporate as precipitation falls, or be stored in the atmosphere as cloud water.

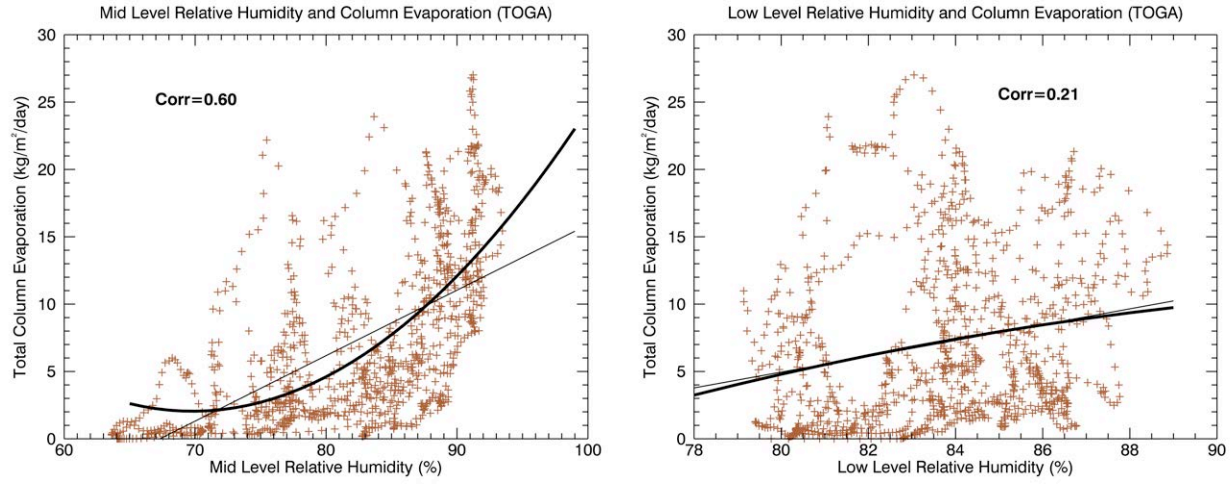

Figure 6.4. Scatter plots of total column precipitation evaporation rate versus mid-level relative humidity (850-500hPa, top) and low-level relative humidity (1000-850hPa, bottom), both smoothed with a 2.5 hr running mean.

Typically, cloud water amounts are much smaller than precipitation or vapor amounts, so we neglect these, and create a ratio for precipitation efficiency similar to the one used by the Zhang-McFarlane scheme (see Equation 1). We define precipitation efficiency as

$$PEff = \frac{P}{[P+E]} \quad (4)$$

where P is the surface precipitation rate, and E is the total column evaporation rate. The surface precipitation rate, total column evaporation rate and precipitation efficiency (PEff) for the duration of the TOGA run are plotted in Figure 6.5. The PEff in our simulation ranges from near 0.8 to below 0.1. The highest peaks in PEff occur in periods with lower precipitation, as do the lowest values. Higher surface precipitation tends to relate to a relatively high PEff, though, the relationship between surface precipitation and PEff is not clear from Figure 6.5. Figure 6.6 shows the correlation between surface precipitation and PEff (note that the non-linear nature of the distribution skews our polynomial fit unrealistically here). There is a positive correlation of 0.43 between surface

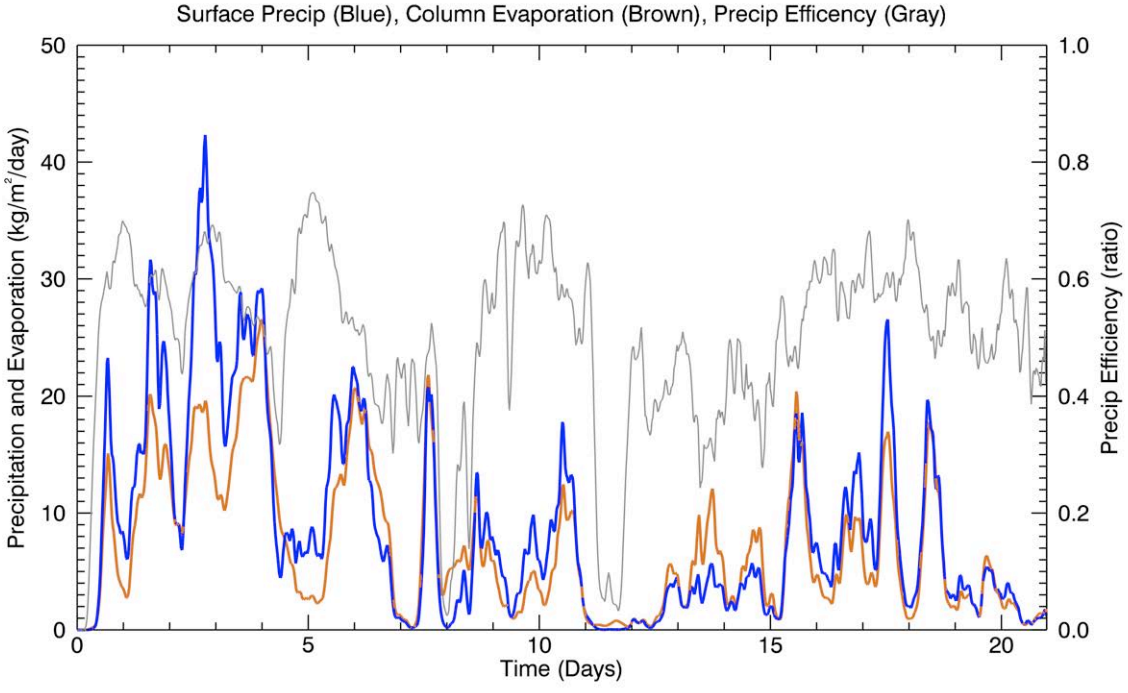

Figure 6.5. Surface precipitation (blue), total column evaporation (orange) and precipitation efficiency (gray) during the TOGA simulation.

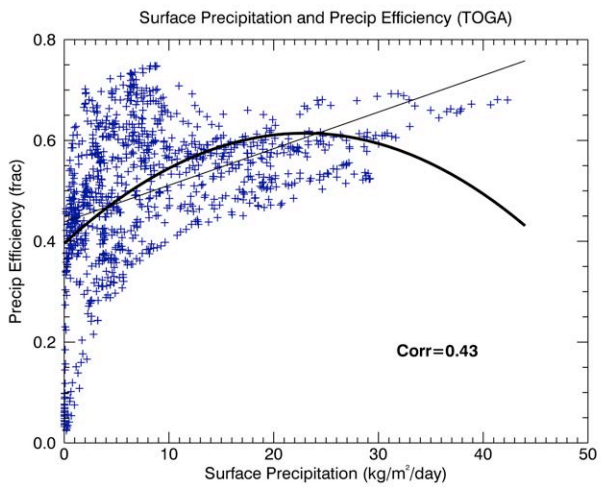

Figure 6.6. Surface precipitation correlated with precipitation efficiency during TOGA.

precipitation and precipitation efficiency. So, increasing precipitation is associated with increasing efficiency, but the highest values of PEff (above 0.65) are grouped around light surface precipitation (below 10 kg/m^2/ day).

If we look at precipitation efficiency and relative humidity, we see a relationship that does follow our original hypothesis. In Figure 6.7, PEff is positively correlated with relative humidity, so increased humidity leads to less fractional precipitation evaporation and a more efficient precipitation process. The correlation at low levels is relatively strong at 0.67. So, the fractional amount of precipitation evaporated is somewhat sensitive to the relative humidity below cloud base, and this part of our downdraft cooling cycle is possible. However, the total amount of precipitation evaporated and available for downdraft cooling increases with increased relative humidity (Figure 6.4). This means that cooler, or simply more, downdrafts will likely occur during high relative humidity periods (as seen in Figure 6.3).

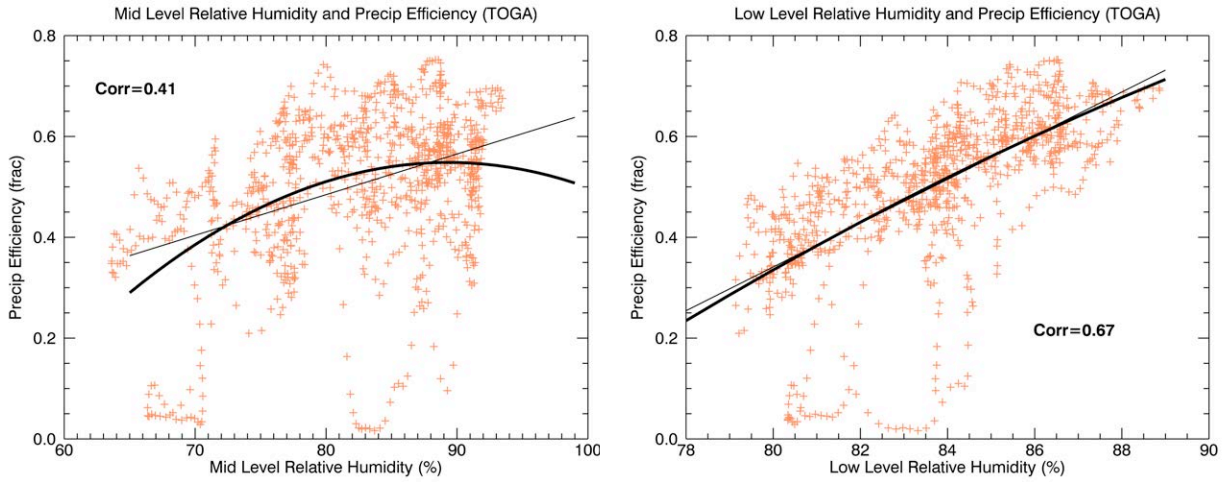

Figure 6.7. Precipitation efficiency versus mid-level relative humidity (850-500hPa, top) and low-level relative humidity (1000-850hPa, bottom), both smoothed with a 2.5 hr running mean.

If precipitation evaporation increases with increased relative humidity, *and* the precipitation efficiency increases with increased relative humidity, then the amount of precipitation hitting the surface must also increase with increased relative humidity. Figure 6.8 shows the tight linkages between precipitation, evaporation and downdraft cooling in our model. Surface precipitation and the total column evaporation are tightly coupled, with a correlation of 0.90. Downdraft cooling is also highly correlated with both surface precipitation and evaporation at about 0.75 for each. It seems that, in our model, intense convection and high precipitation rates form in moist regions. The evaporation rate is much more sensitive to the amount of precipitation than the environmental relative humidity, so the evaporation rate and downdraft cooling rate are *higher* in high relative humidity regions.

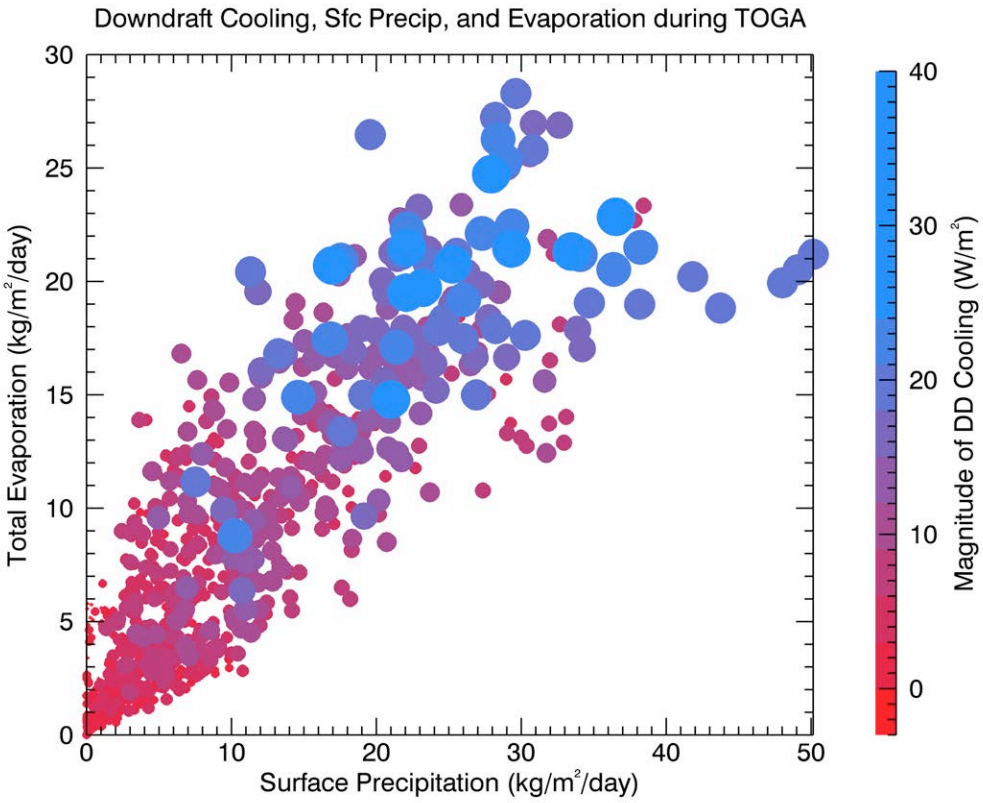

Figure 6.8. A scatter plot of surface precipitation versus total column evaporation, where each point is colored by the magnitude of downdraft cooling for that time. The size of each point is a function of the category of downdraft cooling magnitude. Precipitation and evaporation are correlated at 0.90, precipitation and downdraft cooling are correlated at 0.76, and evaporation and downdraft cooling are correlated at 0.75.

Returning to the questions first posed in this chapter, downdraft cooling in our model is not very sensitive to environmental relative humidity. Downdrafts are tightly correlated to the evaporation in the column, and the evaporation is dependent on the amount of precipitation. In tropical regions, higher rain rates occur in moist regions, so our most intense downdraft cooling occurs when relative humidities are higher, not lower. A relatively dry tropical environment does not produce stronger downdraft cooling as intense convection does not occur in those regions, and precipitation strong enough to create downdraft cooling simply is not present. We do see an increase in precipitation efficiency with increased relative humidity, but the fractional increase is not enough to overcome the intense correlation between rainfall and evaporation rates. A clear exception to this occurs in the mid-latitudes, where intense convection can occur above a dry sub-cloud layer, and produce destructive downbursts (see Chapter 1). Based on our results, in the tropics, updraft entrainment is far more important in coupling convection to the environmental relative humidity.

Assumption: Downdrafts must have a lower virtual temperature than the environment.

We have shown that downdrafts are tightly coupled to the precipitation amount in our model, and that the cooling by downdrafts is not particularly sensitive to environmental relative humidity. This indicates that there could be a problem with the basic assumption used in so many convective parameterizations: that downdrafts entrain environmental air to evaporate enough precipitation to keep their region cooler than the environment. We show in Chapter 4 that a large source of mass for downdrafts is actually from updrafts, rather than the environment. So, what are the resulting thermodynamic profiles of updrafts and downdrafts? How are updrafts and downdrafts vertically structured in these model clouds? And what are the main drivers of negative buoyancy in our downdrafts?

The difference between the MSE in downdrafts (or updrafts) and the environment is shown in Figure 6.11. The profiles of MSE surpluses are binned by the downdraft cooling rate for that

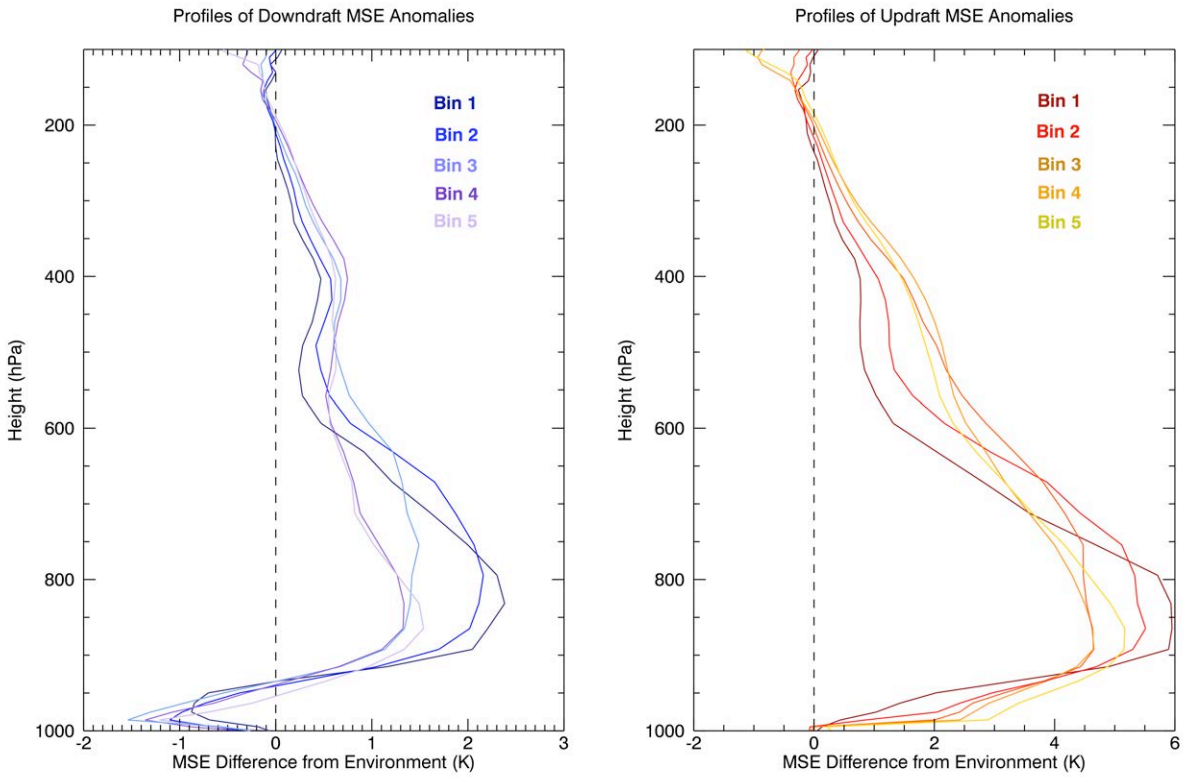

Figure 6.11. Profiles of MSE deficits (difference from environmental values) for Downdrafts (left) and Updrafts (right), binned by downdraft cooling. Bin 1: Cooling less than 0 W/m^2. Bin 2: Cooling greater than 0 W/m^2 and less than 2 W/m^2. Bin 3: Cooling greater than 2 W/m^2 and less than 7 W/m^2. Bin 4: Cooling greater than 7 W/m^2 and less than 15 W/m^2. Bin 5: Cooling greater than 15 W/m^2.

output time period (every half hour) and then averaged into five bins, as described in the caption. Bin 1 is very light downdraft cooling and Bin 5 is relatively intense cooling. Each of these bins had more than 200 profiles averaged to create the composite shown in Figure 6.11 (except for Bin 5 which had only 35). The most interesting part of this figure is that for all bins, downdrafts have a higher MSE than the environment through most of the column. Only in the lower levels (below 900hPa) do downdrafts have less MSE than the environment. Updrafts have a greater MSE surplus than downdrafts through the majority column for all bins.

Saturation moist static energy is often used to approximate the buoyancy or calculate approximate CAPE of a parcel. Clearly, this approximation is not very good here, as all of our downdrafts would be positively buoyant. Though, the buoyancy of downdrafts has long been a source of discussion and difficult to observe, as mentioned at the beginning of the chapter. Here,

we have a model and we can see exactly how buoyancy is calculated for any air parcel. Our model, SAM v6.8.2 is anelastic, and therefore does not predict local density perturbations. SAM uses a virtual temperature approximation to calculate the acceleration due to buoyancy that includes local temperature, pressure and moisture perturbations. The acceleration due to buoyancy is given by

$$Buoy = -g\left(\frac{\rho'}{\rho}\right) \approx g\left(\frac{T'}{T} + 0.608q_v' - q_n - q_p - \frac{p'}{p}\right) \qquad (5)$$

where g is the acceleration due to gravity, a prime quantity is the deviation from the horizontal mean, ϱ is the air density, p is pressure, T is temperature, q_v is the water vapor mixing ratio, q_n is the non-precipitating ice-liquid water mixing ratio (cloud water and ice), and q_p is the total precipitating water mixing ratio (Khairoutdinov and Randall, 2003).

We reproduced this calculation at each point in our 3D output snapshots and categorized each snapshot by downdraft cooling rate at that time step as described for Figure 6.11. The acceleration due to this buoyancy term for updrafts, downdrafts and the environment for bins 3 and 5 are shown in Figure 6.12. Even though the downdraft cooling is 10 W/m^2 different between these two bins, the profiles of buoyancy accelerations are very similar. Profiles from bins 1, 2, and 4 are not shown as they are similar to these as well. Downdrafts in our model are generally negatively

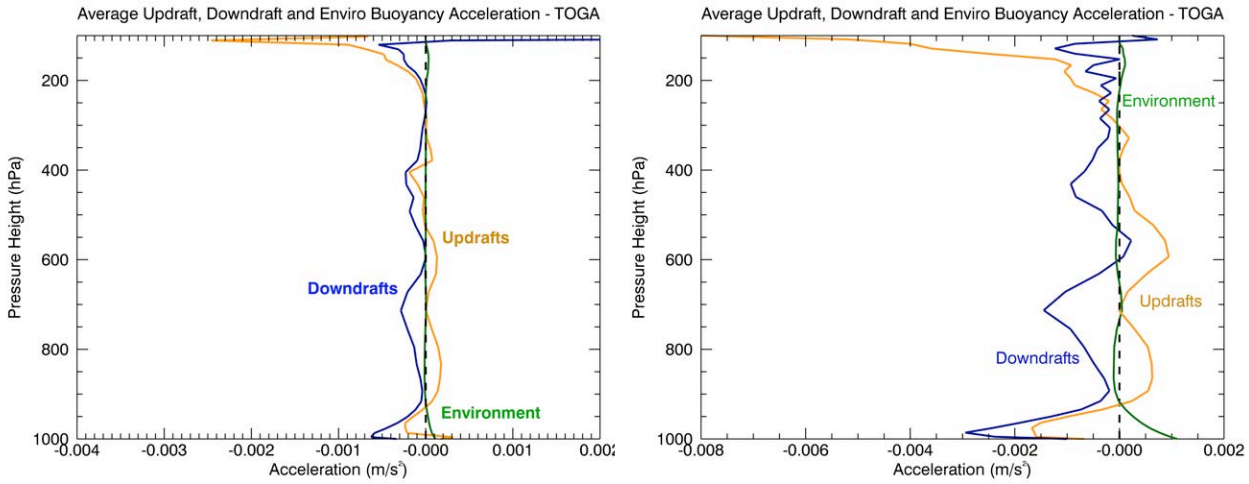

Figure 6.12. Acceleration due to buoyancy for updrafts, downdrafts and the environment during Bin 3 time steps (left) and Bin 5 time steps (right).

buoyant, though there are positive accelerations at the top of the clouds (likely gravity wave or overshooting top activity) and at around 600hPa in Bin 5. Updrafts are generally positively buoyant (as expected), though they have large negative buoyancy at the highest levels (overshooting tops once again), and negative buoyancy in the boundary layer.

There are two main reasons why downdrafts have positive MSE anomalies but negative buoyancies in our model. The first is that MSE does not take into account the weight of condensate, which can greatly reduce the buoyancy of a parcel. The second is that MSE weights water vapor heavily, and the virtual temperature does less so (see Chapter 5 equation 3, and equation 5 in this chapter). To really understand the buoyancy drivers in our model, we plot the vertical profiles of the components of Equation 5 in Figure 6.13. For downdrafts, the vapor and pressure perturbations are almost always sources of positive buoyancy, suggesting that air within a downdraft is very moist, both through entrainment and the evaporation of precipitation. Temperature perturbations oscillate between negative and positive in both profiles. Downdrafts are warmer than the surrounding environment near the top of the boundary layer (about 900hPa), near the freezing level (at 600hPa) and in the upper part of the clouds (between 300 and 200hPa). Condensate loading is a constant source of negative buoyancy for downdrafts. It seems that as soon as a parcel cools off enough to no longer be able to support the condensate within, it rapidly descends in a downdraft.

Another way to look at how downdrafts may be interacting with the environment is to examine their location within a cloud. Downdrafts buried deep within a cloud as part of an intense precipitation core are less likely to be forced by evaporation, and downdrafts on the edges of clouds, distant from the precipitation cores, are less likely to be forced by condensate loading. Figure 6.14 shows a series of horizontal cross-sections from one three dimensional snapshot from TOGA. Each cross-section is increasing in height, and showing us a "slice" view of the clouds and drafts, much like an MRI shows "slice" images of a brain. In these figures, we have contours of precipitation in green through pink, cloud in gray, updrafts as orange boxes and downdrafts as blue boxes. These are

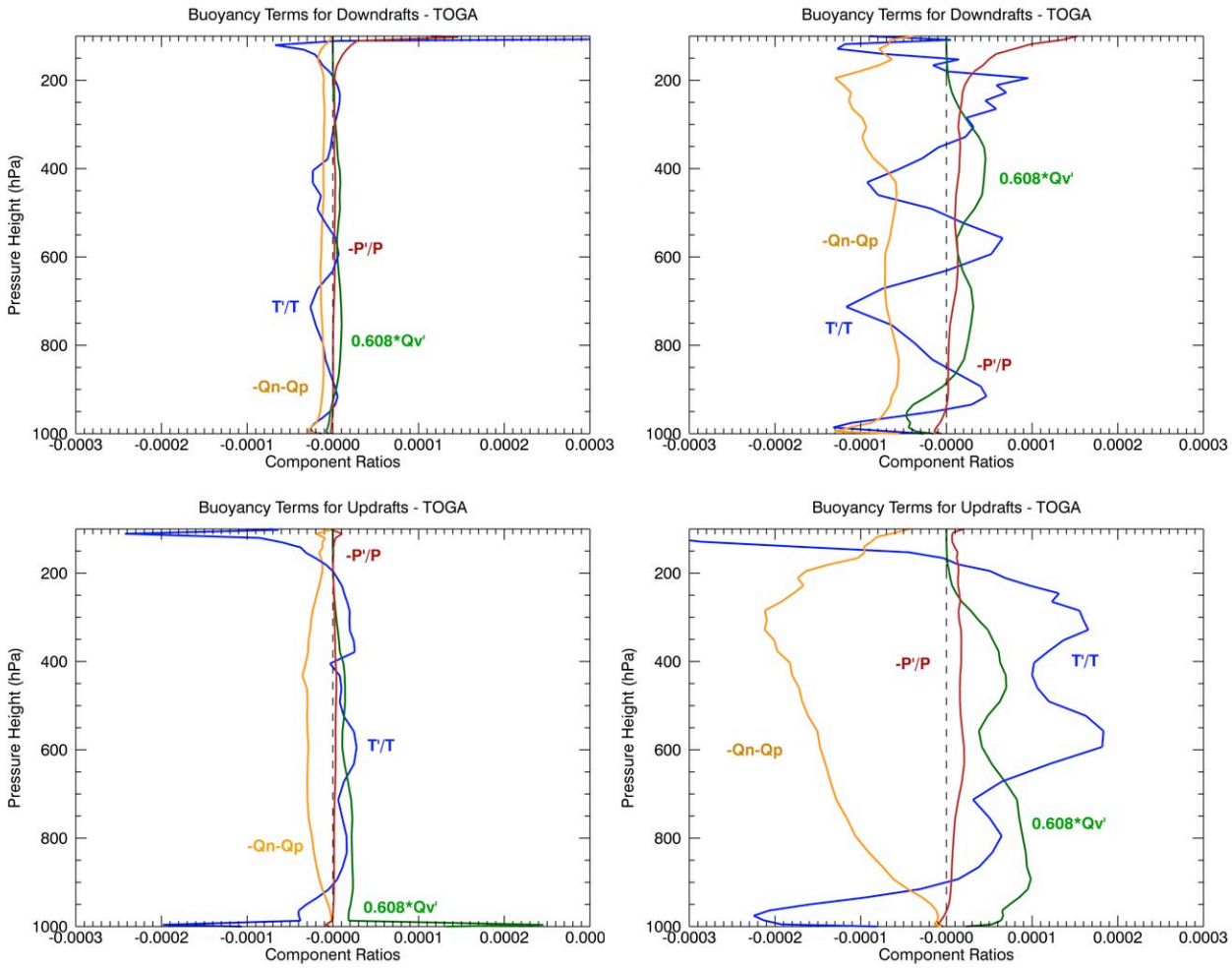

Figure 6.13. Profiles of buoyancy terms for downdrafts (top row) and updrafts (bottom row) during Bin 3 timesteps (left column) and Bin 5 timesteps (right column).

"core" defined updrafts and downdrafts, whose vertical velocities are greater than 1 m/s or less than -1 m/s.

Near the surface, in the top row of Figure 6.14, there are far more downdraft gridcells than updrafts. These downdrafts are generally in the center of the precipitation field, which has a wide coverage and is fairly intense at low levels. As we move up in the column (second row), the cloud and precipitating region narrow, and updrafts begin to dominate. Downdrafts are still associated with precipitation inside of a cloud, but they move to the outer edges of the cloud, where cloud water and precipitation are interacting more with the environment. At these mid-levels, we see the tops of some mid-height congestus clouds, and each of these have some precipitation and one or two

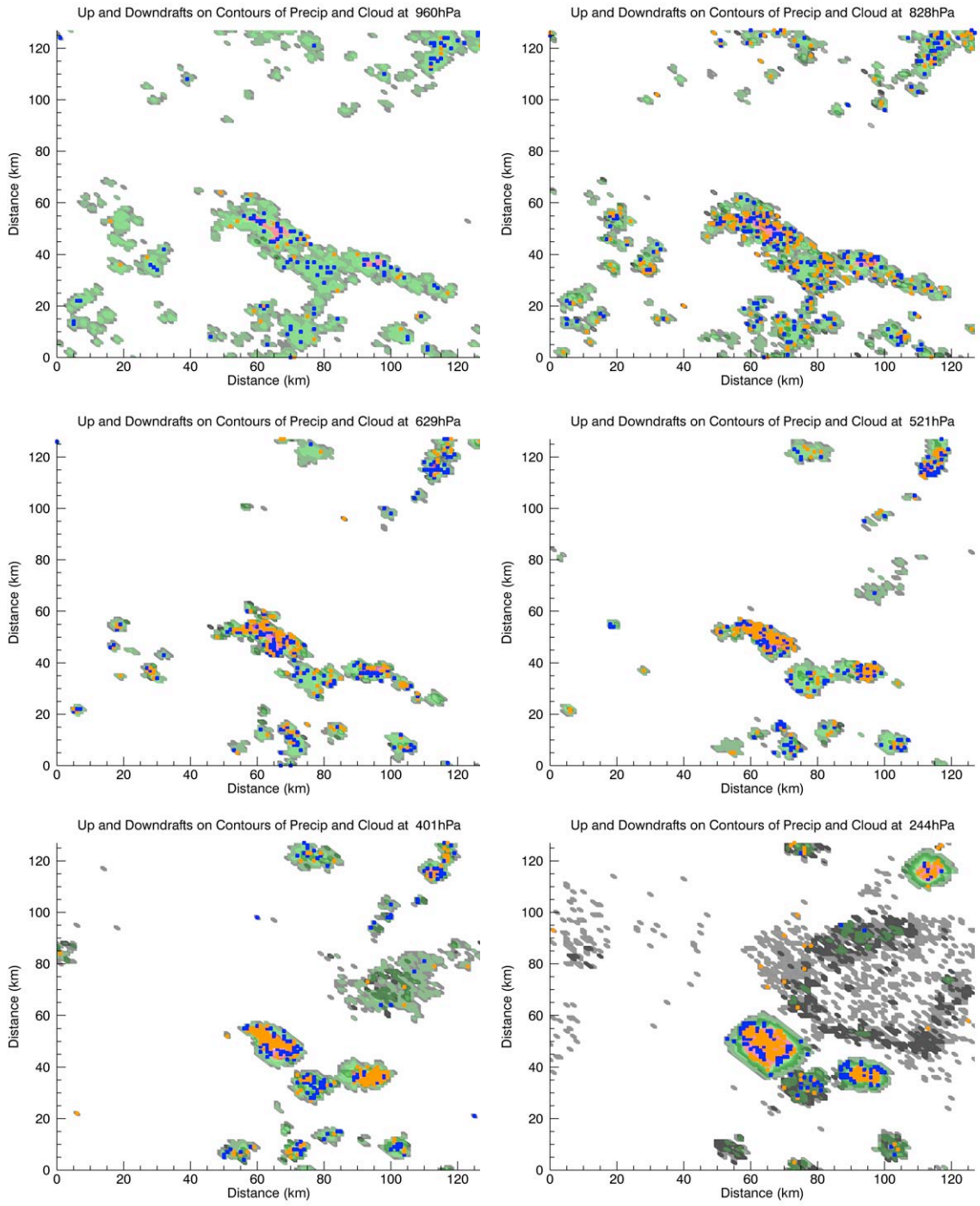

Figure 6.14. Horizontal cross-sections of the domain at increasing height (left to right, top to bottom) showing precipitation (green and pink contours), cloud (gray contours), updraft gridcells (orange squares) and downdraft gridcells (blue squares) for one three dimensional snapshot during TOGA.

updrafts and downdrafts designated, even at the top of small clouds. In the upper levels (bottom row), we enter the evaporating precipitation and cloud field from the anvil of the main convective tower. Interestingly, even though this precipitation evaporates before completely reaching the surface, it does not form a deep or penetrating downdraft. In fact, there are not as many downdraft cells in the anvil as there are surrounding the core precipitating regions and updrafts. It looks like this cloud tower has two deep updraft cells, which contain warm, moist, heavily precipitating air. At the edges of the cloud, where precipitation would slough-off and evaporation of cloud water can occur, downdrafts dominate.

It is difficult to diagnose exactly which process dominates in producing negative buoyancy. Condensate loading is clearly an important aspect, and the fact that our downdrafts are not very sensitive to environmental relative humidity suggests that they are mainly driven by precipitation loading. However, they do contain negative temperature anomalies at many heights above cloud base, and those are likely formed through evaporation of either cloud water or precipitation. Based on these results, it seems both processes are important in this model, and neither one should be dismissed as secondary.

Recommendation: Downdrafts should be tightly correlated to the available precipitation, but also sensitive to evaporation.

The goals of climate models have shifted in the past few years, from attempting to accurately simulate annual and monthly-mean climate patterns, to better simulation and even prediction of seasonal and sub-seasonal variability. These are lofty goals, and it is not surprising that models often struggle with convectively-coupled variability in phenomena such as the MJO and the monsoon. Convection is a complex and multi-scale process that is difficult to capture in the statistics and generalizations of convective parameterization. Downdrafts are clearly one of many possible weak areas in today's global climate models.

The results of this chapter suggest several possible areas of improvement in coupling convection to mid-tropospheric relative humidity.

1) The likely best method for ensuring that deep convection mainly occurs in a moist environment is to improve the formulation of convective entrainment. Downdrafts in our model are dependent on precipitation, and not very sensitive to environmental relative humidity, so cannot be used to regulate convection in this way.
2) Downdraft cooling is directly linked to precipitation evaporation, and evaporation is directly linked to the amount of precipitation. While the fraction of precipitation that can be evaporated is variable, the logarithmic distribution of precipitation means that high precipitation periods have orders of magnitude more potential cooling available than low precipitation periods. Heavy precipitation periods can have a higher precipitation efficiency, but still evaporate plenty of precipitation to drive intense downdrafts at the same time.
3) Above cloud base, downdrafts often have positive MSE perturbations. They are negatively buoyant due to cool temperature perturbations *and* condensate loading. The weight of cloud water and precipitation should not be neglected in a downdraft parameterization.
4) Downdrafts in our model form in the regions of clouds where intense precipitation and relatively dry environmental air interact. This allows for both evaporation and condensate loading to drive negatively buoyant drafts.

It should be noted that precipitation evaporation is a microphysical process, and dependent on a range of factors from the phase of precipitation (ice or liquid) to the droplet size distribution and the local wind dynamics. Our models uses only a single moment microphysical scheme, which may slightly simplify these interactions unrealistically. A necessary direction for future research would be to determine the impacts of microphysics on downdraft cooling, and ensure that our convective parameterizations are in-line with those relationships.

Chapter 7: Downdrafts and Wind Shear

Assumption: The impact of wind shear on downdrafts can be neglected.

Many convective parameterizations with simple saturated downdrafts allow just enough precipitation to evaporate to keep the downdraft saturated as it mixes with dry environmental air. The amount of mixing is determined by the downdraft mass flux, which is often a prescribed fraction of the updraft mass flux (Tiedke, 1988; Zhang and McFarlane, 1995; etc). None of these parameterizations take into account vertical wind shear in their formulations.

The impact of vertical wind shear on downdrafts has been investigated previously. Weisman and Klemp (1982) show that storms in a no-shear environment have downdraft outflows that cut-off warm updraft inflows. Storms in a weak to moderate sheared environment have new cells form on the edges of the outflow, as shear adds to the convergence at the edges of the cold pool. Abel and Shipway (2007) suggest that shear can tilt updrafts in the trade-wind regime, allowing more precipitation to fall out of the upper portions of the cloud. These updrafts have less condensate loading and are more buoyant, and the downdrafts have more evaporation and are more negatively buoyant. Kirkpatrick et al. (2009) examine seven controlled parameters in 139 simulations looking for the environmental variables that most closely correlate to the strength of updrafts and downdrafts. They find downdrafts to be very complex and nonlinear, but the best parameters are shear strength and column temperature. Storms in stronger shear environments organize to produce more intense downdrafts, and storms in warm columns have deeper layers for the warm rain processes that drive downdrafts.

These studies generally support the idea that a sheared profile adds to updraft tilt and stronger convergence along the edges of downdraft outflow boundaries. This creates more organized convective systems, with powerful up- and downdrafts. Shear can help tilt updrafts, allowing precipitation to fall out of the cloud and through dry air. Updrafts are then free of their

condensate load and can be more buoyant, and downdrafts form in the shafts of precipitation with enhanced evaporation as they are more exposed to the dry environment.

This is applicable in the tropics as well, as equatorial waves have enhanced vertical wind shear. Kiladis et al. (2009) show that many tropical waves are associated with tilted regions of temperature and moisture perturbations, and both low and upper level wind shear. Convectively coupled Kelvin waves have convergence near the surface and divergence aloft, resulting in a deep layer of zonal wind shear. Equatorial Rossby waves, which follow the passage of an MJO event, create a huge region of low-level intense westerly wind, with easterlies in the upper levels, behind the convective envelope. These wind shear profiles come hand-in-hand with organized convectively-coupled tropical waves. It is difficult to say if the winds are the result of the organized convection, or if the winds are instrumental in organizing the convection (Kiladis et al., 2009).

Despite the observed impact of shear on the organization of convection and convective processes, there are almost no convective parameterizations that include the impact of shear. Kain and Fritsch (1990) published a convective parameterization that linked precipitation efficiency (and thereby the downdraft/updraft mass flux ratio) on vertical shear and cloud base. However, in the most recent revision of this parameterization (Kain, 2004), this dependency is removed. Another of the few convective parameterizations that proposes to include the effects of updraft tilt is Cheng and Arakawa (1997). This parameterization includes a detailed rain water budget, and liquid water loading effects on the buoyancy of up- and downdrafts. They also include the effects of a tilted updraft, modeling the geometry of an updraft plume as a cylinder, which can be either vertical or have as much as a 55-degree tilt. This tilt allows precipitation to fall out of the cloud and create stronger up- and downdrafts as a result. While Cheng and Arakawa (1997) mention that shear could be an influence on the tilted structure of the updraft, they choose the actual tilt angle to be the smallest angle that produces a stable solution for their cloud model. The result is that wind shear does not actually impact their convective parameterization at all.

To examine the impact of shear on downdrafts, we use our model in a type of weak temperature gradient approximation large-scale forcing (Sobel and Bretherton, 2000; Raymond and Zeng, 2005; Raymond, 2007). In the tropics, temperature anomalies are quickly dispersed through gravity wave activity, so most of the tropics exist in the same mean vertical sounding profile. We simulate this process in two steps. The first step defines the basic mean profile by running an un-forced simulation of radiative-convective equilibrium. In our case, we run this simulation with a fixed high surface temperature (303K), and initialize with a moist tropical sounding. There is no diurnal forcing, no Coriolis effect, and no seasonality. There is no large-scale wind or radiative forcing either. This run lasts 50 days, and we average the temperature and moisture profiles over the last ten days to create our "basic state."

We then run the model three more times, with each run nudged back to the basic state temperature and moisture profiles (as would be required to create the weak temperature gradient of the tropics). Each one of these three nudged simulations are run for 30 more days, and forced with a different large-scale wind profile. The nudging in each simulation occurs every two hours. Figure 7.1 shows the prescribed zonal (U) wind profiles that each simulation is nudged towards, and the

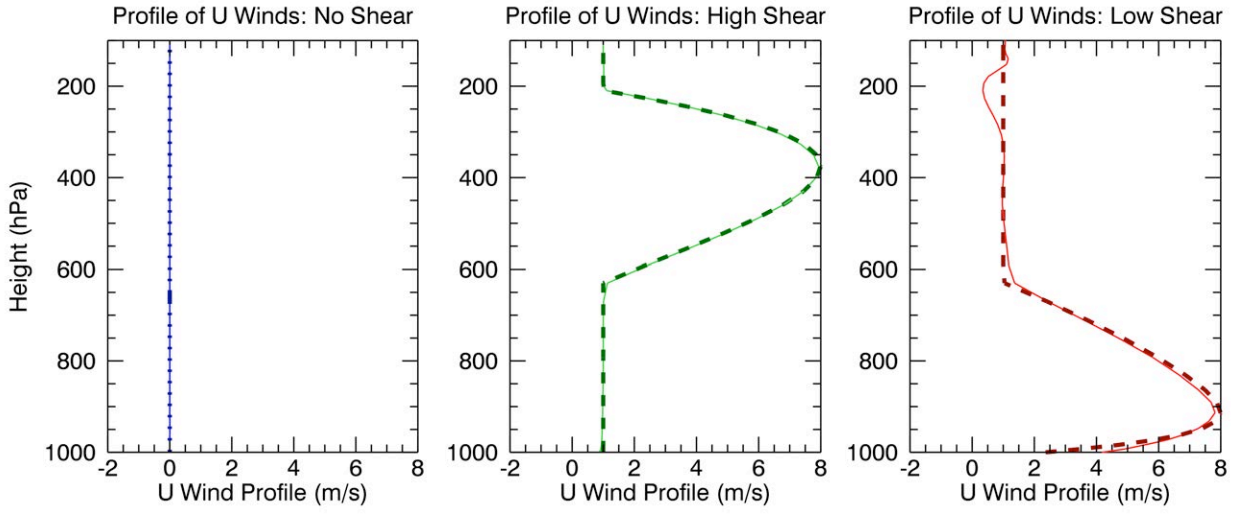

Figure 7.1. Prescribed zonal wind profiles for each weak temperature gradient simulation (dashed line), and average zonal winds simulated in the last 10 days of each run (solid line). Blue lines are the NS case, green lines are the HLS case, and red lines are the LLS case.

actual mean zonal wind profile of the last 10 days. There is no prescribed meridional wind or vertical lift in these simulations.

In our "No Shear" simulation (hereafter NS), the vertical profile of U winds is nudged to be zero at all levels. In our "High-Level Shear" case (hereafter HLS), the vertical profile of U winds is nudged to 1 m/s at all levels, except the convective layers above the freezing level. These are nudged to increase smoothly starting at just below 600hPa to 8 m/s around 400hPa, and then decrease smoothly back to 1 m/s. In our "Low-Level Shear" case (hereafter LLS), the vertical profile of U winds is again prescribed to be 1 m/s at all levels, except in the very lowest layers of the atmosphere. The wind is nudged to increase from 2 m/s at the surface to peak near the sub-cloud layer at about 900hPa and then decrease smoothly towards 1 m/s at the freezing level. We see in Figure 7.1 that the simulations adhere well to their nudged profiles in the NS and HLS cases, but the actual simulated winds in the LLS case are a bit different. The surface winds are twice as high as the nudging winds, and upper level winds near the tropopause are quite a bit lower than prescribed. This indicates that convection in this simulation is working to transport momentum out of the shear zone. All three simulations have the same nudging time scale, so it is interesting that the LLS case is the only one with this feature.

The LLS case does have much higher convective activity than the other two simulations. Figure 7.2 shows the time series of surface precipitation, integrated column water vapor, latent heat flux and sensible heat flux for the last 10 days of all three simulations. Clearly, the LLS simulation has much more precipitation, and much higher latent and sensible heat fluxes than the other two simulations. The increased surface fluxes could be the result of increased surface winds, and the higher energy inputs from these surface fluxes could help drive the more intense convection in the LLS case. However, the column water vapor in the LLS case is quite a bit lower than in the other two, indicating that convection is doing a better job of condensing and raining out the excess moisture from the surface.

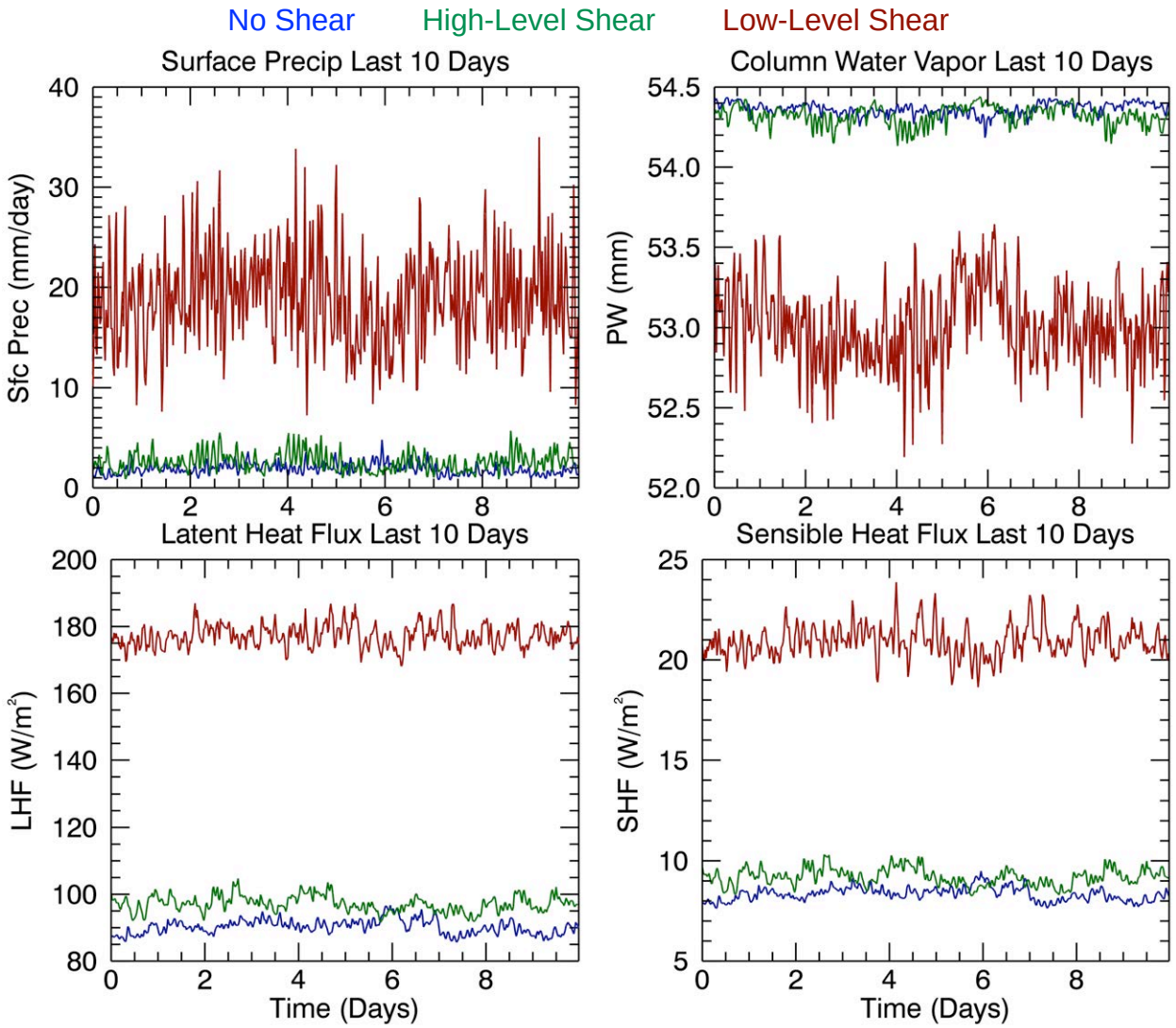

Figure 7.2. Properties of the three simulations shown for the last 10 days of their runs. Blue lines are the NS case, green lines are the HLS case, and red lines are the LLS case.

Several modeling and observational studies have pointed out the connection between low-level shear and the long-term maintenance and propagation of convective squall lines. Rotunno et al. (1988) show that low level shear creates vorticity anomalies that cause a convective updraft to tilt upshear, but the buoyancy anomalies in a cold pool incense an updraft to tilt downshear. When these tendencies are nearly balanced, the system becomes a long-lived, deep penetrating squall line, propagating normal to the shear. Nicholls et al. (1988) confirmed these findings and suggested that the impacts of precipitation loading and upper-level shear should be taken into account as well. They find that strong shear aloft results in tilted updrafts, and with the inclusion of environmental

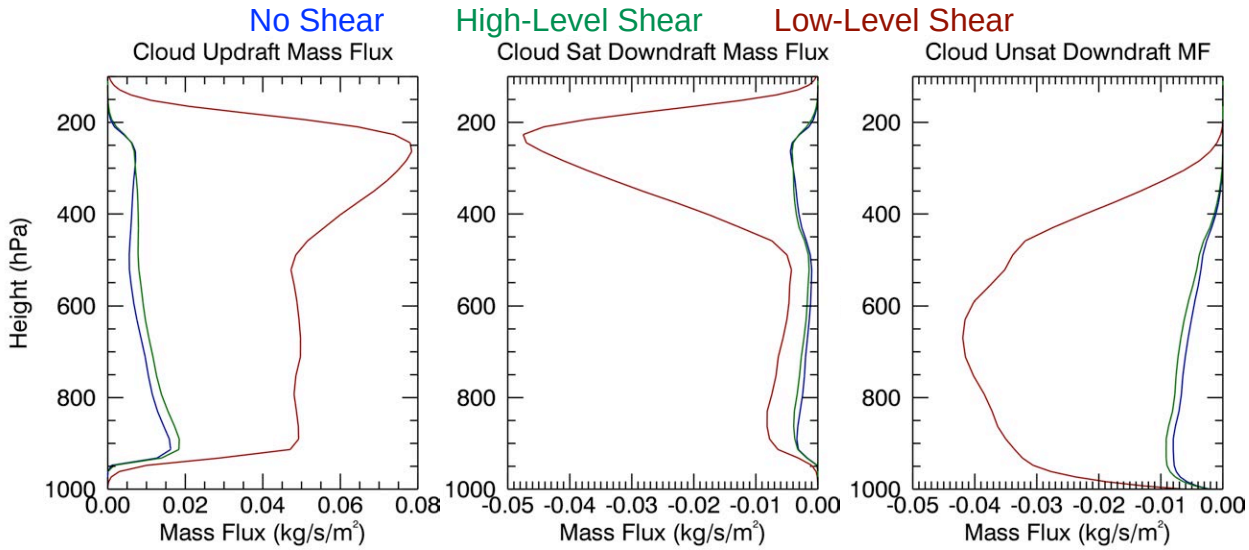

Figure 7.3. Vertical profiles of mean cloud updraft and downdraft mass fluxes from the last 10 days of each simulation. Saturated downdrafts have some cloud water/ice present, unsaturated downdrafts have only precipitation. Blue lines are the NS case, green lines are the HLS case, and red lines are the LLS case.

factors (such as a lower relative humidity in the mid-troposphere), can result in stronger, deeper cold-pools. Once a cold-pool becomes too large, and without balancing low-level shear, it can overrun the warm updraft source of the system and lead to the decay of the squall line.

Based simply on the theory that the presence of any shear creates tilted, and therefore stronger updrafts and downdrafts, it is surprising that the HLS case is so similar to the NS case. However, the findings of Nicholls et al. (1988) and other studies suggest that shear aloft is not conducive to convective organization. The HLS case has only slightly more precipitation, latent heat flux and sensible heat flux than the NS case. This is despite the fact that the HLS case does have an imposed large-scale wind at the surface as well, and strong upper-level winds that should be effective at tilting deep convective updrafts and creating more stratiform clouds and rain.

Profiles of the average updraft and downdraft cloud mass fluxes are shown in Figure 7.3. In this figure, we separate the downdraft into the "saturated" mass flux, that contains some cloud liquid water, and the "unsaturated" mass flux, that contains only rain. The LLS case has much more updraft mass flux through the entire column, and more downdraft mass flux as well. The increase in saturated, or in-cloud, downdraft mass flux is primarily in the upper levels, above the melting level

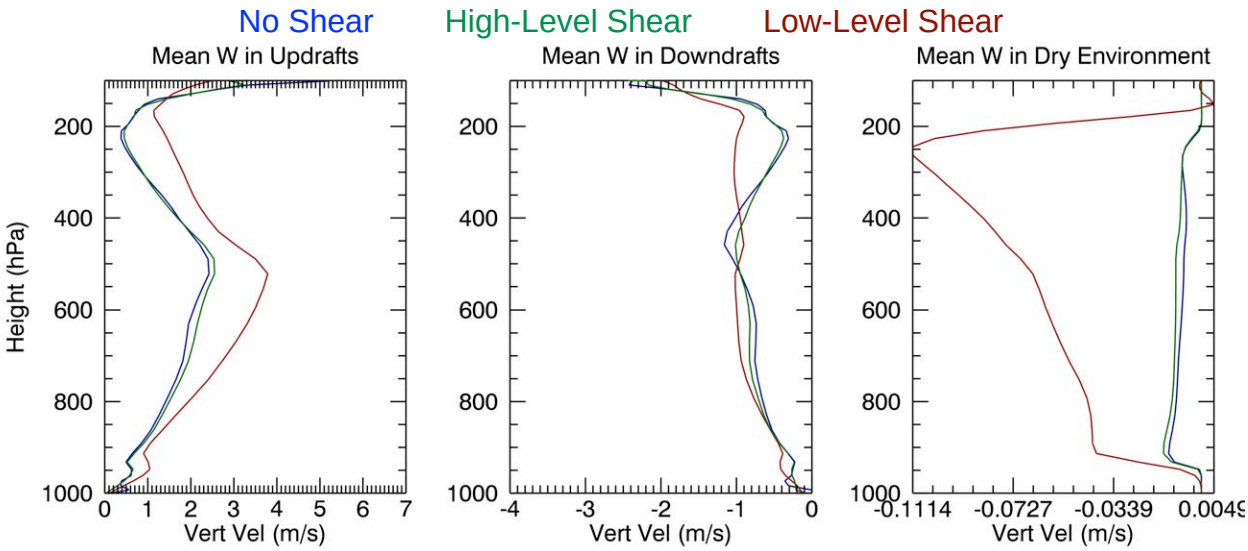

Figure 7.4. Vertical profiles of mean cloud updraft and downdraft, and dry environmental vertical velocities from the last 10 days of each simulation. Blue lines are the NS case, green lines are the HLS case, and red lines are the LLS case.

and above our shear layer. The increase in unsaturated, or out-of-cloud, mass flux occurs through most of the column, but is at its peak right where the shear level tops out at 650hPa. The huge increase in updraft mass flux is balanced primarily through this large increase in unsaturated downdrafts. If we expect these unsaturated downdrafts to increase the moisture in the column, then the decreased precipitable water in Figure 7.2 is surprising. However, the increased updraft mass flux

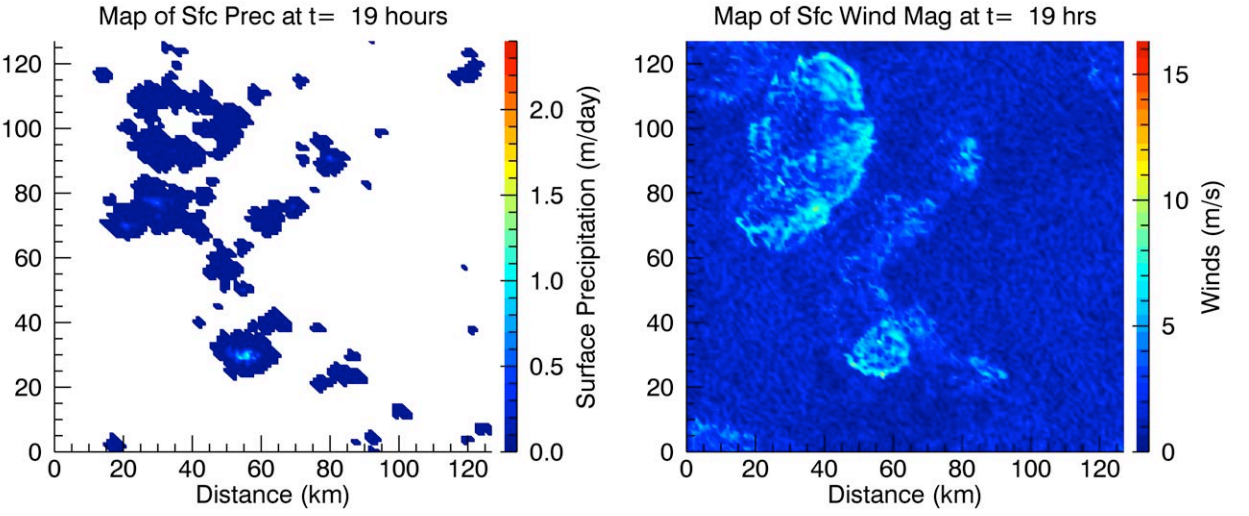

Figure 7.5. Map of surface precipitation (left) and surface wind magnitudes (right) from Day 20 (+19 hr) of the HLS simulation.

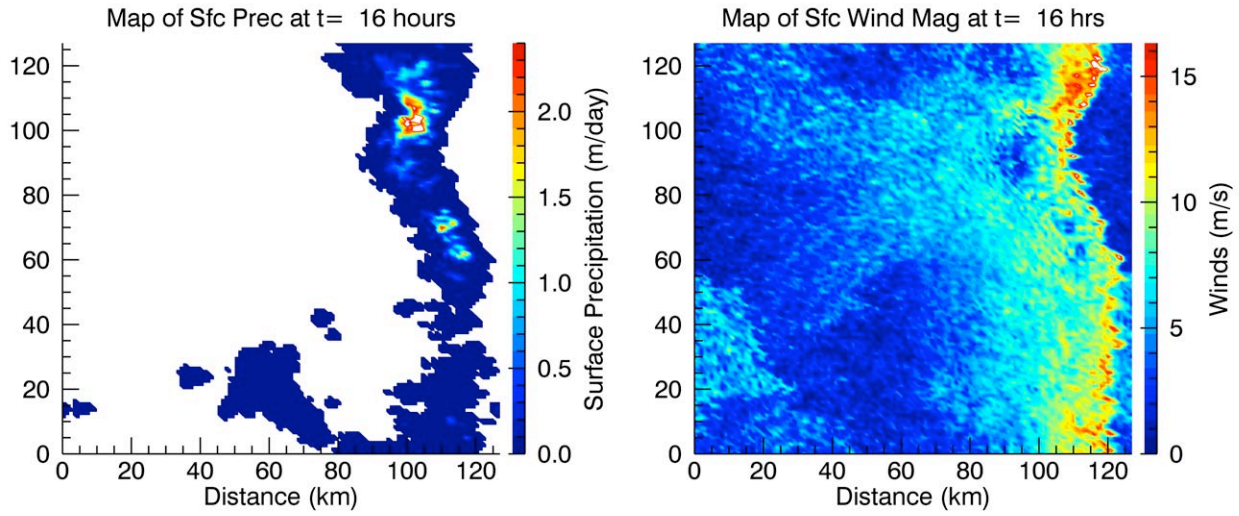

Figure 7.6. Map of surface precipitation (left) and surface wind magnitudes (right) from Day 20 (+16 hr) of the LLS simulation.

is also balanced by an increase in the dry environmental mass flux, which could be another explanation for the slightly dryer column in the LLS case.

Figure 7.4 shows profiles the mean vertical velocities of updrafts, downdrafts and the dry environment for the last 10 days of the simulations. In the LLS case, there is a significant increase in updraft velocity, very little change in downdraft velocity, and a very large increase in the mean vertical velocity of the dry environment. As expected from the drier environmental sounding, our between-cloud subsidence has increased dramatically in the LLS case. Especially in the upper levels where the unsaturated downdraft mass flux is less prominent. This creates a higher and stronger low-level inversion, and the vertical velocity profiles indicate that updrafts and downdrafts are both a little bit less intense in the region of this inversion (around 900hPa). The overall small increase in updraft velocity, and the very small increase in the intensity of downdraft velocity, in the LLS case is surprising given the increase in cloud mass fluxes shown in Figure 7.3. To get this result, the area covered by cloud mass fluxes must have increased instead.

What is happening to our convection that makes it so much more powerful in the LLS simulation? Figures 7.5 and 7.6 show maps of surface precipitation and wind magnitudes from a single 3-dimensional output time step. These were chosen almost at random from the last 10 days of

each simulation, where convection is in equilibrium, and these maps all look similar. In the HLS simulation, convection is disorganized and weaker. The precipitation field is dominated by a few scattered convective cells. The wind field indicates that these cells are strong enough to produce cold outflow, but the cold pools are nearly circular below the convection. In the LLS simulation, convection has organized into a single eastward-propagating band. It moves very quickly across the domain (with a period of approximately 4 hours). The gust front is east of the precipitation band, and consists of a strong north-south line of intense winds just ahead of the convection.

In the HLS and NS cases, the downdrafts are not powerful enough to enhance new convective elements, but their presence below the local convective updraft is enough to reduce the input of warmth and energy in that convective cell, as suggested by the results of Nichols et al (1988). The HLS case does not prevent the updraft from being co-located with its precipitation, especially in these warm clouds where most of the falling precipitation is located below the shear level. The LLS case has strong winds blowing along the converging regions of the cold pools, creating stronger convergence and more impetus for the production of new convection. These results follow those of Rotunno et al (1988), and we see the impact of cold pools balanced against

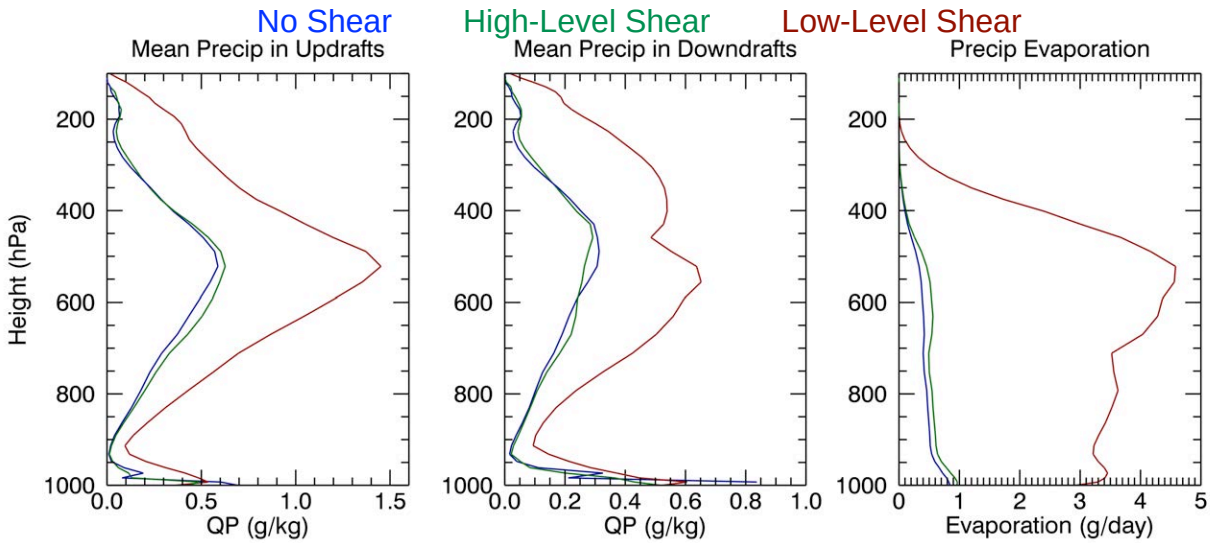

Figure 7.7. Profiles of precipitating condensate mixing ratios in updrafts (left) and downdrafts (middle), and the profile of evaporated precipitation (right) averaged for the last 10 days of the simulation. Blue lines are the NS case, green lines are the HLS case, and red lines are the LLS case.

low-level shear. Figure 7.7 shows the average mixing ratio of condensate in updrafts and downdrafts in the last ten days of the three simulations. The LLS case has more precipitation in both the updrafts and downdrafts. However, this occurs above the peak of the shear layer. Below 800hPa, the amount of condensate in the drafts of all three cases are more closely related. There is virtually no difference in condensate loading between the HLS and NS cases.

Figure 7.7 shows that evaporation is greatly enhanced in the LLS simulation. This could be due to the increased winds in the lower levels or to the increase in precipitation in this run. The effects of this increased evaporation on the downdrafts are important, though. Figure 7.8 shows that the downdrafts in the LLS run are slightly colder and far more moist than downdrafts in the other simulations. If the temperature anomaly and increased precipitation loading are stronger than the moisture anomaly, this could mean our downdrafts have lower virtual temperatures, and are more powerful downdrafts.

If we return to the idea of tilting due to shear, it is possible that the wind in the LLS case is strong enough to blow precipitation out of both the updrafts and the downdrafts in the shear layer. The profile of precipitation evaporation in Figure 7.7 shows that there is a large increase in this process in the LLS case. Is this the result of tilted updrafts or simply the presence of much more precipitation? Table 7.1 shows the mean and standard deviations of precipitation efficiency (as defined in Chapter 6) for the three simulations. The mean

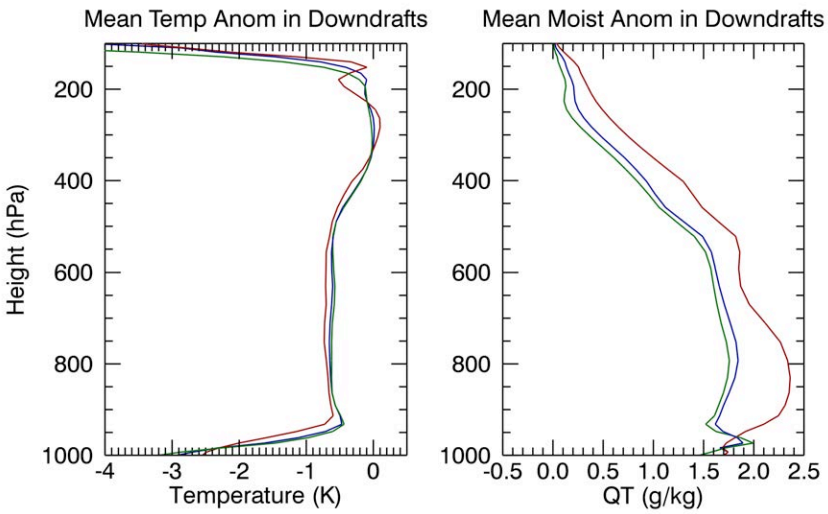

Figure 7.8. Profiles of temperature anomalies (left) and vapor +cloud water anomalies (right) averaged for the last 10 days of the simulation. Blue lines are the NS case, green lines are the HLS case, and red lines are the LLS case.

Table 7.1. Mean and standard deviations of precipitation efficiency, as defined in Chapter 6, for the last 10 days of all three simulations.

	Mean PrecEff	Standard Deviation
No Shear	**0.41**	**0.034**
High-Level Shear	**0.44**	**0.045**
Low-Level Shear	**0.43**	**0.060**

precipitation efficiency is almost the same for all three runs, but the standard deviation increases from the NS to the HLS case, and again to the LLS case. The standard deviation is not particularly large, suggesting even in the LLS case, 90% of the time period is within a range of only 0.24. Basically, the precipitation efficiency does not change much in these simulations, indicating that the evaporation is due mainly to the presence of increased precipitation, rather than environmental relative humidity.

We should point out that while downdrafts are colder and associated with more precipitation evaporation in this run, it is difficult to say that stronger downdrafts have produced more intense cold pools and convergence in the surface levels. The surface-level winds in the LLS case are slightly stronger than the other two, at 3.2 m/s instead of 1.0 m/s. To see if this is the cause of our increased convection, we did one more WTG simulation with a prescribed 3.2 m/s wind through the entire convective column, called the "No Shear 3.2" (NS3.2) case. Here the winds near the surface will be enhanced, but there are no shear effects in this simulation. The prescribed wind profile and actual mean winds for the last 10 days of the simulation are shown in Figure 7.9. The actual winds are very close to those prescribed for almost the entire column, though they are slightly lower near the surface. The precipitation for the run is shown in Figure 7.9 as well, with the time series of precipitation for the other runs as a comparison. This simulation does have a higher surface precipitation amount to balance stronger surface fluxes created by the large-scale wind field. But it is still not as much precipitation as we see in the LLS case where convection is organized into a propagating squall line. Figure 7.10 shows maps of the surface precipitation and surface wind

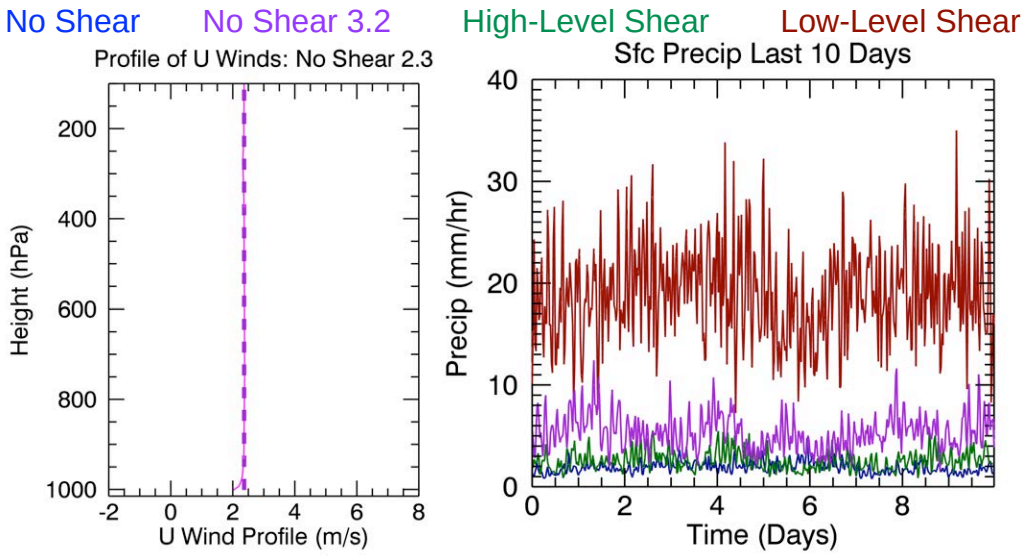

Figure 7.9. Prescribed profile of U Wind in the No Shear 3.2 case (left), and surface precipitation for the last 10 days of the simulations (right). Blue lines are the NS case, green lines are the HLS case, red lines are the LLS case, and purple lines are the NS3.2 case.

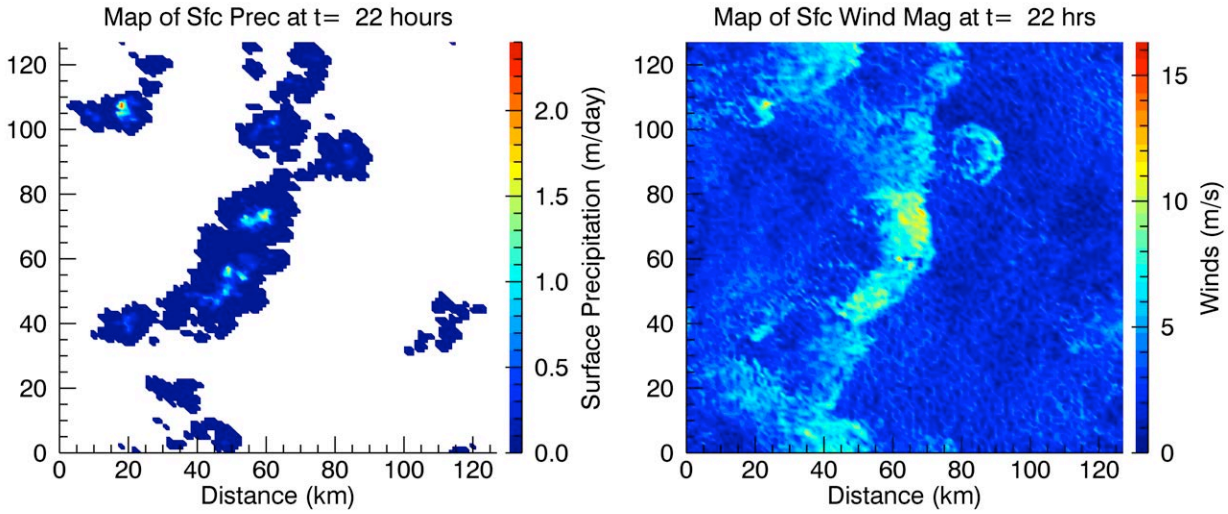

Figure 7.10. Map of surface precipitation (left) and surface wind magnitudes (right) from Day 20 (+22 hr) of the No Shear 3.2 simulation.

magnitudes for one example time period in the NS3.2 simulation. The convection in this case moves eastward at a pretty fast pace, and attempts to organize repeatedly, but is unable to build the wave structure seen in the LLS case.

The results of these simulations show that vertical wind shear does have a large impact on the organization of convective elements. Increased shear in the lower levels adds to the convergence created at the edge of cold pools and increases convective activity ahead of existing convective cells.

This leads to more and stronger updrafts, more condensation and precipitation formation, and more downdrafts. The presence of increased downdraft activity feeds back into the system, creating more potent cold pools, more gust front convection and resulting in a very intense propagating squall line. There is an increase in evaporation when low-level shear is present, but no change in precipitation efficiency, so it is difficult to say if tilting is the cause. Figure 7.11 shows 3D renderings of the precipitation fields from the HLS and LLS simulations. The HLS precipitation shafts are tilted, with the upper portions of the shafts further east than the bases of the tallest elements. The rain shafts, like the convective cells in this run, are scattered and disorganized. The squall line in the LLS case has a tilt as well, but the upper portions of these rain shafts are further west than the lower parts. This creates a profile of building and propagating convection, with shallow convection ahead of gradually deepening convection. As the mature cells rain out, their downdrafts enhance new convection along the gust front, and the system continues to the east.

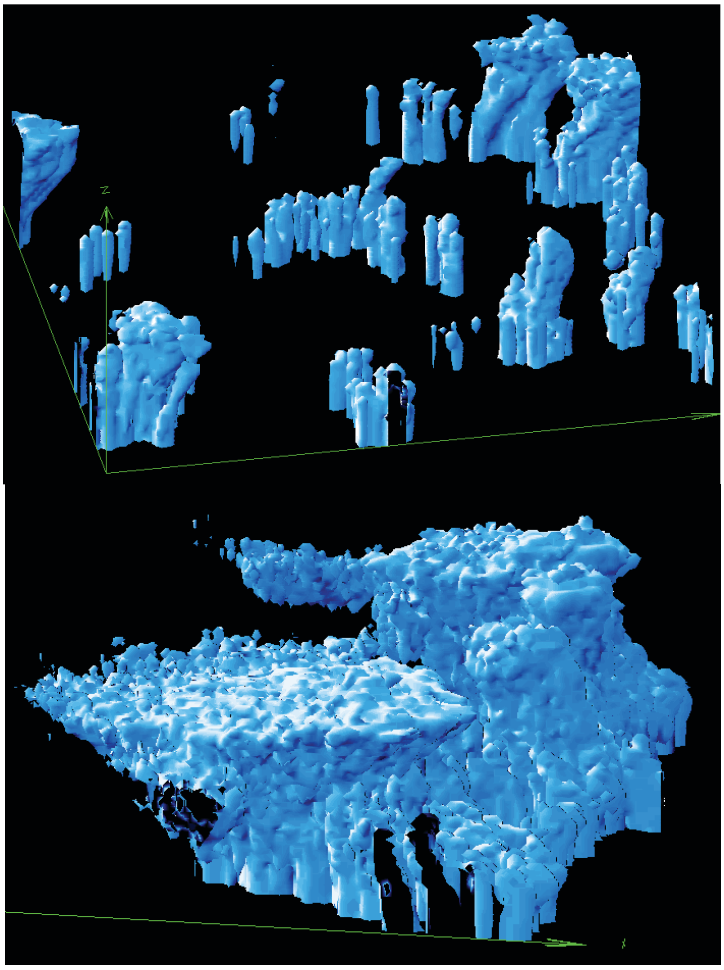

Figure 7.11. Three dimensional rendering of the precipitation fields from a single 3D snapshot of the High-Level shear case (top) and the Low-Level shear case (bottom).

Recommendation: Downdrafts should be influenced by low-level wind shear.

In this chapter we examined two different assumptions about the relationships between downdrafts (and convection in general) and wind shear in convective parameterizations. The first is that wind shear effects on convection are negligible. Our simulations, and many other studies, suggest that shear can help organize convection into systems that behave very differently from disorganized convection (Weisman and Klemp, 1982). The increased winds in and above the boundary layer, in particular, enhance downdraft convection and produce much stronger convective cells. The impact of shear on the organization of mesoscale convective systems has been studied for many years (eg. Houze, 1993), and recent work has focused on the impact of cold pool convergence on the propagation direction and speed of MCSs (Corfidi, 2003). Our results here are supported by much research from mesoscale meteorology, but the impacts of shear on tropical organization may not be as well understood (Kiladis et al., 2009)

The second assumption is that wind shear creates a tilted updraft structure, and rain falls out of the cloud, creating stronger downdrafts. The slight tilt of convective cells in our simulations can

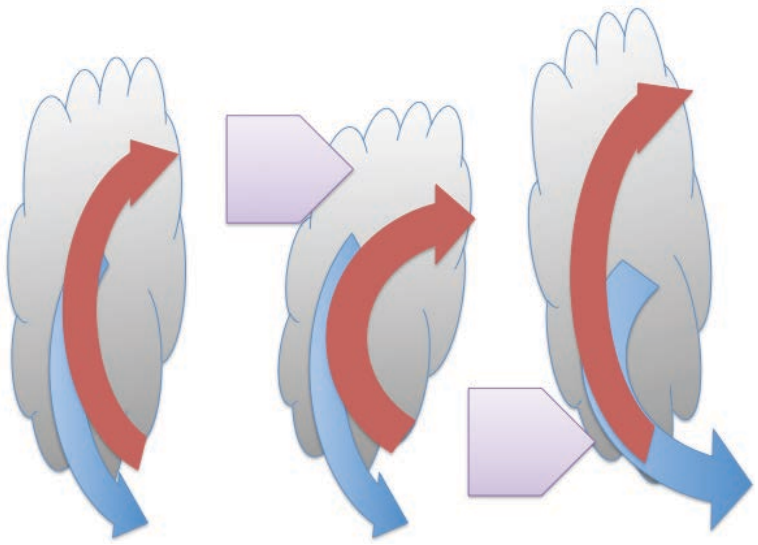

Figure 7.12. Schematic view of how increased winds impact the structure of convective updrafts and downdrafts in our study. The left-most cloud is vertical in an unsheared environment. The second cloud is tilted with increased upper-level winds. The right-most cloud is tilted the opposite direction with low-level shear.

be seen in both the cloud fields and the precipitation shafts. Our forcing winds are strong enough to tilt both the drafts and the precipitation shafts, not only the drafts as assumed in many studies (Cheng and Arakawa, 1997; Abel and Shipway, 2007). This means that updraft source regions are co-located with downdraft cold pools even in the presence of some vertical tilt. The difference occurs when the increased shear adds to the strength of downdrafts, and the cold pool convergence. This increases surface gustiness and increases the mechanical lifting of parcels. We diagram these effects in Figure 7.12.

This work addresses some important questions and assumptions made in the design of convective parameterizations, but does not point to a full parameterization of the downdraft-cold pool-shear relationship. To really quantify the impacts of low-level shear on convection, an ensemble study would be a good course of action. Performing multiple simulations with slowly increasing magnitudes and depths of the shear layer would build a dataset capable of illuminating the general relationship in question. However, our work here points out a possible weakness in current parameterizations that should be addressed in future development.

Chapter 8: Boundary Layer Quasi-Equilibrium

Assumption: Surface flux warming and moistening in the boundary layer is mainly balanced by downdraft cooling and drying.

Emanuel (1987; 1993) and Raymond (1995) propose that the tropical boundary layer exists in its own state of quasi-equilibrium. They show that the low-level moist entropy changes very little on a daily time-scale, and suggest that this is due mainly to a balance between surface fluxes and downdraft cooling. A simple theory known as boundary layer quasi-equilibrium (BLQE) is described clearly in Raymond (1995) as follows:

> "Convection can only occur when the boundary-layer equivalent potential temperature exceeds a threshold value determined by the tropospheric virtual temperature profile. Surface fluxes increase the boundary layer equivalent potential temperature and downdrafts from convection decrease it. This results in a balance in which the amount of convection, which scales with downdraft amount, is determined by the surface fluxes. Clear-air entrainment from above and direct radiative cooling of the boundary layer usually play only secondary roles in the boundary-layer budget of equivalent potential temperature." (Raymond, 1995)

Boundary layer quasi-equilibrium is the theory that downdrafts, and by extension all convective activity, are regulated by the amount of cooling and drying required to balance warming and moistening by surface fluxes. By this theory, entrainment from the environment is secondary to downdraft effects, and removal of high MSE by updrafts is unimportant within the boundary layer. On the other hand, Arakawa and Schubert (1974) suggest that increases in atmospheric CAPE created by surface fluxes in the boundary layer are balanced by entrainment of cooler, drier air in the cloudless environment.This is a basic disagreement that has wide ranging impacts for developing convective parameterizations. Should a convective parameterization balance low-level MSE build-up with convective downdraft activity or clear-air entrainment?

In our study, we do not question the fact that the tropics exist mainly in a state of equilibrium between large-scale destabilization and convective stabilization. We do, however, question the mechanism of convective re-stabilization. As CAPE is produced by surface fluxes and radiative cooling, does convection reduce CAPE mainly via downdrafts in the boundary layer, or is environmental entrainment more important? To investigate this balance and the processes involved, we simply calculate the moist static energy budget in the boundary layer. Moist static energy (MSE) for a parcel is defined in Chapter 5 eqn 3, and we write it again here for convenience,

$$h \equiv C_p T + gz + Lq_v \quad (1)$$

where C_p is the specific heat of dry air, T is the parcel temperature, g is the acceleration due to gravity, z is the height above the surface of the parcel, L is the latent heat of vaporization and q is the water vapor mixing ratio of the parcel.

Following Raymond (1995), but using MSE, we can write a budget for MSE averaged over the boundary layer of our model as

$$\frac{\partial h_b}{\partial t} = Q_{hb} + \frac{F_s}{z_{bl}} - \frac{\overline{wh}}{z_{bl}} + LS_{hb} \quad (2)$$

where, Q_{hb} is the net radiative heating of the boundary layer, F_s are the surface fluxes, and LS_{hb} are tendencies due to prescribed large scale forcing (advection and lifting). The third term on the right-hand side of Equation 2 is the cooling due to the transport of MSE across the top of the boundary layer. Even though MSE contains both moisture and temperature terms, we use the term "cooling" to, somewhat colloquially, indicate a reduction in MSE throughout this chapter. In this transport term, w is the vertical velocity and h is the MSE in each gridcell, and the bar is a mean over the entire top of the boundary layer. The top of the boundary layer can be defined or calculated in many different ways, for simplicity we use 500m through the entire simulation. Each of the right-hand side terms are relatively easy to calculate, except for the exact flux of h. Our model, SAM, uses a positive-definite monotonic advection scheme (Khairoutdinov and Randall, 2003; Smolakiewicz and

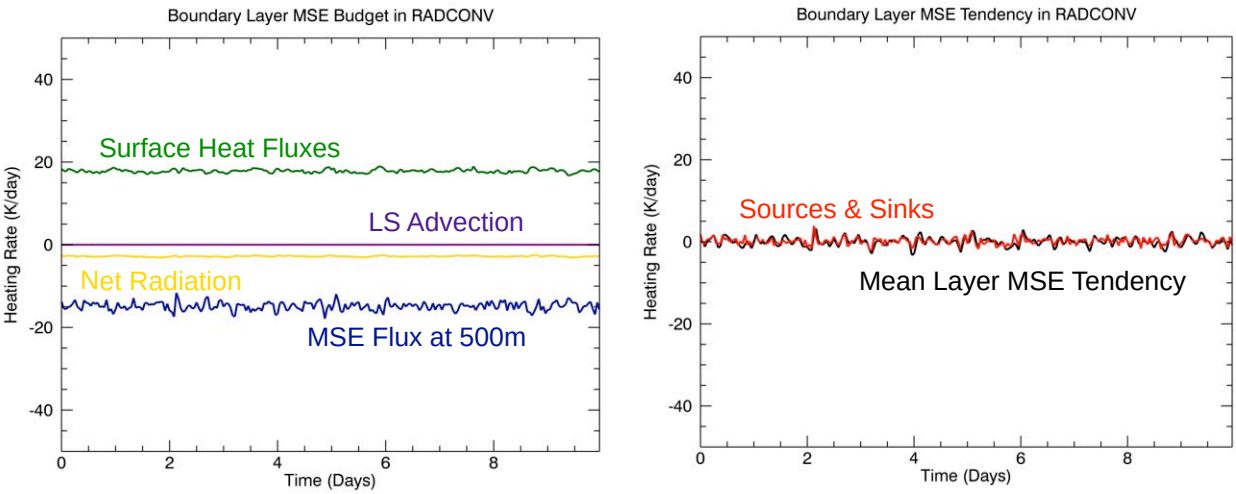

Figure 8.1. MSE budget for the boundary layer during the last 10 days of the RADCONV run. Sources and sinks (left) and their total compared to the BL MSE tendency (right).

Grabowski, 1990). We approximate the vertical advection using the local vertical velocity only, and this is less accurate as the gradient of MSE gets larger near the top of the boundary layer.

The results of this calculation for the last 10 days of the RADCONV simulation are shown in Figure 8.1. This is a simple simulation with a large, constant surface temperature but no large-scale lifting or forcing. The tendency of the total boundary layer MSE is shown as a heavy black line in the right panel, and the sum of all the terms from the right-hand side of Equation 2 is a corresponding red line. The boundary layer MSE changes very little in this simulation, and sources and sinks of MSE are well balanced. As expected from the budget, the surface flux inputs to the boundary layer are balanced by radiative cooling and cooling through the fluxes of MSE into and out of the boundary layer. The relative impacts of the convective fluxes and the environment are not shown in these figures. To do this, we need to break apart the flux of MSE into its eddy terms. If we allow both the vertical velocity and the MSE to be composed of a mean value and the deviations from that mean, we can write

$$wh = \left(\overline{w} + w'\right)\left(\overline{h} + h'\right)$$

$$\overline{wh} = \overline{\overline{w}\overline{h} + w'\overline{h} + \overline{w}h' + w'h'}$$

$$\overline{wh} = \overline{w}\,\overline{h} + \overline{w'h'} \quad (3).$$

In our model, the mean vertical velocity is zero, and the mean of all deviations must be zero, so we do not have the two middle terms. In Equation (3), we are left with the transport by the mean vertical velocity and the eddy covariance of vertical velocity and MSE. In our model, the vertical velocity is required to be zero at each level, so the first term on the right hand side of (3) is zero. While the mean vertical velocities of updrafts, downdrafts and the environment are not zero themselves, if we calculate an average flux of MSE for each type, they all sum to zero and are not a part of the eddy flux of MSE that actually balances surface fluxes. Because the mean vertical velocity is zero at each level, the advection of MSE must be due entirely to eddy fluxes.

We now separate the transport of MSE according to draft type. Because we are dealing with boundary layer cloud effects, we use the more inclusive cloud fluxes here. All air moving upward in a cloud is considered "updraft" transport, all air moving downward in a cloud or precipitation shaft is considered "downdraft" transport, and all clear air outside of clouds is categorized as the "environment." Figure 8.2 shows the flux of MSE at 500m separated into eddy covariances for updrafts, downdrafts and the environment. Here, we are plotting

$$\overline{w'h'} = \left(\overline{w'h'}\right)_{UD} + \left(\overline{w'h'}\right)_{DD} + \left(\overline{w'h'}\right)_{ENV} \quad (4).$$

By Equation (3), the sum of these eddy covariances is the same as the total flux of MSE shown in Figure 8.1. All three terms contribute to the cooling and transport of MSE across the top of the boundary layer. Updrafts lift excessively warm parcels, leaving the boundary layer cooler. Downdrafts inject parcels with lower MSE, and the environment can do either through a multitude of turbulent eddies. However, unlike the the balance as described in Emanuel (1993) and Raymond (1995), in Figure 8.2 we see that the majority of the boundary layer cooling is done through environmental entrainment, and not downdrafts. For the last 10 days of the RADCONV run, environmental eddy covariance accounts for 3-4 times more cooling than the downdrafts. This is

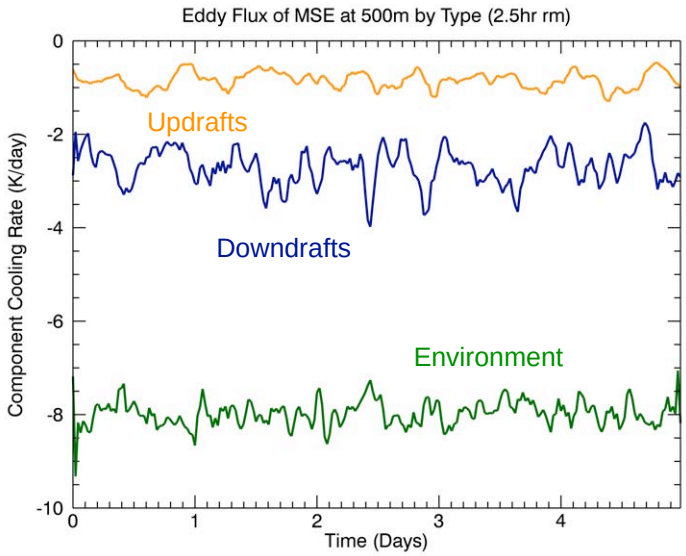

Figure 8.2. Eddy covariances of vertical velocity and MSE at 500m averaged over the whole domain during the last 10 days of the RADCONV run with a 2.5 hour running mean. These are multiplied by -1 to allow the upward (out of the BL) transport of MSE to be a sink or cooling term.

surprising, because we have shown that downdrafts are colder than the environment in the boundary layer, and that the average mass fluxed by downdrafts is much larger than that of the environment. Indeed, the net transport of MSE for downdrafts is *much* larger than that for the environment (not shown), but again, this is balanced by updraft transport and these terms sum to zero and do not contribute to the overall cooling of the layer in our model. In the end, the environment has a larger impact because there is so much more of it. When you average the eddy fluxes of downdrafts and updrafts over the entire domain, they have difficulty competing with the wide area of entrainment from the dry environment.

Our RADCONV simulation really only encompasses light tropical convection. A more realistic simulation of tropical convective variability is our TOGA run. The budget for MSE (as given in Equation 2) for the TOGA simulation is shown in Figure 8.3. In this case, a large-scale forcing term is added because of the forcing data that drive the simulation. Also, our net radiation term now includes a solar cycle. In this case, the boundary layer MSE tendency is far more variable. It fluctuates between more than -20 and nearly +20 K/day during the simulation. In periods of suppressed convection between days 11-15, when the gradient of MSE at the top of the layer is very

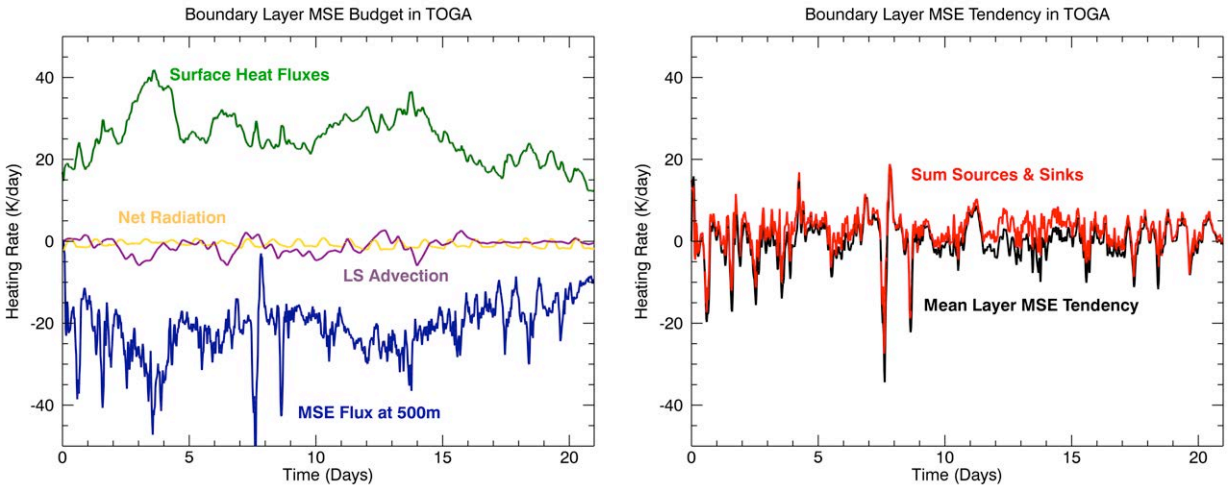

Figure 8.3. MSE budget for the boundary layer during TOGA run. Sources and sinks (left) and their total compared to the BL MSE tendency (right).

strong, our approximation to the advection scheme used in SAM breaks down and the budget does not quite match the actual MSE tendency. This simulation has much more active convection, and the flux of MSE is, of course, the main cooling source to balance the increased surface fluxes.

Again, we break apart the flux of MSE into its eddy components in order to ascertain the relative importance of downdrafts and the environment in these convectively active regions, shown in Figure 8.4. Interestingly, these results are even more contradictory of the hypothesis of downdraft

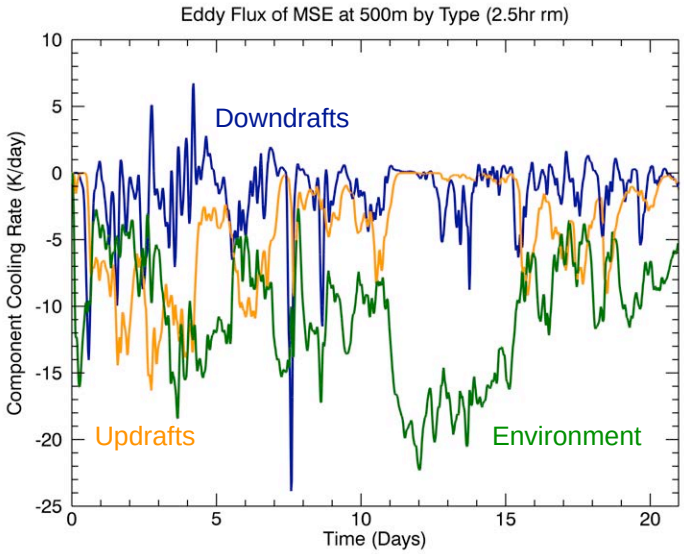

Figure 8.4. Eddy covariances of vertical velocity and MSE at 500m averaged over the whole domain during the TOGA run with a 2.5 hour running mean. These are multiplied by -1 to allow the upward (out of the BL) transport of MSE to be a sink or cooling term.

dominance proposed in Emanuel (1987; 1993) and Raymond (1995). Through most of the simulation, the environmental fluxes dominate the cooling term again, and the updraft cooling term is stronger than downdrafts as well. There are only a very few instances where downdraft cooling dominates. In the very convectively active MJO-like period of days 1-7, updrafts cool more than the environmental entrainment. And, in these days, downdrafts often have a negative eddy covariance (shown in Figure 8.4 as a positive heating rate), where they are warming the boundary layer rather than cooling it. We discussed in Chapter 6 the observation that downdrafts in our model often have positive MSE perturbations through a large part of our column. In these regions, the eddy covariance of MSE in downdrafts would be negative, and show up as a warming in our layer.

In our TOGA simulation, the downdraft cooling term is not as strong as the environmental entrainment term. Again, this is mostly because the amount of area covered by downdrafts and their cooling is much smaller than the environmental entrainment area. However, Figure 8.5 gives us another clue as to why downdrafts may not influence the boundary layer MSE very much, especially in high convective periods. These plots show the average vertical profiles of updraft, downdraft, and environmental MSE in the lowest 2000m of our domain. Generally, the profile of MSE is assumed to be similar to the green line in the left panel of Figure 8.5. There is a well mixed region in the

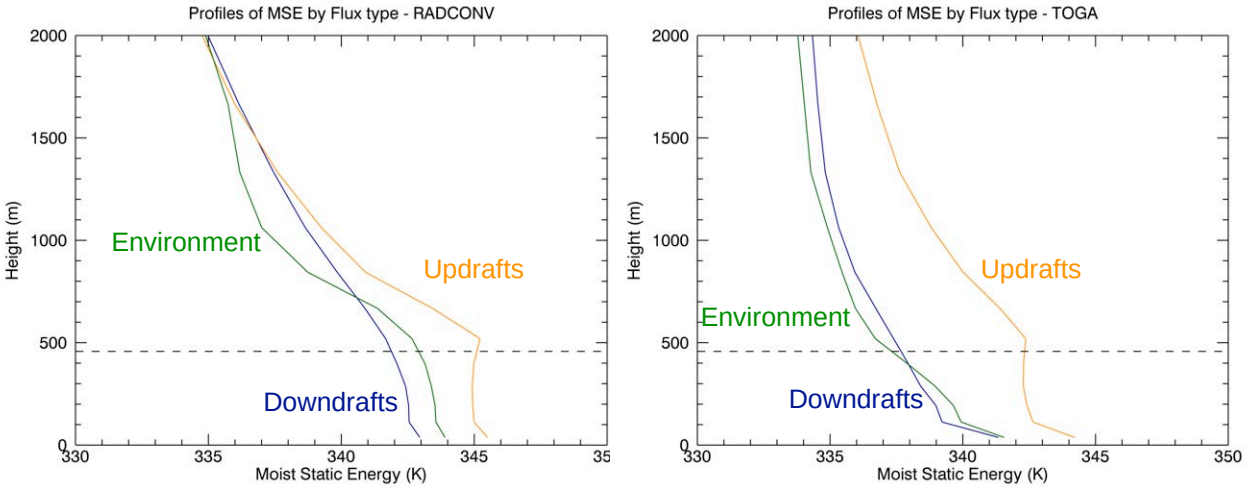

Figure 8.5. MSE profiles in the lowest 2000m. The top of our boundary layer is marked as a dashed line. The RADCONV profiles are averaged over 1 day, the TOGA profiles averaged over 1 hour.

boundary layer where the MSE does not change much with height. There is then a rapid drop-off in the dryer troposphere above cloud base. Updrafts have a high MSE for most of their profiles, but downdrafts are cooler only below the discontinuity at the top of the boundary layer. Above this, downdrafts are often in cloudy or moist regions, and have higher MSE than the environment (see Chapter 6 for more discussion). The right hand panel in Figure 8.5 shows that the top of the mixed layer does not stay above our 500m level all of the time in TOGA. In periods of intense convection, the well-mixed sub-cloud layer is very shallow, and downdrafts bring their high MSE anomalies down into the lowest levels.

We also note that the mean MSE anomaly for downdrafts is much closer to the environmental profile than updrafts are in our model. This is shown well in the updraft and downdraft MSE PDFs in Chapter 5 (Figure 5.11). This means that even though updrafts are a very small portion of the overall domain, if their anomalous vertical velocity and MSE are high enough, they can create a significant mean eddy covariance in the domain. The fact that updrafts have a stronger cooling here is not completely unrelated to downdrafts, of course. We showed in Chapter 5 that updrafts have a higher MSE that is associated with convergence around the edges of cold pools.

To examine one more case with intense downdrafts but a system in near steady-state, we can take a quick look at the Low Level Shear (LLS) weak temperature gradient simulation discussed in Chapter 7. The MSE budget and tendency for the last 10 days of this simulation is shown in Figure 8.6. Here, the surface fluxes are higher, and the compensating flux of MSE across the 500m level is higher as well. The tendency of MSE in the boundary layer is much more stable than in the TOGA simulation, and oscillates between about -5 and +5 K/day. In this simulation, we see much less radiative cooling than in the RADCONV case, because more than half of the domain is covered in deep convective clouds at any given time (see Chapter 7). The break-down of eddy MSE fluxes is shown in Figure 8.7, and, as before, the environmental entrainment dominates. In this case, however, updrafts and downdrafts are more equivalent in their amount of cooling. Downdraft cooling is

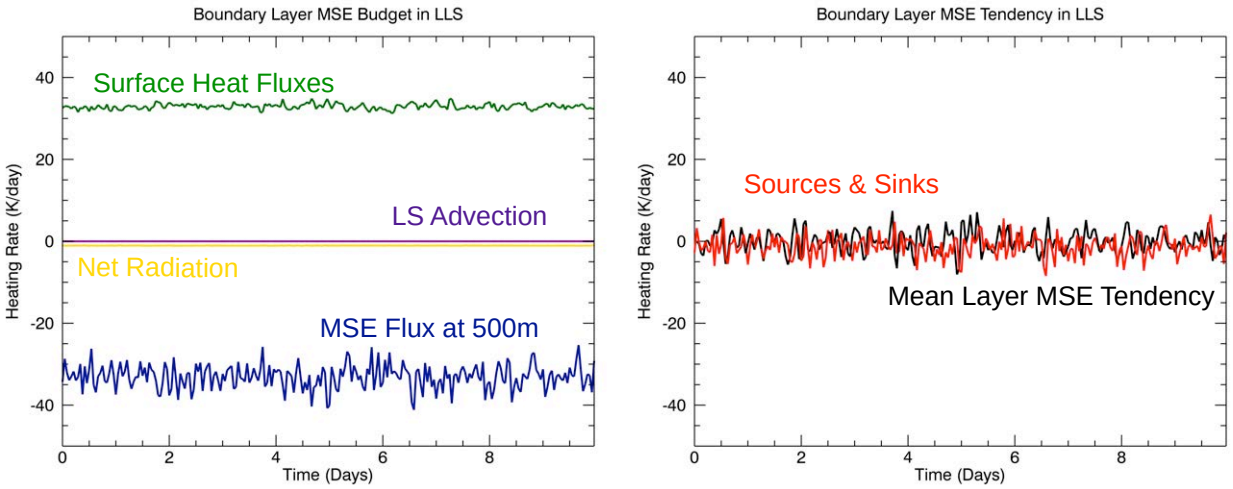

Figure 8.6. MSE budget for the boundary layer during TOGA run. Sources and sinks (left) and their total compared to the BL MSE tendency (right).

clearly more variable, but updraft cooling in this case is much stronger than in the RADCONV case. The average profiles of MSE in Figure 8.8 show us that the mixed layer is deep in this simulation, and that the drop-off into dry tropospheric MSE values is not quite as steep as that seen in RADCONV. Updrafts have a very high MSE anomaly, and this probably contributes to the extra boundary layer cooling seen in Figure 8.7.

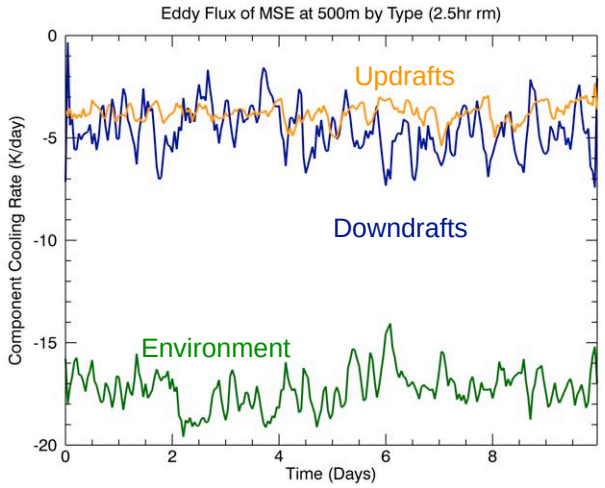

Figure 8.7. Eddy covariances of vertical velocity and MSE at 500m averaged over the whole domain during the last 10 days of the LLS run with a 2.5 hour running mean. These are multiplied by -1 to allow the upward (out of the BL) transport of MSE to be a sink or cooling term.

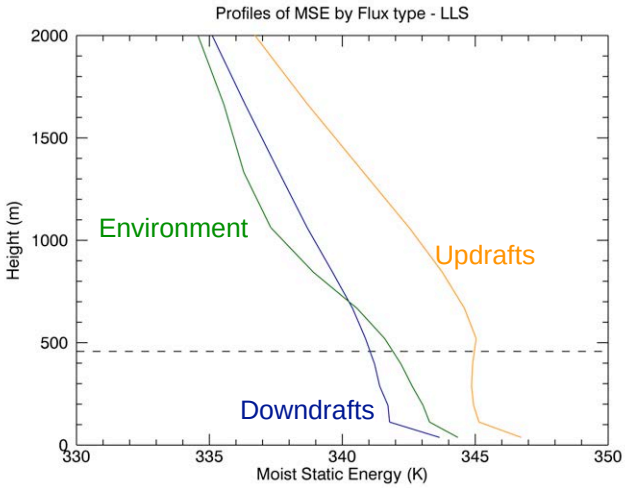

Figure 8.8. MSE profiles in the lowest 2000m of the LLS run, averaged over 1 day. The top of our boundary layer is marked as a dashed line.

Our results do not support the boundary layer quasi-equilibrium hypothesis proposed by Emanuel (1987; 1993) and described in Raymond (1995). Tropical quasi-equilibrium is well supported by both observations and our results here. The MSE of the boundary layer in our simulations stays relatively constant - even in the TOGA simulation, there are no persistent increases and decreases in MSE. However, the mechanisms required for this are more complex than a simple balance involving mainly downdrafts. Radiation and large-scale influences are very minor, but the major source of boundary layer cooling is the environment, not downdrafts.

In our study, we have shown that downdrafts move plenty of mass downward, and they increase the variability of the boundary layer. It is possible that downdrafts might not be a major source of low MSE, but they could still influence the cooling of the boundary layer. Environmental entrainment occurs by wave breaking and turbulent mixing at the top of layer. Without these turbulent disturbances, the stable layer at the top of the boundary layer would keep cooler environmental air from being entrained. It is possible that downdrafts and cold pool gust fronts could increase environmental entrainment by increasing the turbulence in the clear air boundary layer.

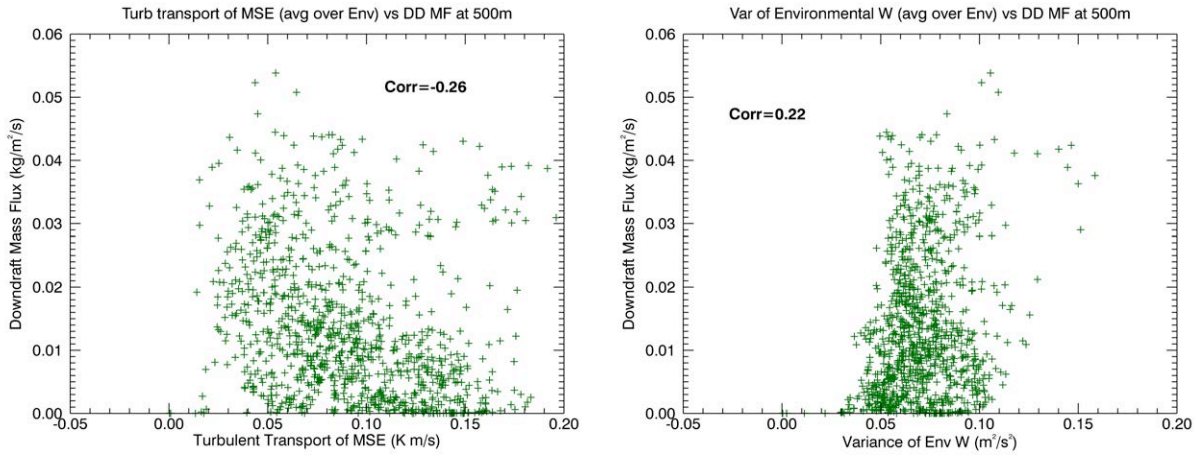

Figure 8.9. Correlation between turbulent transport of MSE by the environment, averaged only over environmental gridcells versus downdraft mass flux (left). Variance of environmental vertical velocities at 500m averaged only over the environment versus downdraft mass flux (right).

We look at the relationship between environmental turbulent transport of MSE and downdraft mass flux in Figure 8.9. Here, we average the environmental flux variables only over the environmental gridcells, to try to capture the turbulent motions rather than mean subsidence. The turbulent transport of MSE by the environment at 500m is not well correlated with downdraft mass flux at only -0.26. And the negative correlation suggests that turbulent entrainment in the environment decreases when downdrafts become more active. However, the variance of environmental vertical velocity has a small positive correlation. Our hypothesis that downdrafts increase boundary layer turbulence may not be entirely wrong, but it is not exactly supported by our results. This is a complex system, and further work is necessary to really understand these interactions. Another possibility is that in the tropics, clouds too small to resolve on our grid scale (less than 1km), can help entrain low MSE air into the boundary layer (Esbensen, 1978). Because we are not capturing these effects, our dry environment may be excessively entraining.

Our results clearly show that, in our model, environmental entrainment of lower MSE is the primary mechanism for balancing surface flux increases in MSE. These results support the description of boundary layer forcing in Arakawa and Schubert (1974), and contradict the idea of Boundary Layer Quasi-Equilibrium from Emanuel (1987; 1993), and Raymond (1995). In RADCONV, we see that the environment moves more high MSE up and low MSE down across the 500m layer than either updrafts or downdrafts. In the TOGA case, we see that intense convection can actually result in downdrafts that transport high MSE into the lowest levels. And in the LLS case, we see that intense, organized convection tends to increase the cooling power of updrafts rather than downdrafts. We still have many questions about these processes. Do downdrafts have an affect on the boundary layer depth in our model? How does this mechanism work over larger regions of the tropics or large gridcells in GCMs? And how should we parameterize this relationship? Does it need to be included in GCMs or is a simple cooling by the environment sufficient? Is cooling by downdrafts currently *over represented* in convective parameterizations?

Chapter 9: A Lagrangian View of Downdrafts

What is a 'Lagrangian View'?

There are two main methods for describing the motion of a fluid. The first is the Eulerian method, which uses a fixed three dimensional space and describes the fluid as it flows through the space. The second method is a Lagrangian method, where fluid motions are described from the point of view of a parcel moving within that fluid. In the Eulerian method, we are describing convection as if we are an observer on a near-by mountain top, watching the clouds roll by. In the Lagrangian method, we describe motions from the perspective of a balloon floating up and down and in and out of the clouds as they grow and dissolve over time. So far in this study, we have exclusively used Eulerian methods in diagnosing and compiling statistics on downdrafts. However, there is much to be learned from the Lagrangian view of downdrafts as well.

Yamaguchi and Randall (2012 - hereafter YR12) describe a tool for tracking parcels using a Lagrangian method in SAM. The Lagrangian Parcel Tracker (LPT) is a tool added into our CRM that initializes a distribution of massless parcels and predicts their location and properties over time. Unlike other LPT tools, the YR12 method allows the thermodynamic properties of parcels to change as they are advected around the domain. Parcel position is predicted using a third-order iterative time differencing, and fifth order interpolation is available. We use a simple trilinear interpolation in our simulation due to a lower vertical resolution near the surface than was used in YR12. The LPT spatially interpolates the prognostic thermodynamic fields from SAM, but actually diagnoses other fields (such as cloud water and temperature) using SAM's microphysics scheme to ensure the most consistency. In order to use the LPT, we changed the advection scheme to a fifth-order scheme described in Yamaguchi et al. (2011).

Our current version of the LPT requires a uniform vertical grid, and since we needed vertical resolution on the order of 100m in the boundary layer, we had to continue this trend

through the troposphere an into the stratosphere. To be economical in our time constraints, we ran SAM in two dimensions with 280 levels in the vertical (up to 28km) and 500m horizontal resolution (on a 128km horizontal domain). Our time step shortened to 5 seconds, and we ran our model with TOGA forcing for 100 hours. At 3.8 days, we release 256,000 parcels distributed on 20 levels, 500m apart from 1000m to 11000m. We then run the model with parcel tracking for another 8.3 hours (6,000 time steps), and collect output from all parcels ever minute.

The TOGA LPT simulation

The same 8.3 hour time period in the three dimensional TOGA simulations produced a propagating squall line feature that was relatively stable. Downdrafts during this period are significant, but not necessarily the strongest in the entire TOGA run. Our two dimensional simulation produced a similar squall line, as seen in Figure 9.1. Our goal was to get as many parcels

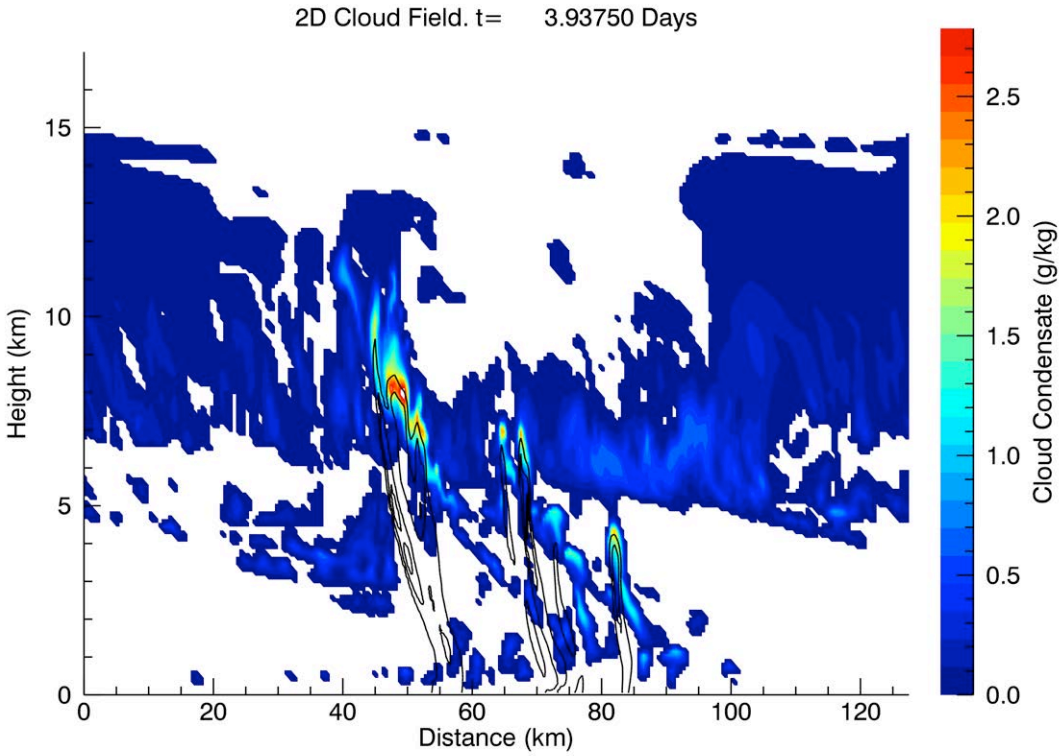

Figure 9.1. A snapshot of clouds (color contours) and precipitation (line contours) from our high-resolution two dimensional TOGA simulation with Lagrangian Parcel Tracking.

as possible entrained into downdrafts, and learn about downdraft properties from within. Over the 8 hour simulation, many parcels experienced significant downward motion. We categorize downdraft periods as those where a parcel's negative vertical velocity exceeds 3 m/s. Out of 256,000 parcels, only 4360 (or about 1.7 percent) of them experience an event of this magnitude. After finding a time where the parcel sees this intense downward motion, we search backwards and forwards in time to find the point where the parcel's vertical velocities pass through zero. The first zero vertical velocity is considered the point where the parcel is entrained into the downdraft and the second zero is the location of detrainment.

With this definition, we make a few assumptions. The first is that we do not check for clouds or precipitation in determining downdrafts in this system. It is unlikely that a parcel would experience a 3 m/s or greater motion outside of a cloud. The second is that we do not assume the parcel defines the entire downdraft. It is very possible that parcels could be entrained on the way down or detrained before a downdraft reaches its minimum height. Figure 9.2 shows histograms of

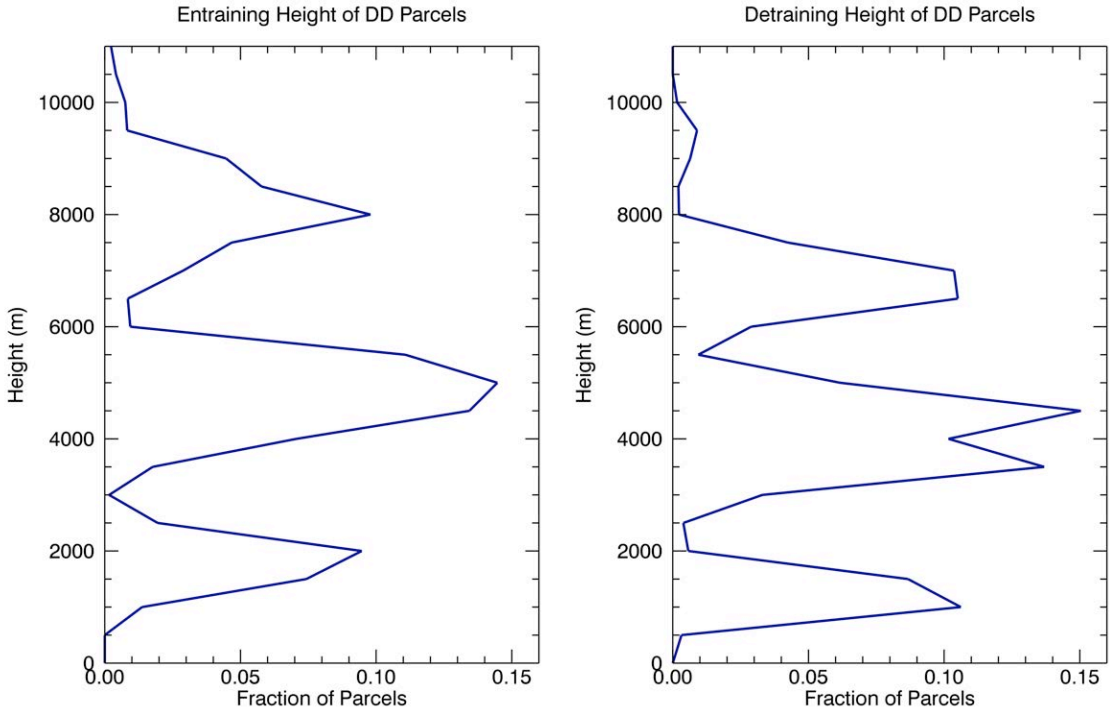

Figure 9.2. Height of parcel entrainment (left) and detrainment (right) through downdrafts in the TOGA LPT simulation.

the heights of entrainment and detrainment from the 4360 downdraft parcels. These plots show a strong trimodal structure, with parcels entering downdrafts primarily between 7 to 9 km, 4 to 6 km, and 1 to 2 km. The detrainment heights are just below the entrainment heights. The average distance traveled by parcel within a downdraft is about 1 km, and the maximum values are just above 2 km. We are not prepared to say that this means downdrafts are only 2 km long in our model. It is just as likely that parcels are tossed out of the turbulent downdraft, or our analysis method does not allow for any turbulent lifting within the downdraft region. It is also possible that none of our parcels made it into the small cores of the penetrating downdrafts.

Figure 9.3 shows the heights of a few parcels during the 8 hours of LPT simulation. These parcels were chosen because they all experience some of the longest downdraft travel. It is interesting to see that all of these parcels are entrained into the same updraft motion, though at different heights. They all then transition into the downdraft at a similar time. The period at the

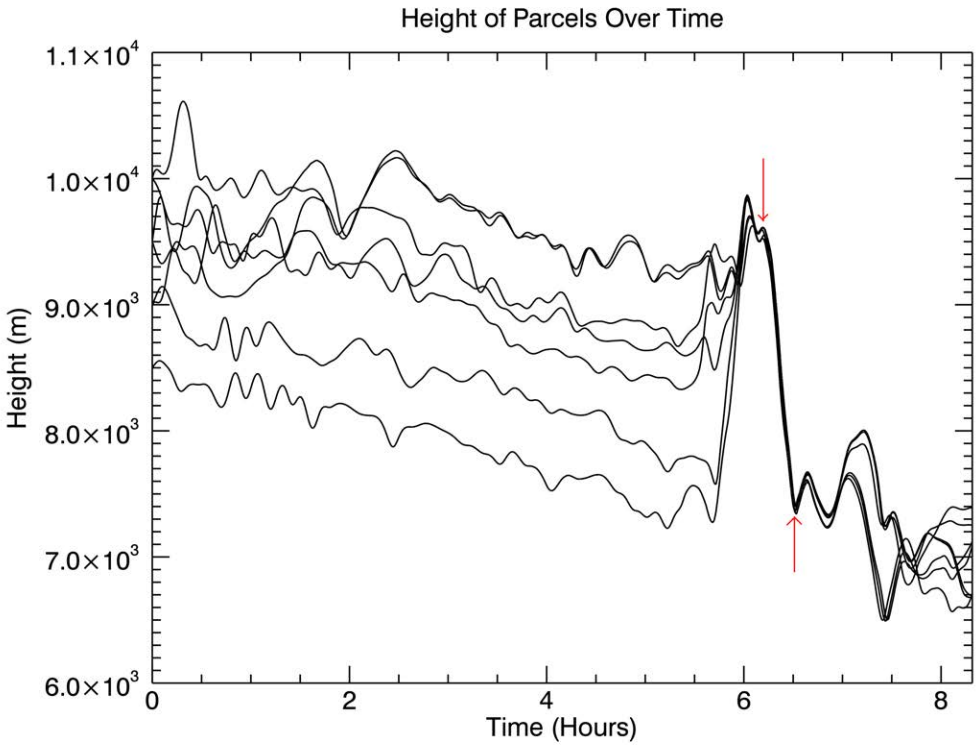

Figure 9.3. Time-Height plots of a few parcel trajectories that are entrained into an updraft and then move into and out of a downdraft during the TOGA LPT simulation.

beginning and end of their downdraft travel is rather turbulent. Our definition of downdrafts by the location of their zero values of vertical velocity will truncate the time within the downdraft to the period between the two red arrows shown in Figure 9.3. Even though some of these parcels continue to descend after the initial drop, we do not include those data points in our analysis.

Downdraft Moisture and Buoyancy

A common assumption in downdraft parameterizations is that downdrafts are saturated as they descend. This makes sense if the downdraft is falling through cloudy air, though the core of the downdraft could be insulated by precipitation and be less than saturated (theoretically). And certainly, as downdrafts exit the cloud, they may or may not maintain their saturation through the evaporation of precipitation. Using parcels from the LPT simulation, we can ask the question, how saturated are these downdrafts?

Figure 9.4 shows a little more than 10% of our downdraft parcel trajectories, with their relative humidity plotted against their height. Because downdraft parcels are defined to have a negative velocity for the entire period, we can read this plot from top to bottom. All parcels here start high and end low. We immediately see a common trend. These downdrafts almost all start at saturation (or slightly above) and their relative humidities rapidly drop off as the parcel descends. The curve away from 100% relative

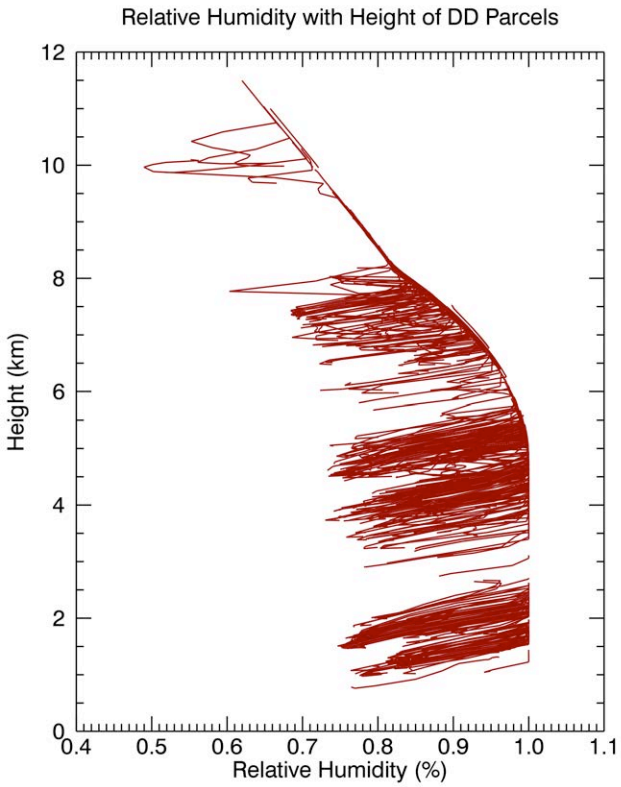

Figure 9.4. Downdraft parcel trajectories in height-relative humidity space in the TOGA LPT simulation. By definition, all parcels must be going downwards, so all trajectories start high and end lower.

humidity above 5500m signals the glaciation of the cloud and downdrafts. At a given temperature, the saturation vapor pressure over ice is lower than that of water, so the relative humidity at saturation over ice will seem to be lower than 100% if you do not take this into account.

Clearly, our downdrafts are not likely falling through cloudy air here. Figure 9.1 shows the cloud configuration during this simulation is tilted, and precipitation quickly falls out of the clouds. It appears from Figure 9.4 that these downdrafts are not evaporating enough precipitation to maintain saturation. In fact, the rate of decrease of relative humidity (the slope of the heigh-relative humidity line each parcel makes) is very similar for all parcels at all heights. A final feature worth noting is the "hook" at the end of many of these trajectories. There are many parcels here with a slight increase in relative humidity right at the end of their downdraft trajectory. Sometimes the increase is very small, and occasionally it is quite large (almost a loop back towards saturation in some cases), but it is nearly always there.

To see how the evaporation of precipitation may be impacting these changes in downdraft relative humidity, we added the rate of evaporation of precipitation to the YR12 parcel tracking code. Figure 9.5 shows the trajectories of 10% of downdraft parcels in height-evaporation space. Again, each of these trajectories starts high and ends low. Here we see most downdraft parcels start with zero or very little evaporation and the rate increases as they descend. This follows

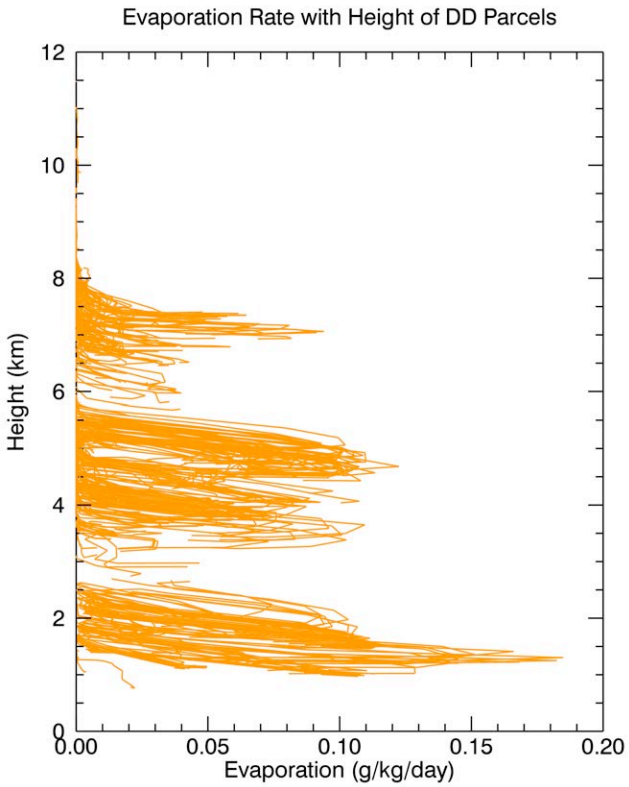

Figure 9.5. Downdraft parcel trajectories in height-evaporation rate space in the TOGA LPT simulation. By definition, all parcels must be going downwards, so all trajectories start high and end lower.

with the decrease in relative humidity. Even though there is increased evaporation along the parcel trajectory, it is not enough to maintain saturation in the downdraft. Trajectories in Figure 9.4 also have a similar "hook" or trend reversal near the end. These are much larger for evaporation, however. The slope of the evaporation trajectories seem a bit more variable than the relative humidity trajectories. The highest values of evaporation rate appear in a nearly horizontal line, suggesting a very rapid increase with very little parcel descent. The slope of the trajectories near the zero value are much steeper. These are areas where evaporation is increasing more slowly than others.

Most of the downdrafts sampled by our parcels do not maintain saturation as they descend. The parcels tend to start at saturation and then dry more and more as they descend. This could be because our downdrafts form near the base of cloud layers and rapidly descend through clear air. The linear decrease in relative humidity is likely due to adiabatic warming of downdraft parcels. This decrease in relative humidity does pump up the evaporation rate as parcels descend, but near the bottom of the downdraft trajectory, the evaporation rate tends to decrease as well. If these trajectories are capturing the lowest regions of a short-lived downdraft, this decrease in evaporation would likely lead to an increase in buoyancy (since temperature is increasing, and it seems unlikely that new precipitation is forming), and upwards acceleration. The fact that parcels continue to descend after this turn-around suggests that our downdrafts do have "undershooting bottoms", or places where they are continuing downward motion despite having slightly positive buoyancy.

The possibility of undershooting bottoms is supported in Figure 9.6, where we plot the trajectory of downdraft parcels in height and virtual temperature anomalies from the 8 hour mean virtual temperature profile. Here, we define virtual temperature as in Chapter 6, and include the negative effects of cloud water and precipitation on parcel buoyancy. Figure 9.6 shows that downdrafts adhere tightly to the average environmental moist adiabat. The trajectories in this space are slightly shorter, indicating that downdraft virtual temperature does not change much as the

parcels descend. These trajectories are somewhat noisy, and this could be due to the use of the average sounding. Even though the environmental virtual temperature sounding does not change much, a fraction of a degree can add noticeable noise in the trajectories in Figure 9.6. However, some general trends are apparent. The downdraft parcels tend to begin and spend most of their descent time with a negative anomaly, and then, near the end of the their trajectories, they gain a positive anomaly. This is the movement of a downdraft from negatively buoyant to positively buoyant at the end of its lifetime. These downdrafts do continue to descend for several to hundreds of meters with this positive buoyancy. This is probably due mainly to momentum, just as overshooting tops are the result of updraft momentum carrying them past their level of neutral buoyancy. The undershooting bottoms seen here could be the positively buoyant downdrafts that so concerned Wei et al. (1998) as they analyzed flight data from TOGA-COARE, and are discussed by Igau et al. (1999) as well.

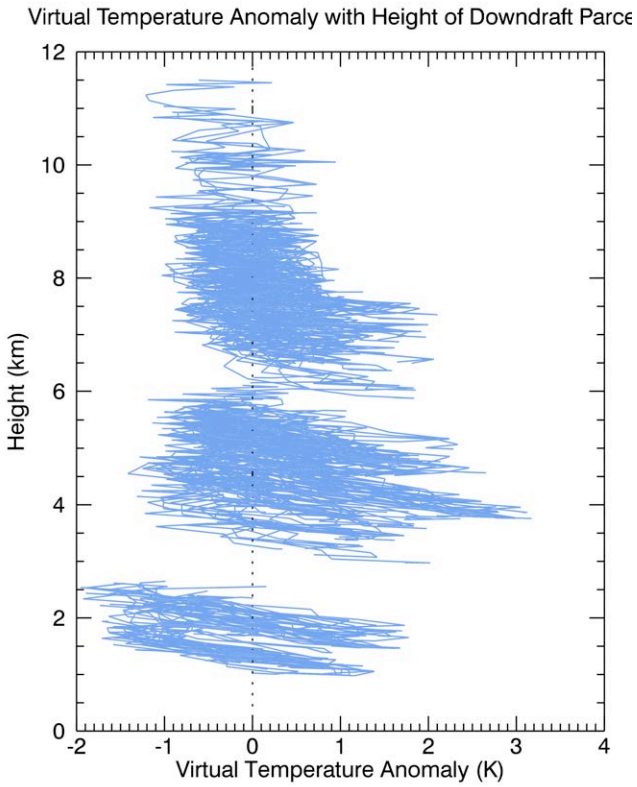

Figure 9.6. Downdraft parcel trajectories in height-virtual temperature space in the TOGA LPT simulation. By definition, all parcels must be going downwards, so all trajectories start high and end lower. The level-average virtual temperature sounding is plotted as a thin black dashed line.

This chapter is a short analysis and really constitutes a technology test of the Lagragian Parcel Tracker. This is a very nice tool for investigating processes like entrainment and detrainment, and could be useful for updrafts and downdrafts. However, since the data is presented in such a different manner, it is sometimes difficult to determine if a parcel is entrained or detrained near the beginning or end of a cloud draft, if the parcel is brushing the edge or within the core of the draft,

and how the properties of the parcel relate to the mean state at that time. Our parcel output is in one minute time increments, but we could not do this for the full three dimensional output as well. So comparing parcel anomalies to mean state variables will require extra code in the parcel tracker or time and space interpolation of traditional model output. This tool has great potential to increase insight into local downdraft properties, or changes in those properties as the parcel descends.

Chapter 10: Summary and Future Work

Downdraft Impacts on Convection

Downdrafts are more than a simple side-effect of convection. They are part of a complex and multi-scale process that influences the convection that spawned them. In our study, we have outlined several ways in which downdrafts impact local convection and climate, and explored these using the high-resolution output from our cloud resolving model (CRM). We illustrate the most important processes discussed in our work in Figure 10.1. Downdrafts impact the area near convective storms through local cooling, increased surface fluxes and increased boundary layer turbulence. They influence the climate by decreasing the mass of subsiding air outside of clouds, as well as organizing and maintaining convective elements in propagating cloud systems.

We illustrate the four main effects of downdrafts discussed by our work in Figure 10.1. The first, and likely most important impact of downdrafts is that they provide an important downward mass flux to counter-balance updraft mass flux in clouds (labeled 1 in Figure 10.1). We show in Chapter 4 that downdrafts are a significant part of the mass budget in almost every cloud system simulated in our model. In the RADCONV simulations, downdrafts have a much larger net downward mass flux than the environment, while in the TOGA simulation, they are of a similar

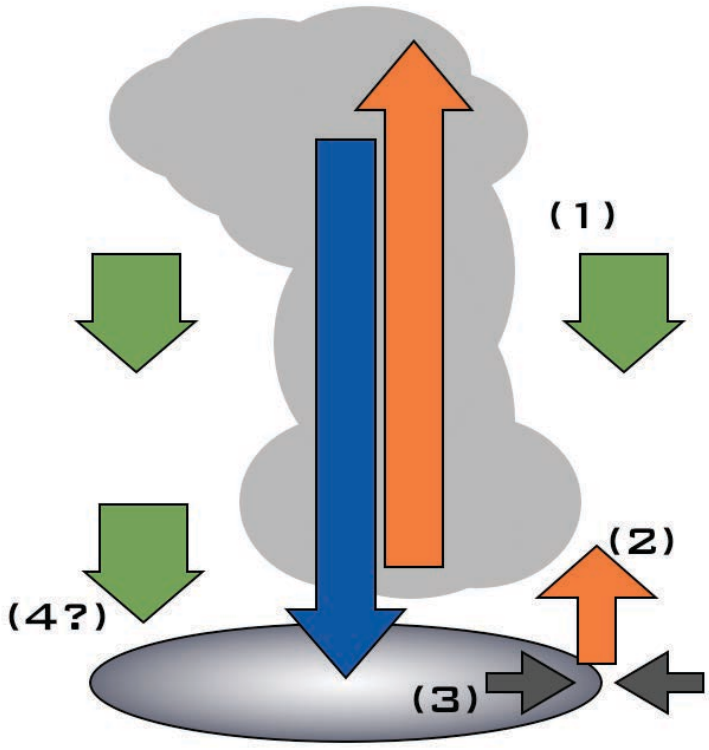

Figure 10.1. Downdrafts in the convective system impact (1) the subsiding environment, (2) new convection, (3) surface fluxes, and (4) possibly boundary layer entrainment.

magnitude. The mass flux from downdrafts begins at the same level as the updraft mass flux tops out at, but has a maximum just above cloud base. This mass flux is also important for the transport of tracers and pollutants, as it provides a mechanism for the injection of free tropospheric air into the boundary layer. And the presence of a downdraft mass flux reduces the amount of air in the subsiding environment surrounding deep convection, decreasing the warming and drying influence of subsidence on the entire atmosphere.

A second critical effect of downdrafts is the impact of cold pools on the formation of new convection (labeled 2 in Figure 10.1). We show in Chapter 5 that the cool air flowing out of downdrafts forms a bubble of cold air below the cloud, known as a cold pool. There is increased convergence around the edges of cold pools, as the cold air spreads out in all directions and converges against the warmer, boundary layer air. We show that updrafts form preferentially in this convergence zone, and that these updrafts have much higher MSE anomalies and higher CAPE than would be expected using only layer mean values. We also show, in Chapter 7, that adding a low-level sheared wind profile can compound this convergence, and create long-lived propagating mesoscale systems. This organized system then produces much stronger convective mass fluxes than non-organized systems using the same large-scale temperature and moisture profiles. This indicates the presence of a self-maintaining cycle, where downdraft cold pools organize convection in a system that produces even more downdrafts and more cold pool air.

The third important impact of downdrafts shown in Figure 10.1, is the influence of downdrafts on surface fluxes. While we did not investigate this as deeply as the previous two topics, it is still an important feedback from downdrafts into future convection. We found that downdrafts are very tightly correlated with sensible heat flux from the ocean surface in Chapter 5, and that gusty winds surrounding cold pools can increase local latent heat flux. In Chapter 5 we note that there are many non-convective processes that increase latent heat flux as well, such as high sea surface temperatures and stronger large-scale winds. This produces a near decoupling between downdraft

mass flux and latent heat flux in our model. But looking at the impacts of local winds, we see a clear increase in latent heat flux on the edges of cold pools, where new convection is forming.

The fourth impact of downdrafts in Figure 10.1 is still unclear and hypothetical. We show in Chapter 8 that downdrafts do contribute to boundary layer cooling and reduction of low-level MSE, but not as much as the environmental entrainment at the top of the boundary layer. However, we show a correlation between downdrafts and boundary layer variance in this study that could result in stronger environmental entrainment when downdrafts increase the turbulence of the boundary layer. Our hypothesis is that downdraft mass flux in the boundary layer, and cold pool or gust-front turbulent eddies, increases turbulence throughout the boundary layer, and adds to the ability of the clear environment to entrain through wave breaking at the top of the boundary layer. However, the possibility exists that cloud processes that impact entrainment are not well enough resolved in this study, so more work needs to be done on this subject.

There are several other secondary impacts and relationships discussed in our work here. In Chapter 4, we discuss the flow of mass from updrafts into downdrafts, suggesting that updrafts bleed some of their buoyancy off into downdrafts. This results in less buoyant updrafts, and more buoyant downdrafts, similar to observations described in Chapter 1. We show in Chapter 6 that downdrafts are not as sensitive to environmental relative humidity as expected, and point out the importance of entrainment for the formation of a strong relationship between deep convection and moisture in the troposphere. And we show in Chapter 6 that downdrafts have positive MSE anomalies as they entrain air from updrafts. We show that, in our model, negative buoyancy in downdrafts is initially due to the presence of condensate loading rather than precipitation evaporation using LPT in Chapter 9. The high-resolution, three dimensional output from our CRM is an invaluable resource for investigating these types of convective processes that we are still struggling to observe in the real world.

Improving Downdrafts in Global Climate Models

All of these findings lead us to evaluation and improvement of downdrafts in convective parameterizations in global climate models (GCMs). Actually, most modern convective parameterizations are not too far off the mark. In Chapter 2, we discuss the current state of convective parameterizations, and note that all of the most modern GCMs include a mass flux for downdrafts in their parameterizations. We show in Chapter 5 that a direct relationship between updraft and downdraft mass flux is a poor choice for capturing true natural variability, but is probably not too bad for the climatological mean state. And our analyses in Chapter 6 suggests that downdrafts that are closely tied to precipitation evaporation may be over-doing a process that is present (and important) in our model, but not quite that important.

The main changes we suggest for downdrafts in convective parameterizations can be distilled into two subjects. The first is downdraft thermodynamic properties and drivers. We show in Chapter 4 that downdrafts and updrafts have plenty of interaction in our model, and the old method of taking a blob of cloud air and entraining only environmental air as it descends is not supported by our results (or real world observations for that matter, see Chapter 1). In order to better simulate the real world, updrafts should be entraining from the environment, and shedding mass, momentum and energy into downdrafts as they ascend. Our thermodynamic profiles in Chapter 6 suggest that downdrafts do not need anomalously negative MSE to maintain descent, and precipitation loading should be included in negative buoyancy calculations. This could cause downdrafts to be warmer and wetter than we see in current models, and might actually decrease the cooling and moistening they currently provide. This moisture source could be replaced by detrainment from shallow convection.

The second subject that needs to be addressed in the current parameterization of convective downdrafts is the presence of cold pools and the variability of the boundary layer. We show in Chapter 5 that the MSE and CAPE of updraft parcels leaving the boundary layer is far

higher than mean values currently used in convective parameterizations. We show that cold pool gustiness and convergence increase surface fluxes and act to organize convection. In Chapter 7, we show that shear influences on boundary layer convergence helps to organize and sustain more powerful convection. And in Chapter 8 we discuss the most active source of low MSE entrainment in the boundary layer, which we find to be the environment rather than downdrafts.

Basically, we are suggesting a shift in the current conceptual paradigm for deep convection. Figure 10.2 illustrates the difference between current simple saturated downdraft parameterizations, and convection in image we describe here. Most modern parameterizations have spectrums of lightly entraining updrafts, and use the mean CAPE in the column as their measure of buoyancy. These parameterizations also have a single, saturated downdraft, and typically detrain only at the final levels of both updrafts and downdrafts. We suggest a convective parameterization that starts from the boundary layer. A calm boundary layer will require a high amount of CAPE to overcome

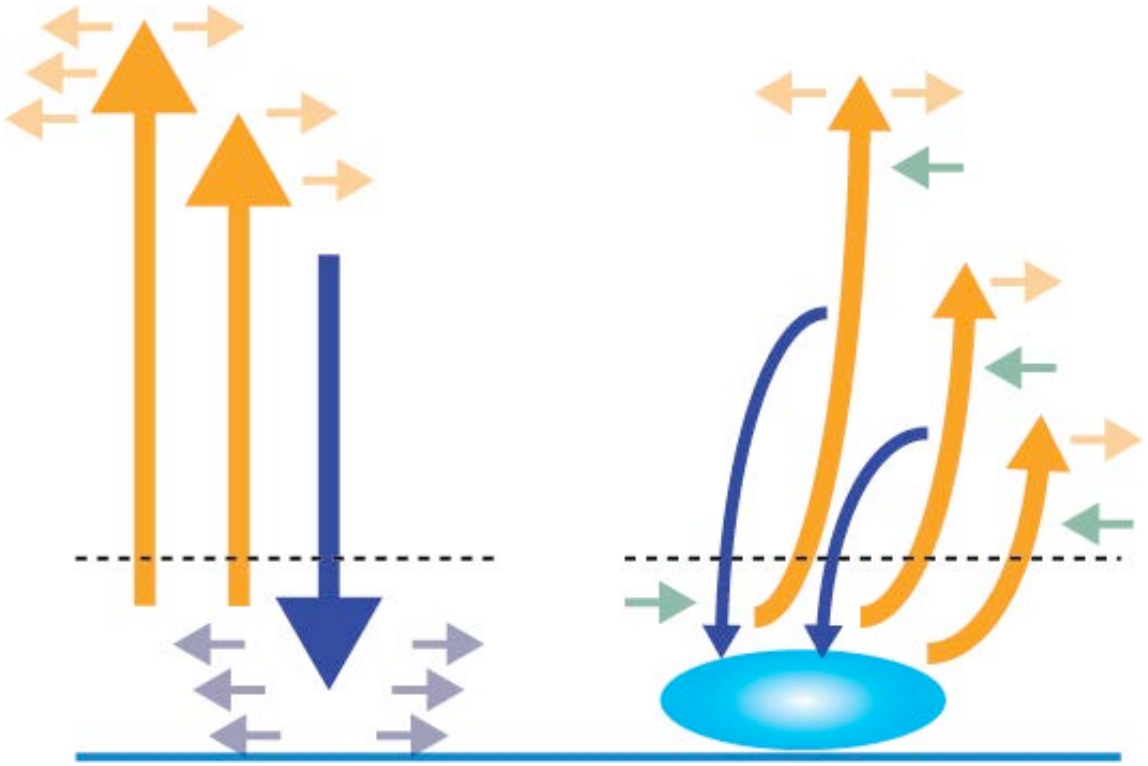

Figure 10.2. A traditional view of updrafts and downdrafts detraining at specific levels (left) versus our view of highly entraining updrafts, lower entraining downdrafts, and cold pool induced variability.

any local CIN, but a disturbed boundary layer, perhaps containing a cold pool, will require less (see Chapter 6). Our updrafts would generally have CAPE values higher than the mean, but would entrain more dramatically than those of other parameterizations. They would also detrain at all levels, into the environment at upper levels and into downdrafts closer to the boundary layer. These downdrafts should be tied to the plume precipitation amounts, and evaporate as they descend, but not necessarily to saturation. Maintaining a cold pool allows us to parameterize organization as well, and we can reduce entrainment in plumes around vigorous cold pools. We could even include the effects of shear, if not on our convective plumes, including a low-level shear invigoration of the cold pool would be an improvement.

This increase in entrainment and the added effects of mesoscale organization could lead to a spectrum of clouds that looks very different from those in current GCMs. Rather than a few deep clouds, we might see a lot more constant shallow convection, and deep convection only when the cold pool becomes large enough. D. Randall has described quasi-equilibrium in the tropics as similar to a flock of sheep. The clouds are like sheep, and they wander along, grazing on CAPE. The question we need to ask is, what kind of sheep do we want in our flock? Do we need one made up of several very efficient grazers, or do we want a larger flock, with many small sheep only nibbling on the best grass, and the occasional pass of a lawn mower?

Future Work

Often, at the end of a project, it seems more questions have appeared than have been answered. We have attempted to answer many long-standing questions about downdrafts, but there are plenty more to conquer. Our results are suspect in that we used only a single model and single microphysical scheme. To really validate these results, we need to see many more studies with similar findings, using different models and different microphysical schemes. A test of downdraft sensitivity to microphysics would be extremely helpful.

It would also be very good to look at downdrafts in other case studies. Continental mid-latitude downdrafts are very different from those in the tropics, as the cloud bases are higher and there is more precipitation evaporation. There are many other types of convection where we suspect that downdrafts play a critical role in timing or organization, but little has been written about downdrafts in CRM simulations of these cases. Hurricanes, mesoscale convective systems, the diurnal on-set of deep convection, and large desert dust storms (haboobs) would all be very interesting downdraft test cases. Also, if we really want to understand the impact of downdrafts on tropical waves, it would be good to do some larger-scale "aqua-planet" type CRM runs. These have been shown to form propagating convection on an MJO or Kelvin wave scale, but little has been written about how downdrafts influence the convection in those waves.

Finally, there are several unfinished portions of this project, each could use a lot more time and work. The questions surrounding our boundary layer quasi-equilibrium results stand out the strongest. This is an area that could use a detailed statistical analysis of clear-air boundary layer turbulence and entrainment processes in the presence of downdrafts. The results from the LPT method run are interesting and very encouraging. This is a tool that will definitely give good insights into convective processes in the future. Finally, our results and hypothesis need to move into the GCM world. We could learn a lot about downdrafts by doing GCM runs and simply adjusting a current scheme in minor ways. The parameterization recommendations discussed here deserve to be fully developed and tested in a GCM simulation some day as well.

This project has given us a chance to question some established assumptions and investigate new ways of thinking about complex convective processes. The cloud resolving model is a powerful tool, and while it has its own assumptions and limitations, it is very useful for learning about clouds and cloud processes. We hope the work presented here is useful in the design and understanding of future convective parameterizations. As computers become more and more powerful, we will see CRMs become higher resolution, allowing us all to assume less and illuminate more.

References

Abel, S. J. and B. J. Shipway, 2007: A comparison of cloud-resolving model simulations of trade wind cumulus with aircraft observations taken during RICO. *Q. J. R. Meteorol. Soc.*, **133**, 781-794.

Arakawa, A. and W. H. Schubert, 1974: Interaction of a cumulus cloud ensemble with the large-scale environment, Part 1. *J. Atmos. Sci.*, **45**, 3188-3211.

Betts, A. K., L. V. Gatti, A. M. Cordova, M. A. F. Silva Dias, and J. D. Fuentes, 2002: Transport of ozone to the surface by convective downdrafts at night. *J. Geophys. Res.*, **107(D20)**, 8046, doi: 10.10129/2000JD000158.

Bohren, C. F. and B. A. Albrect, 1998: *Atmospheric Thermodynamics*. 402pp, Oxford University Press, New York, New York.

Bretherton, C., M. E. Peters, and L. E. Back, 2004: Relationships between water vapor path and precipitation over the tropical oceans. *J. Climate*, **17**, 1517-1528.

Byers, H. R. and R. R. Braham, 1948: Thunderstorm Structure and Circulation. *J. Meteor.*, **5**, 71-86.

Byers, H. R. and R. R. Braham, 1949: *The Thunderstorm*. 287 pp, U.S. Weather Bureau, Washington, D. C.

Cheng, M.-D., and A. Arakawa, 1997: Inclusion of Rainwater Budget and Convective Downdrafts in the Arakawa-Schubert Cumulus Parameterization. *J. Atmos. Sci.*, **54**, 1359-1378.

Chikira, M. and M. Sugiyama, 2010: A Cumulus Parameterization with State-Dependent Entrainment Rate. Part I: Description and Sensitivity to Temperature and Humidity Profiles. *J. Atmos. Sci.*, **67**, 2171-2193.

Collins, W. D., P. J. Rash, B. A. Boville, J. J. Hack, J. R. McCaa, D. L. Williamson, J. T. Kiehl, and B. Briegleb, 2004: Description of the NCAR Community Atmosphere Model (CAM 3.0), *Tech. Rep. NCAR/TN-464+STR*.

Corfidi, S. F., 2003: Cold Pools and MCS Propagation: Forecasting the Motion of Downwind-Developing MCSs. *Wea. Fore.*, **18**, 997-1017.

DeMott, C. A., D. A. Randall, and M. F. Khairoutdinov, 2007: Convective precipitation variability as a tool for general circulation model analysis. *J. Climate*, **20**, 91-112.

Donner, L. J., 1993: A cumulus parameterization including mass fluxes, vertical momentum dynamics, and mesoscale effects. *J. Atmos. Sci.*, **50**, 889-906.

Donner, L. J., C. J. Seman, and R. S. Hemler, 1999: Three-dimensional Cloud-System Modeling of GATE Convection. *J. Atmos. Sci.*, **56**, 1885-1912.

Donner, L. J., and coauthors, 2011: The dynamical core, physical parameterizations, and basic simulation characteristics of the atmospheric component AM3 of the GFDL global coupled model CM3. *J. Climate*, **24**, 3484-3519.

Elsaesser, G. S. and C. D. Kummerow, 2013. A Multi-Sensor Observational Depiction of the Transition from Light to Heavy Rainfall on Sub-Daily Timescales. *J. Atmos. Sci.*, in press.

Emanuel, K. A., 1987: An air-sea interaction theory for tropical cyclones, Part I. *J. Atmos. Sci.,* **44**, 2324-2340.

Emanuel, K. A., 1989: The Finite-Amplitude Nature of Tropical Cyclogenesis. *J. Atmos. Sci.*, **52**, 3431-3456.

Emanuel, K. A., 1991: A scheme for representing cumulus convection in large-scale models. *J. Atmos. Sci.*, **44**, 2313-2329.

Emanuel, K. A., 1993: The Effect of Convective Response Time on WISHE Modes. *J. Atmos. Sci.*, **50**, 1763-1775.

Emori, S., T. Nozawa, A. Numaguti, and I. Uno, 2001: Importance of cumulus parameterization for precipitation simulation over East Asia in June. *J. Meteor. Soc. Japan*, **79**, 939-947.

Esbensen, S., 1978: Bulk Thermodynamic Effects and Properties of Small Tropical Cumuli. *J. Atmos. Sci.*, **35**, 826-837.

Fujita, T. T. and F. Caracena, 1977: An Analysis of Three Weather-Related Aircraft Accidents. *Bull. Am. Meteor. Soc.*, **58**, 1164-1181.

Fujita, T. T. and R. M. Wakimoto, 1981: Five scales of airflow associated with a series of downbursts on 16 July 1980. *Mon. Wea. Rev.*, **109**, 1438-1456.

Grell, G. A., 1993: Prognostic evaluation of assumptions used by cumulus parameterizations. *Mon. Wea. Rev.*, **121**, 764-787.

Hallett, J., R. I. Sax, D. Lab, and A. S. Ramachandra Murty, 1978: Aircraft measurements of ice in Florida cumuli. *Q. J. R. Meteorol. Soc.*, **104**, 631-651.

Hannah, W. M. and E. D. Maloney, 2011: The Role of Moisture-Convection Feedbacks in Simulating the Madden-Julian Oscillation. *J. Climate*, **24**, 2754-2770.

Hong, S.-Y. and H.-L. Pan, 1998: Convective trigger function for a mass-flux cumulus parameterization scheme. *Mon. Wea. Rev.*, **126**, 2599-2620.

Houze, R. A., 1993: *Cloud Dynamics*. 573pp, Academic Press, San Diego, California.

Humphreys, W. J., 1914: The Thunderstorm and its phenomena. *Mon. Wea. Rev.*, **42**, 348-380.

Igau, R. C., M. A. LeMone, and D. Wei, 1999: Updraft and Downdraft Cores in TOGA COARE: Why So Many Buoyant Downdraft Cores? *J. Atmos. Sci.*, **56**, 2232-2245.

Johnson, R. H., 1976: The Role of Convective-Scale Precipitation Downdrafts in Cumulus and Synoptic-Scale Interactions. *J. Atmos. Sci.*, **33**, 1890-1910.

Johnson, R. H. and M. E. Nicholls, 1983: A Composite Analysis of the Boundary Layer Accompanying a Tropical Squall Line. *Mon. Wea. Rev.*, **111**, 308-319.

Johnson, R. H., T. M. Rickenbach, S. A. Rutledge, P. E. Ciesielski, and W. H. Schubert, 1999: Trimodal Characteristics of Tropical Convection. *J. Climate*, **12**, 2397-2418.

Jorgensen, D. P., E. J. Spser, and M. A. LeMone, 1985: Vertical motions in intense hurricanes. *J. Atmos. Sci.*, **42**, 839-856.

Jorgensen, D. P. and M. A. LeMone, 1989: Vertical Velocity Characteristics of Oceanic Convection. *J. Atmos. Sci.*, **46**, 621-640.

Jorgensen, D. P., M. A. LeMone and S. B. Trier, 1997: Structure and Evolution of the 22 February 1993 TOGA COARE Squall Line: Aircraft Observations of Precipitation, Circulation, and Surface Energy Fluxes. *J. Atmos. Sci.*, **54**, 1961-1985.

Kain, J. S. and J. M. Fritsch, 1990: A one-dimensional entraining/detraining plume model and its application in convective parameterization. *J. Atmos. Sci.*, **47**, 2784-2802.

Kain, J. S., 2004: The Kain-Fritsch Convective Parameterization: An Update. *J. Applied Meteor.*, **43**, 170-181.

Keller, V. W., and R. I. Sax, 1981: Microphysical development of a pulsating cumulus tower: a case study. *Q. J. R. Meteorol. Soc.*, **107**, 679-697.

Khairoutdinov, M. F. and D. A. Randall, 2001: A cloud resolving model as a cloud parameterization in the NCAR Community Climate System Model: Preliminary results. *Geophys. Res. Lett.*, **28**, 3617-3620.

Khairoutdinov, M. F. and D. A. Randall, 2003: Cloud Resolving Modeling of the ARM Summer 1997 IOP: Model Formulation, results, Uncertainties, and Sensitivities. *J. Atmos. Sci.*, **60**, 607-625.

Khairoutdinov, M. F., D. A. Randall, and C. DeMott, 2005: Simulations of the atmospheric general circulation using a cloud-resolving model as a super-parameterization of physical processes. *J. Atmos. Sci.*, **62**, 2136-2154.

Khairoutdinov, M. F., S. K. Krueger, C.-H. Moeng, P. A. Bogenschutz and D. A. Randall, 2010: Large-Eddy Simulation of maritime Deep Tropical Convection. *J. Adv. Model. Earth Syst.*, **1**, Art #15, 13pp.

Kiladis, G. N., M. C. Wheeler, P. T. Haertel, K. H. Straub, and P. E. Roundy, 2009: Convectively coupled equatorial waves, *Rev. Geophys.*, **47**, RG2003, doi:10.1029/2008RG000266.

Kim, D., K. Sperber, W. Stern, D. Waliser, I-S Kang, E. Maloney, W. Wang, K. Weickmann, J. Benedict, M. Khairoutdinov, M-I Lee, R. Neale, M. Suarez, K. Thayer-Calder, G. Zhang, 2009: Application of MJO Simulation diagnostics to climate models. *J. Climate*, **22**, 6413-6436.

Kirkpatrick, C., E. W. McCaul Jr., and C. Cohen, 2009: Variability of updraft and downdraft characteristics in a large parameter space study of convective storms. *Mon. Wea. Rev.*, **137**, 1550-1561.

Knupp, K. R., and W. R. Cotton, 1985: Convective Cloud Downdraft Structure: An Interpretive Survey. *Rev. of Geophys.*, **23**, 183-215.

LeMone, M. A., and E. J. Zipser, 1980: Cumulonimbus vertical velocity events in GATE, I, Diameter, intensity and mass flux. *J. Atmos. Sci.*, **37**, 2444-2457.

Liu, P., B. Wang, K. R. Sperber, T. Li, and G. A. Meehl, 2005: MJO in the NCAR CAM2 with the Tiedke convective scheme. *J. Climate*, **18**, 3007-3020.

Malkus, J. S., 1954: Some Results of a Trade-Cumulus Cloud Investigation. *J. Meteor.*, **11**, 220-237.

Malkus, J. S., 1955: On the Formation and Structure of Downdrafts in Cumulus Clouds. *J. Meteor.*, **12**, 350-354.

Maloney, E. D. and D. L. Hartmann, 2001: The Sensitivity of Intraseasonal Variability in the NCAR CCM3 to Changes in Convective Parameterization. *J. Climate*, **14**, 2015-2034.

Mapes, B. and R. Neale, 2011: Parameterizing convective organization to escape the entrainment dilemma. *J. Adv. Model. Earth Syst.*, **3**, M06004, 20p.

Middleton, N. J. and Q. Z. Chaudhary, 1988: Severe dust storm at Karachi, 31 May 1986. *Weather*, **43**, 298-301.

Moorthi, S. and M. J. Suarez, 1992: Relaxed Arakawa-Schubert: A Parameterization of Moist Convection for General Circulation Models. *Mon. Wea. Rev.*, **120**, 978-1002.

Neale, R. B., J. H. Richter and M. Jochum, 2008: The impact of convection on ENSO: From a delayed oscillator to a series of events. *J. Climate*, **21**, 5904-5924.

Nicholls, M. E., R. H. Johnson and W. R. Cotton, 1988: The Sensitivity of Two-Dimensional Simulations of Tropical Squall Lines to Environmental Profiles. *J. Atmos. Sci.*, **45**, 3625-3649.

Noppel, H., U. Blahak, A. Seifert, and K. D. Beheng, 2010: Simulations of a hailstorm and the impact of CCN using an advanced two-moment cloud microphysical scheme. *Atmos. Res.*, **96**, 286-301.

Nordeng, T. E., 1994: Extended versions of the convective parameterization scheme at ECMWF and their impact on the mean and transient activity of the model in the tropics. Tech. Memo. 206, European Centre for Medium-Range Weather Forecasts, Reading, United Kingdom, 41p.

Pan, D.-M. and D. A. Randall, 1998: A cumulus parameterization with a prognostic closure. *Q. J. R. Meteorol. Soc.*, **124**, 949-981.

Park and Bretherton, 2009: The University of Washington Shallow Convection and Moist Turbulence Schemes and Their Impact on Climate Simulations with the Community Atmosphere Model. *J. Climate,* **22**, 3449-3469.

Pincus, R., H. W. Barker, and J.-J. Morcrette, 2003: A fast, flexible, approximation technique for computing radiative transfer in inhomogeneous cloud fields, J. Geophys. Res., 108(D13), 4376, doi:10.1029/2002JD003322.

Pritchard, M. S., M. W. Moncrieff, and R. C. J. Somerville, 2011: Orogenic propagating precipitation systems over the United States in a global climate model with embedded explicit convection. *J. Atmos. Sci.*, **68**, 1821-1840.

Qian, L., G. S. Young, and W. M. Frank, 1998: A Convective Wake Parameterization Scheme for Use in General Circulation Models. *Mon. Wea. Rev.*, **126**, 456-469.

Randall, D. A., K.-M. Xu, R. J. C. Somerville and S. Iacobellis, 1996: Single-Column Models and Cloud Ensemble Models as Links between Observations and Climate Models. *J. Climate*, **9**, 1683-1697.

Raymond, D. J., 1995: Regulation of Moist Convection over the West Pacific Warm Pool. *J. Atmos. Sci.*, **52**, 3945-3959.

Raymond, D. J. and X. Zeng, 2005: Modelling tropical atmospheric convection in the context of the weak temperature gradient approximation. *Q. J. R. Meteorol. Soc.*, **131**, 1301-1320.

Raymond, D. J., 2007: Testing a cumulus parametrization with a cumulus ensemble model in weak-temperature-gradient mode. *Q. J. R. Meteorol. Soc.*, **133**, 1073-1085.

Romps, D. M. and Z. Kuang, 2010: Do undiluted convective plumes exist in the upper tropical troposphere? *J. Atmos. Sci.*, **67**, 468-484.

Rotunno, R., J. B. Klemp and M. L. Weisman, 1988: A Theory for Strong, Long-Lived Squall Lines. *J. Atmos. Sci.*, **45**, 463-485.

Sahany, S. and R. S. Nanjundiah, 2008: Impact of convective downdrafts on model simulations: results from aqua-planet integrations. *Ann. Geophys.,* **26**, 1877-1887.

Sinclair, P. C., 1973: Severe storm velocity and temperature structure deduced from penetrating aircraft, in *Preprints 8th Conference Severe Local Storms*, p 25-31, American Meteorological Society, Boston, Mass.

Smolarkiewicz, P. K. and W. W. Grabowski, 1990: The multi-dimensional positive definite advection transport algorithm: Non-oscillatory option. *J. Comput. Phys.*, **86**, 355-375.

Sobel, A. H. and C. S. Bretherton, 2000: Modeling tropical precipitation in a single column. *J. Climate*, **13**, 4378-4392.

Straub, K. H., P. T. Haertel, and G. N. Kiladis, 2010: An Analysis of Convectively Coupled Kelvin Waves in 20 WCRP CMIP3 Global Coupled Climate Models. *J. Climate*, **23**, 3031-3056.

Stull, R. B., 1988: *An Introduction to Boundary Layer Meteorology*. Kluwer Academic Publ., Dordrecht, The Netherlands.

Sud, Y. C. and G. K. Walker, 1993: A rain evaporation and downdraft parameterization to complement a cumulus updraft scheme and its evaluation using GATE data. *Mon. Wea. Rev.*, **121**, 3019-3019.

Sun, R., S. K. Krueger, M. A. Jenkins, M. A. Zulauf and J. J. Charney, 2009: The importance of fire-atmosphere coupling and boundary-layer turbulence to wildfire spread. *Intrnl. J. Wildland Fire*, **18**, 50-60.

Thayer-Calder, K. and D. A. Randall, 2009: The Role of Convective Moistening in the Madden Julien Oscillation. *J. Atmos. Sci.*, **66**, 3291-3312.

Tiedke, M., 1989: A comprehensive mass flux scheme for cumulus parameterization in large-scale models. *Mon. Wea. Rev.*, **117**, 1779-1800.

Tokioka, T., K. Yamazaki, A. Kitoh, and T. Ose, 1988: The equatorial 30-60 day oscillation and the Arakawa-Schubert penetrative cumulus parameterization. *J. Meteor. Soc. Japan*, **66**, 883-901.

Van Den Heever, S. C., G. L. Stephens and N. B. Wood, 2011: Aerosol Indirect Effects on Tropical Convection Characteristics under Conditions of Radiative-Convective Equilibrium. *J. Atmos. Sci.*, **68**, 699-718.

Warner, J., 1977: Time variation of updraft and water content in small cumulus clouds. *J. Atmos. Sci.*, **34**, 1306-1312.

Wei, D., A. M. Blyth and D. J. Raymond, 1998: Buoyancy of Convective Clouds in TOGA COARE. *J. Atmos. Sci.*, **55**, 3381-3391.

Weisman, M. L. and J. B. Klemp, 1982: The Dependence of Numerically Simulated Convective Storms on Vertical Wind Shear and Buoyancy. *Mon. Wea. Rev.*, **110**, 504-520.

Wiggert, V., R. I. Sax, and R. L. Holle, 1982: On the modification potential of Illinois summertime convective clouds, with comparison to Florida and FACE observations. *J. Appl. Meteorol.*, **21**, 1293-1322.

Willis, P. T., J. Hallett, and J. A. Jorden, 1982: The development of precipitation near the top of a marine cloud. In *Preprints on Cloud Physics*, p 211-214, American Meteorological Society, Boston, Mass.

Zhang, G. J. and N. A. McFarlane, 1995: Sensitivity of climate simulations to the parameterization of cumulus convection in the Canadian Climate Centre General Circulation Model. *Atmos.-Ocean*, **33**, 407-446.

Zhang, G. J. and M. Mu, 2005: Simulation of the Madden-Julian Oscillation in the NCAR CCM3 Using a Revised Zhang-McFarlane Convection Parameterization Scheme. *J. Climate*, **18**, 4046-4064.

Zipser, E. J. and M. A. LeMone, 1980: Cumulonimbus Vertical Velocity Events in GATE. Part II: Synthesis and Model Core Structure. *J. Atmos. Sci.*, **37**, 2458-2469.

Yamaguchi, T., D. A. Randall, and M. F. Khairoutdinov, 2011: Cloud modeling tests of the ULTIMATE-MACHO scalar advection scheme. *Mon. Wea. Rev.*, **139**, 3248-3264.

Yamaguchi, T. and D. A. Randall, 2012: Cooling of Entrained Parcels in a Large-Eddy Simulation. *J. Atmos. Sci.*, **69**, 1118-1136.